REPORT DOCUMENTATION PAGE

Form Approved
OMB No. 0704-0188

1. AGENCY USE ONLY (Leave blank)	2. REPORT DATE	3. REPORT TYPE AND DATES COVERED
	23 Apr 96	Final Report, 1 Mar 93 - 29 Feb 96

4. TITLE AND SUBTITLE

Micromechanics-Based Failure Model of Granular/Particulate Medium with Reinforcing Fibers

5. FUNDING NUMBERS

G F49620-93-1-0192

6. AUTHOR(S)

Radoslaw L. Michalowski

AFOSR-TR-96 0301

7. PERFORMING ORGANIZATION NAME(S) AND ADDRESS(ES)

The Johns Hopkins University
Department of Civil Engineering
3400 N. Charles Street
Baltimore, MD 21218-2686

9. SPONSORING / MONITORING AGENCY NAME(S) AND ADDRESS(ES)

Air Force Office of Scientific Research
Directorate of Aerospace Sciences
Bolling AFB
Washington, DC 20332

N/A

10. SPONSORING / MONITORING AGENCY REPORT NUMBER

93-1-0192

11. SUPPLEMENTARY NOTES

12a. DISTRIBUTION / AVAILABILITY STATEMENT

Approved for Public Release
Distribution Unlimited

12b. DISTRIBUTION CODE

19960624 263

13. ABSTRACT (Maximum 200 words)

This research has focused on limit behavior of fiber composites with granular matrices (such as fiber-reinforced soils). Dominant mechanisms of fiber-matrix interaction were identified. Mathematical description of the behavior of granular composites on the macro-scale was presented, based on microstructural interactions. The concept of mathematical homogenization was introduced to represent the failure properties of the composite on the macro-scale. Failure criteria for composites both with fibers in a preferred direction and with randomly distributed fibers were derived. A Laboratory technique was devised for preparation of the specimens of fiber-reinforced composites. Experimental test were carried out, and the experimental evidence was collected for validation of the mathematical description. Implementation of the derived criteria in numerical methods for solving boundary value problems was presented.

14. SUBJECT TERMS	15. NUMBER OF PAGES
Composites, Constitutive behavior, Failure, Fiber reinforcement, Granular materials, Homogenization, Soil reinforcement	96
	16. PRICE CODE

17. SECURITY CLASSIFICATION OF REPORT	18. SECURITY CLASSIFICATION OF THIS PAGE	19. SECURITY CLASSIFICATION OF ABSTRACT	20. LIMITATION OF ABSTRACT
Unclassified	Unclassified	Unclassified	UL

TABLE OF CONTENTS

Micromechanics-Based Failure Model of Granular/Particulate Medium with Reinforcing Fibers

SUMMARY

This report contains results from research sponsored by the Air Force Office of Scientific Research, Grant No. F49620-93-1-0192, made to the Johns Hopkins University for research entitled "Micromechanics-Based Failure Model of Granular/Particulate Medium with Reinforcing Fibers". Research results presented in this report are the outcome of a 3-year effort on part of the Principal Investigator and a team of two Graduate Students. Both theoretical and experimental effort was undertaken; computational and experimental facilities at the Johns Hopkins University were used to accomplish the tasks. Results from this research have been published in six technical papers and one doctoral dissertation[1]. This report summarizes the findings.

Research personnel involved: Radoslaw L. Michalowski, Principal Investigator (Associate Professor at the Johns Hokins University), and 2 Graduate Assistants: Aigen Zhao (Ph.D. degree conferred in 1995), and Jan Cermak (Ph.D. expected in academic year 1996/97).

---

[1]R.L. Michalowski and A. Zhao. *Failure criteria for fibrous granular composites*. In: Proceedings, 8th. Int. Conf. International Association for Computer Methods and Advances in Geomechanics, Morgantown WV, 1994, vol. 2, 1385-1390.

R.L. Michalowski. *Failure criterion for a fiber-reinforced granular composite*. In: Proc. ASCE X Engineering Mechanics Conference, ed. S. Sture, Boulder, CO, May 1995, Vol. 2, 1143-1146.

R.L. Michalowski and A. Zhao. *Limit condition for fiber-reinforced granular soil*. Transportation Research Record, 1474(1995), 102-107.

R.L. Michalowski and A. Zhao. *Limit condition for unidirectionally reinforced soils*. In: 5th. Int. Symp. on Numerical Models in Geomechanics, G.N. Pande & S. Pietruszczak, eds., Davos, Switzerland, 1995, 237-242.

R.L. Michalowski and A. Zhao. *Failure of fiber-reinforced granular soils*. Journal of Geotechnical Engineering, 122(1996), No. 3, 226-234.

R.L. Michalowski and A. Zhao. *Failure of unidirectionally reinforced composites with a frictional matrix*. Journal of Engineering Mechanics, 122(1996), No. 11 (in print).

A. Zhao. *Failure Criteria for Reinforced Soils and Analysis of Reinforced Soil Structures*. Doctoral Dissertation, The Johns Hopkins University, 1994.

The objectives of this research were: improvement in understanding of the mechanical behavior of fibrous composites with a granular matrix; identifying the dominant mechanisms of fiber-matrix interaction; formulating mathematical description of the behavior of granular composites on the macro-scale, based on microstructural interactions; deriving failure criteria for composites both with fibers in a preferred direction, and with randomly distributed fibers; collection of experimental evidence for validation of the mathematical description (evidence to corroborate model assumptions).

The report of research findings (pages 11 - 56) is arranged in four subsections. The first two subsections describe the failure criteria derived for fiber composites. These parts include the concept of homogenization, and a theoretical effort toward mathematical description of the failure state of such composites in terms of the macroscopic stresses (stresses averaged over the constituents of the composite). Fiber-reinforced composites with randomly distributed fibers and with fibers oriented in one direction were considered. The former led to an isotropic failure criterion whereas the latter is described with an anisotropic function.

Experimental tests are described in the third part. A technique was devised for preparing specimens of composites with fibers distributed uniformly and with a random distribution of orientation. Over 80 drained triaxial tests were performed on sand and sand - fiber mixtures of different composition. Comparison of these test results with the theoretical predictions indicates that the theoretical model for the failure criterion is a robust one. An interesting phenomenon of induced anisotropy was detected in specimens subjected to large deformation. The experimental results are documented in the Appendix.

The fourth part of the research description contains examples of numerical implementation of the failure criteria derived.

It is suggested in the concluding remarks that this research be continued with a wider scope of including anisotropy and describing the entire elasto-plastic behavior of fiber composites with granular matrices.

INTRODUCTION AND LITERATURE SUMMARY REVIEW

An extensive search of the literature was carried out prior to performing the research. Results of that search are summarized below, as part of this Introduction. While a large body of literature exists on metallic and synthetic composites, anisotropic laminate composites, and composites with a periodic structure, rather modest research results were found in the literature with respect to reinforced frictional (pressure-dependent) materials with low or no cementation (such as soils). None of the reports attempted a systematic analysis of the interfacial force transfer, or its consequences for the behavior of the composite on a macroscopic level. Problems of a similar nature were considered, however, in formulating the strength criteria for media other than the granular/particulate kind (*e.g.*, filament reinforced paper, and in description of cementitious fibrous composites). Most of those, however, are concerned with elastic properties, and much less attention is paid to inelastic behavior, which is so important in granular/particulate materials. Some developments in the area of rock joints (and faults) modeling were found to be common with modeling other frictional interfaces, such as a fiber - granular matrix. Published papers representative of past research are mentioned in this Introduction, and a more extensive bibliography is given in section References and Bibliography.

Traces of systematic research into mechanical behavior of fiber composites can be found in the early fifties (Cox, 1952). Cox considered elastic interaction between a single elastic fiber and a matrix material. His analysis was later called the shear-lag theory, and its clear presentation can be found, for instance, in Piggott (1980). In short, the equilibrium of a single elastic fiber imbedded in a cylindrical elastic matrix element under an axisymmetric strain state is analyzed to give the distribution of the shear stress on the perimeter of the fiber, and the axial stress in the fiber. Following the shear-lag theory the axial stress in the fiber, σ_f, and the distribution of the shear stress, τ_f, along a perfectly bonded interface during elastic deformation, can be written as

$$\begin{aligned} \sigma_f &= E_f \varepsilon_1 [1 - \cosh(nx/r)/\cosh(nL/r)] \\ \tau_f &= \frac{1}{2} n E_f \varepsilon_1 \sinh(nx/r)/\cosh(nL/r) \end{aligned} \tag{1}$$

where ε_1 is the axial strain of the matrix at distance R from the axis of the fiber, E_f is the Young modulus of the fiber material, and n is a parameter dependent on E_f, E_m, ν_m (the last two being the Young modulus of the matrix material and Poisson's ratio), and the

geometrical parameter R/r, where r is the radius of the fiber. It was assumed that the load transfer between the fiber and the matrix takes place only across the cylindrical interface and not through the circular ends of the fiber ($\sigma_f = 0$ for $x = \pm L$, $2L$ = fiber length).

The shear-lag theory may be used to calculate *microscopic*[2] stresses in the composite constituents necessary for calculation of the *macroscopic* stress (homogenization). While this theory, in a variety of forms, is used often today for description of elastic behavior of cementitious composites, its application to granular-based composites is questionable for at least two reasons: (a) flexible fibers do not remain straight in a coarse granular matrix as they follow the shape of granules, and (b) description based on the assumption of a perfect and continuous bond is not realistic for the fiber-granular matrix interface.

Studies of the behavior of a single fiber in the matrix material were carried out to predict the behavior of the composite. Homogenization techniques were used to generalize the results derived from the microstructural studies to the macroscopic (or global) behavior of the composite. These techniques are based on the mixture theory where the magnitude of an average quantity (for instance, stress) assigned to the composite is calculated as a volumetric average of this variable in the constituents (see for instance Aboudi, 1991; Piggott, 1980; Romstad *et al.*, 1976, de Buhan *et al.*, 1989). For instance, the composite normal stress in the direction of the fiber would be represented as: $\bar{\sigma} = \eta_f \bar{\sigma}_f + \eta_m \bar{\sigma}_m$ ($\eta_{()}$ and $\bar{\sigma}_{()}$ being the respective volume fractions, and average stresses in the fibers and in the matrix in a representative element of the composite). If fibers in the composite have a homogeneous orientation and regular spacing, and the volume of the fibers can be neglected with respect to the volume of the matrix ($\eta_f << \eta_m$), the average stress tensor can be written as

$$\bar{\sigma}_{ij} = \sigma_{ij}^m + \frac{T}{ab} n_i n_j \qquad (2)$$

where σ_{ij}^m is the stress tensor in the matrix material, T is the magnitude of the force in a single fiber, a and b are the spacing distances in the plane perpendicular to the fibers, and n_k is the unit vector in the direction of the fibers. Another well-known technique

[2]The term *microscopic* indicates an analysis at the level of interaction among the composite constituents as opposed to *macroscopic* considerations at the level of the entire structure. These terms, here, do not indicate the structure's scale (size).

for homogenizing the stress in the composite can be expressed as

$$\bar{\sigma}_{ij} = \frac{1}{V} \int_S T_i x_j \, dS \tag{3}$$

where $\bar{\sigma}_{ij}$ is the average stress in a representative volume V of the composite material. T_i is the traction vector on boundary S of volume V, and x_j is the co-ordinate of vector T_i on boundary S. Boundary S intersects all phases of the composite, and vector T_i represents forces in all of the constituents. This technique was used by Hill (1963) in considering elastic behavior of reinforced solids, and also is often used to arrive at the average stress tensor in granular materials (see, for instance, Drescher and de Jong, 1972).

A homogenization technique found very useful for granular-based composites is based on what is sometimes referred to as the Hill-Mandel principle of macrohomogeneity (see, for instance, Maugin, 1992). This principle, in a somewhat modified version, was used here to homogenize the stress state in a fiber-reinforced granular material at failure. Due to complexity in the calculations of the energy dissipation in fibers during plastic deformation, a special integration space was introduced. Only an isotropic case of the composite was fully analyzed at the time of writing this report, but the concept of the integration space introduced is clearly applicable (though somewhat more complex) to composites with a non-isotropic distribution of fiber orientation.

A lot of attention has been paid to homogenization techniques in the context of metal matrix composites (*e.g.*, Hill 1964a,b, 1965; Huang, 1973; Tanaka *et al.*, 1973; Wakashima *et al.*, 1979; Dvorak and Bahei-El-Din, 1982; Aboudi, 1986; Pindera *et al.*, 1991). The finite element technique was used to analyze repeating unit cells of periodic arrays (*e.g.*, Adams, 1970; Dvorak *et al.*, 1974). Much of this research was devoted to unidirectional fiber composites. The different nature of the metal and granular/particulate matrices makes it difficult to extend these research results to granular fibrous composites. In addition, the nature of the fiber-matrix interface is quite different in both types of composites. An excellent survey of techniques used for analysis of composite materials was presented by Hashin (1983).

Theoretical considerations of the yielding stresses of a fibrous composite in the context of plane stress structures, such as paper, were presented by McLaughlin and

Batterman (1970) and McLaughlin (1972), and also in more general terms by Spencer (1972). The novelty of the approach by McLaughlin and Batterman was in introducing a kinematically admissible deformation pattern of the composite to obtain the yield stress of the composite (a technique similar to limit analysis). Their approach was restricted, however, to plane-stress structures. A common characteristic of these and earlier efforts was assuming a perfect bond between the fibers and the matrix material, and the global behavior of the composite was obtained through a homogenization process without provisions for slip of the fibers.

The most recent papers involving a reinforced non-cementitious granular matrix (granular soils) involve a similar approach. The case of elasto-plastic behavior was considered most recently by Jommi *el al.* (1995) (for papers in the context of reinforced soil, see also de Buhan and Siad, 1989; Sawicki and Lesniewska, 1989; de Buhan and Taliercio, 1991; and Michalowski and Zhao, 1995). A numerical analysis of this problem, using a homogenization technique based on a "unit cell", was also tried for reinforced soils (Romstad, *et al.*, 1976). An attempt at including the slip of a continuous strip reinforcement in a numerical scheme can be found in Naylor and Richards (1978). The possibility of a snap-back behavior was noted recently by Abramento and Whittle (1995). Analytical results for continuous filament reinforcement are even more limited (Villard and Jouve, 1989; and Prisco and Nova, 1993), even though such composites were proved to be very effective (Leflaive, 1985).

There is a handful of papers with results of tests on specimens of fiber-reinforced and continuous filament-reinforced soils (Andersland and Khattak, 1979; Hoare, 1979; Arenicz and Chowdhury, 1988; Gray and Ohashi, 1983; Maher and Gray, 1990; Liausu and Juran, 1995; Stauffer and Holtz, 1995). An effort was made by Gray and Ohashi (1983) and Maher and Gray (1990) to describe the strength through considerations of soil-fiber interaction in a localized shear band (see also Gray and Al-Refeai, 1986). Strain localization is a bifurcation phenomenon where response of the specimen is no longer representative of unique material properties, as the deformation mode (and the evolution of properties) is no longer uniform. Therefore, a strain localization phenomenon should rather be avoided in homogenization processes.

Research related to that undertaken here is underway in the area of fiber-reinforced cementitious materials, concrete in particular. Of special interest are theoretical and experimental studies to explain and describe the interaction between fibers and the matrix. Experimental results of pull-out of a fiber from a brittle matrix

were reported, for instance, by Pinchin and Tabor (1978) for an unyielding fiber, and by Bowling and Groves (1979) for yielding fibers. Laboratory tests and a modeling effort for fiber-reinforced mortar, based on the shear-lag theory, were also presented (Gopalaratnam and Shah, 1987). After a crack has appeared in the matrix, the fibers are expected to do what is usually referred to as "crack bridging". The fiber pullout process during crack bridging in a brittle matrix, however, is different than that of the fiber slip in a deforming granular matrix. A number of lab tests on fibrous composites in a brittle matrix, along with references, are given in a recent text by Bentur and Mindess (1990). While tests of this kind are useful in estimating the efficiency of fibers to bridge cracks in a brittle matrix, a straightforward interpretation of such tests with respect to a granular matrix would not be possible. A review of theoretical analyses of fiber length influence on the fiber's debonding from the matrix material during pull-out was presented by Gray (1984).

As mentioned earlier, the transition from the analysis of a single fiber-matrix interaction for cementitious composites to *macroscopic* behavior is traditionally made by volumetric averaging, similar to the procedure used in the theory of mixtures. Thus the total stress in the composite is represented as the volumetric average of the stresses in the fibers and matrix arrived at in micromechanical considerations of a single fiber - matrix interaction. Such procedure may be quite artificial for granular materials with flexible fibers where the contribution of fibers to the behavior of the composite (or to the total stress) may be strongly dependent on the deformation pattern of the fibers themselves (*e.g.*, kinking) and the deformation pattern of the entire composite (*e.g.*, localization of shear strain). The importance of the kinking process in analysis of the fiber composites was emphasized by Budiansky (1983) (see also Steif, 1990).

Fiber slip (or pullout) is a known failure mode during a crack opening in fiber-reinforced concrete. However, no attention has been paid to the *process* of fiber slip. Tracing this process is very important for improving our understanding of possible failure modes (and post-failure behavior, softening, snap-back) of the composite microstructure, and the consequences for structures built out of such composites. In a few analyses involving slip (*e.g.*, Piggott, 1980), the slip of a fiber is assumed to be symmetrical (starting from both ends of the fiber), and the shear stress on the slipped interface is assumed constant (the consequence of a simple perfectly plastic bond yield function). True slip, however, can be unstable, and not necessarily symmetrical, owing to the bifurcation of the equilibrium path. Also, no mention of possible scale effects was found in the literature on fiber-reinforced granular materials, due to softening of the

interface with the increase in slip, which is a known phenomenon for materials with an "internal length parameter" (Bazant and Desmorat, 1994). The only scale effect mentioned is the obvious one, due to the length (aspect ratio) of the fibers. Fundamental considerations which shed more light on the slip process can be found in the area of modeling frictional slip on rock joints and faults (Dieterich, 1979; Rice and Ruina, 1983; Ruina, 1984; Plesha, 1987).

SCOPE OF RESEARCH AND OBJECTIVES

This research focuses on the investigation into the limit behavior of fiber reinforced granular materials. In particular, an effort was directed toward derivation of the functions which describe the failure stress state of such composites, and toward collecting experimental evidence to validate the failure criteria derived. The scope of this research is restricted to the time-independent irreversible behavior, with the focus on failure.

The objectives of this research were:

(a) improvement in understanding of the mechanical behavior of fibrous composites with a granular matrix, and identifying the dominant mechanisms of fiber-matrix interaction,

(b) formulating mathematical description of the behavior of granular composites on the macro-scale, based on microstructural interactions, and deriving failure criteria for composites both with fibers in a preferred direction, and with randomly distributed fibers,

(c) collection of experimental evidence for validation of the mathematical description (evidence to corroborate model assumptions).

RESEARCH FINDINGS

The report of research findings is arranged into 3 parts: (a) presentation of the homogenization technique and the failure criteria for fibrous granular composites, (b) description of the experimental technique used, and experimental results, and (c) presentation of a technique for solving for macroscopic stresses in a continuum.

Failure Criterion for Fiber-Reinforced Soil (random fibers)

Macroscopic Failure Stress in Fiber-Reinforced Granular Composite

We introduce here a notion of a *macroscopic* stress as a stress averaged over the constituents of the composite (the stress averaged over the granular matrix and the fibers). An energy-based homogenization (averaging) technique has been proposed. In this approach to homogenization, an incipient deformation for a representative element, such as the one in Fig. 1(a), is assumed first. Next, the energy dissipation rate, $\dot{D}(\dot{\varepsilon}_{ij})$, in the soil and fibers is calculated during the incipient deformation process, and it is equated to the work rate of the macroscopic stress $\bar{\sigma}_{ij}$

$$\bar{\sigma}_{ij}\,\bar{\dot{\varepsilon}}_{ij} = \frac{1}{V}\int_V \dot{D}(\dot{\varepsilon}_{ij})\,dV \tag{4}$$

V is the volume of a representative element of the composite and $\bar{\dot{\varepsilon}}_{ij}$ is the macroscopic (average) strain rate. A similar averaging technique was investigated earlier in the context of cementitious composites by Hashin (1964), Shu and Rosen (1967), and, for two-dimensional membranes, by McLaughlin and Batterman (1970). It was also used very recently to homogenize a unidirectionally reinforced sand (Michalowski and Zhao, 1995).

The specific deformation pattern assumed here in the homogenization process has a linear distribution of velocities, subject to constraints imposed by the dilatancy of the base (matrix) material (such as in Michalowski and Zhao, 1995). It is further assumed that the deformation rate of the granular matrix is identical to the macroscopic deformation ($\dot{\varepsilon}_{ij} = \bar{\dot{\varepsilon}}_{ij}$). The fibers are considered one-dimensional elements, and they can deform at the same rate (upon reaching yield stress), or, they can slip in the matrix.

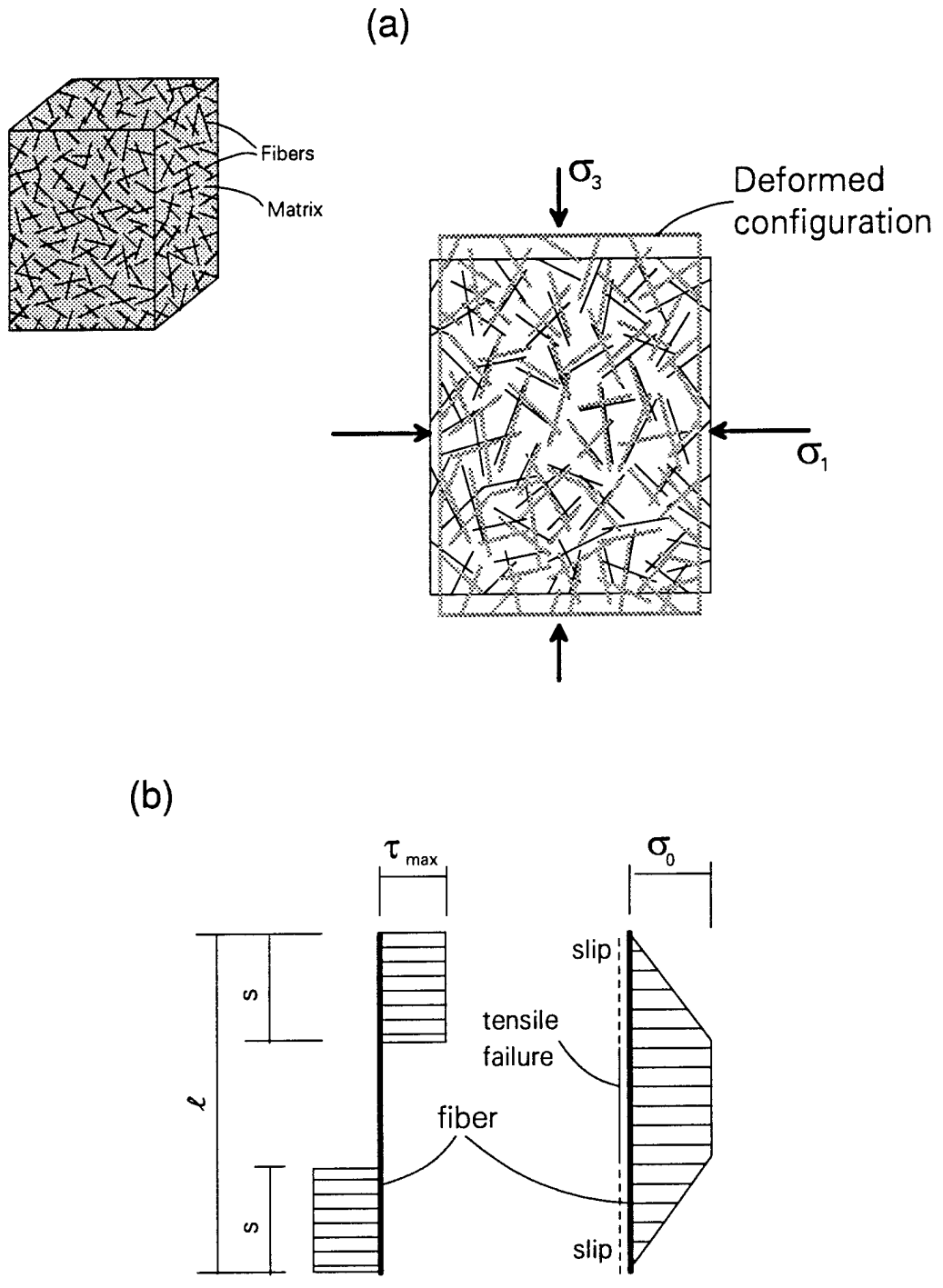

Figure 1. Fiber-reinforced composite: (a) Plane-strain deformation of 3D specimen; (b) Fiber-matrix shear stress and axial stress in rigid-perfectly plastic fiber.

Definitions and Assumptions

We assume here that the fibers are distributed uniformly in the space with a random distribution of orientation. Hence, a representative specimen must exist in which the fiber concentration ρ and the distribution of orientation can be considered uniform. Fiber concentration characterizes the amount of reinforcement and is defined here as

$$\rho = \frac{V_r}{V} \tag{5}$$

where V_r is the volume of the fibers and V is the volume of the entire representative composite element. For practical purposes, such as preparing specimens of fiber-reinforced soil, the weight content may be a more convenient parameter. However, as the mechanical properties of the composite constituents are not necessarily related to their mass densities (and, therefore, to the unit weights), the volumetric content of the fibers is the appropriate parameter to represent the fiber content. Note also that it is the volumetric content of the constituents that governs the averaging schemes in the theory of mixtures.

The fibers are considered to be cylindrical in shape, and their slenderness is described here by the aspect ratio

$$\eta = \frac{l}{2r} \tag{6}$$

where l is the length of the fiber and r is its radius. It is further understood that the length of the fibers is at least one order of magnitude larger than the diameter (say d_{50}) of the sand grains, and the diameter of fibers is at least of the same order as the grains.

Both the fibers and matrix (granular fill) are considered perfectly plastic, described by the Tresca and the Mohr-Coulomb failure criteria, respectively. The influence of the confining stress on the fiber tensile strength is ignored. The kinematics of the granular fill is governed by the normality rule.

Contribution of Fibers to Strength of Composite

Failure of a single fiber in a deforming composite can occur due to fiber slip or tensile rupture. Tensile rupture will be modelled here as incipient plastic flow of fibers.

Notice, however, that even if a tensile rupture occurs, the ends of the fiber will slip as the tensile strength of the fiber material cannot be mobilized throughout the entire fiber length. For a rigid - perfectly plastic behavior of the granular soil, fibers, and the interface, the expected distribution of the shear stress on the fiber surface and the axial stress in the fiber must conform to that in Fig. 1(b).

When a fiber fails in the tensile rupture mode, the slip occurs at both fiber ends up to the distance s

$$s = \frac{r}{2} \frac{\sigma_0}{\sigma_n \tan\varphi_w} \tag{7}$$

σ_0 is the yield stress of the fiber material, σ_n is the stress normal to the fiber surface, and φ_w is the friction angle of the matrix-fiber interface. A pure slip failure mode will occur if the length of fibers l becomes less than $2s$, or when the aspect ratio is

$$\eta < \frac{1}{2} \frac{\sigma_0}{\sigma_n \tan\varphi_w} \tag{8}$$

We further assume that the fibers contribute to the strength of the composite only if they are subjected to tension, whereas their influence in the compressive regime is neglected due to possible buckling and kinking.

Deformation of an Idealized Specimen and Space with "Ordered" Fibers

A plane-strain deformation is considered here for the specimen depicted in Fig.1(a), with a linear velocity distribution. The volume of the specimen is large enough so that its increase does not produce any change in the average properties of the specimen (representative volume).

The consequence of the linear velocity field is a uniform strain-rate throughout the specimen. The deformation process assumed is irreversible (plastic flow) and it is interpreted here as a composite failure. The average stress (macroscopic stress state) at failure is obtained from eq. (4). The kinematics of the granular fill is governed by the flow rule associated with the Mohr-Coulomb yield condition, which leads to the following constraint on dilatancy (plane strain)

$$\frac{\dot{\varepsilon}_1 + \dot{\varepsilon}_3}{\dot{\varepsilon}_1 - \dot{\varepsilon}_3} = -\sin\varphi \qquad \text{or} \qquad \frac{\dot{\varepsilon}_1}{\dot{\varepsilon}_3} = -\tan^2\left(\frac{\pi}{4} - \frac{\varphi}{2}\right) \tag{9}$$

where $\dot{\varepsilon}_1$ and $\dot{\varepsilon}_3$ are the maximum and minimum principal strain rates, respectively, and φ is the internal friction angle of the matrix (for the associative flow rule φ also indicates the rate of dilation).

In order to make integration on the right-hand side of eq. (4) tractable, we introduce a physical space with "ordered" fibers (Fig. 2) where all fibers are moved (in a parallel manner) to the origin of that space. Such transformation is admissible since the energy dissipation rate in fibers is dependent only on their orientation, and is independent of their location in the sample. The sample from Fig. 1(a) (which is three-dimensional, with fibers oriented in three-dimensional space) is now represented by a sphere with radius R_0 (fibers are not shown in Fig. 2). Due to macroscopic isotropy of the composite and symmetry of the deformation pattern, it is sufficient to consider **⅛** of the sphere.

Energy Dissipation Rate in an Idealized Specimen

The energy dissipation rate during plastic deformation of soil conforming to the Mohr-Coulomb failure condition is zero, therefore only the fibers will contribute to the dissipation in the composite specimen.

First, the region of fibers under compression in space in Fig. 2 needs to be found. A uniform plane deformation is considered with axes x and y (Fig. 2) coinciding with directions 1 and 3 [Fig. 1(a)], respectively. The regions with fibers in tension and compression are separated by a plane of inclination θ_0 (plane OBC in Fig. 2). All fibers in plane OBC undergo no deformation

$$\dot{\varepsilon}_{\theta_0} = \dot{\varepsilon}_1 \cos^2\theta_0 + \dot{\varepsilon}_3 \sin^2\theta_0 = 0 \tag{10}$$

which leads to

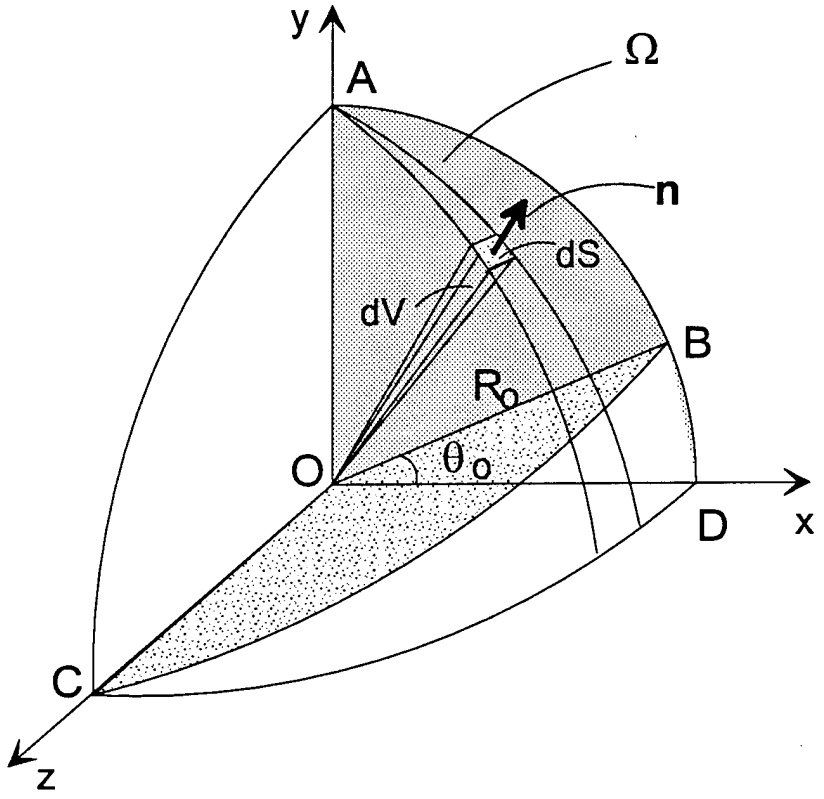

Figure 2. Integration space for isotropic fiber-reinforced representative element (fibers not shown).

$$\frac{\dot{\varepsilon}_1}{\dot{\varepsilon}_3} = -\tan^2\theta_0 \tag{11}$$

and, considering eq. (9), angle θ_0 can be determined as

$$\theta_0 = \frac{\pi}{4} - \frac{\varphi}{2} \tag{12}$$

The energy dissipation rate in a single fiber oriented in direction θ, due to slip along end sections s and due to plastic extension in the middle section of length l - $2s$, is

$$\dot{d} = 2\pi r s^2 \sigma_n \tan\varphi_w \langle\dot{\varepsilon}_\theta\rangle + \pi r^2 (l-2s)\,\sigma_0 \langle\dot{\varepsilon}_\theta\rangle = \pi r^2 \sigma_0 \left(l - \frac{r\sigma_0}{2\sigma_n \tan\varphi_w}\right)\langle\dot{\varepsilon}_\theta\rangle \tag{13}$$

Since the number of fibers per unit volume of the composite is $\rho/\pi r^2 l$, the energy dissipation rate in fibers per unit volume of the composite is

$$\dot{D}_r = \frac{1}{V}\int_V \pi r^2 \sigma_0 \left(l - \frac{r\sigma_0}{2\bar{\sigma}_n \tan\varphi_w}\right)\frac{\rho}{\pi r^2 l}\,\langle\dot{\varepsilon}_\theta\rangle\, dV \tag{14}$$

where $\bar{\sigma}_n$ is now the average normal stress to the fibers in volume V, and $\langle\dot{\varepsilon}_\theta\rangle$ is the strain rate in the direction of the fiber (tension is taken here as negative)

$$\langle\dot{\varepsilon}_\theta\rangle = \begin{cases} |\dot{\varepsilon}_\theta| & \text{if } \dot{\varepsilon}_\theta < 0 \\ 0 & \text{otherwise} \end{cases} \tag{15}$$

The energy dissipation rate per unit volume of the composite from eq. (14) can be written as

$$\dot{D}_r = \frac{1}{\frac{1}{6}\pi R_0^3}\int_V \left(1 - \frac{1}{4\eta}\frac{\sigma_0}{\bar{\sigma}_n \tan\varphi_w}\right)\rho\,\sigma_0 \langle\dot{\varepsilon}_\theta\rangle\, dV \tag{16}$$

where dV is an infinitesimal volume shown in Fig. 2. The exact magnitude of the average stress normal to the soil/fiber interface cannot be found since the distribution of the microstress is not considered here. An approximation is made where $\bar{\sigma}_n$ is

assumed constant for all fibers, and equal to the mean of the maximum and minimum principal stress in the composite [$p = (\bar{\sigma}_1 + \bar{\sigma}_3)/2$]. Such an assumption is a realistic estimate of $\bar{\sigma}_n$ for randomly distributed fibers.

Having assumed that $\bar{\sigma}_n$ can be approximated by p, and noting that $dV = \frac{1}{3}R_0\,dS$ (Fig. 2), eq. (16) can be written as

$$\dot{D}_r = 2\frac{\rho\sigma_0}{\pi R_0^2}\left(1 - \frac{1}{4\eta}\frac{\sigma_0}{p\tan\varphi_w}\right)\int_S \langle\dot{\varepsilon}_\theta\rangle\, dS \tag{17}$$

The unit vector normal to the spherical surface in Fig. 2 is

$$\underline{n} = \frac{x}{R_0}\underline{i} + \frac{y}{R_0}\underline{j} + \frac{z}{R_0}\underline{k} \tag{18}$$

and the velocity vector is

$$\underline{v} = -\dot{\varepsilon}_1 x\underline{i} - \dot{\varepsilon}_3 y\underline{j} \tag{19}$$

thus the magnitude of the velocity component along $\underline{n}$ becomes

$$v_\theta = \underline{v}\cdot\underline{n} = -\frac{x^2}{R_0}\dot{\varepsilon}_1 - \frac{y^2}{R_0}\dot{\varepsilon}_3 \tag{20}$$

and the strain rate along a fiber identified by co-ordinates x-y on the sphere's surface in the "ordered" space is

$$\dot{\varepsilon}_\theta = -\frac{v_\theta}{R_0} = \frac{\dot{\varepsilon}_1 x^2 + \dot{\varepsilon}_3 y^2}{R_0^2} \tag{21}$$

Substituting (21) into (17) one obtains

$$\dot{D}_r = 2\frac{\rho\sigma_0}{\pi R_0^4}\left(1 - \frac{1}{4\eta}\frac{\sigma_0}{p\tan\varphi_w}\right)\int_S (-\dot{\varepsilon}_1 x^2 - \dot{\varepsilon}_3 y^2)\, dS \tag{22}$$

Notice that because of the definition of $\langle\dot{\varepsilon}_\theta\rangle$ [eq. (15)] a minus sign appears in the integral expression, and S is part of the surface associated with fibers under tension only (ABC, Fig. 2). The following transformation is used to solve analytically the integral in eq. (22)

$$\iint_S f(x,y,z)dS = \iint_\Omega f[x,y,z(x,y)]\sqrt{1+\left(\frac{\partial z}{\partial x}\right)^2+\left(\frac{\partial z}{\partial y}\right)^2}\,dx\,dy \tag{23}$$

where Ω is the projection of area S on plane x-y (projection of surface ABCA in Fig. 2 on plane x-y). Note that $z = (R_0^2 - x^2 - y^2)^{1/2}$ thus

$$\frac{\partial z}{\partial x} = \frac{-x}{\sqrt{R_0^2 - x^2 - y^2}}, \qquad \frac{\partial z}{\partial y} = \frac{-y}{\sqrt{R_0^2 - x^2 - y^2}} \tag{24}$$

Eq.(22) now becomes

$$\dot{D}_r = 2\frac{\rho\sigma_0}{\pi R_0^3}\left(1 - \frac{1}{4\eta}\frac{\sigma_0}{p\tan\varphi_w}\right) \iint_\Omega (-\dot{e}_1 x^2 - \dot{e}_3 y^2)\frac{1}{\sqrt{R_0^2 - x^2 - y^2}}\,dx\,dy \tag{25}$$

Introducing new variables ζ and θ [$\zeta = (x^2 + y^2)^{1/2}$, $\theta = \tan^{-1}(y/x)$], and using (11), the expression in (25) becomes

$$\dot{D}_r = 2\frac{\rho\sigma_0}{\pi R_0^3}\left(1 - \frac{1}{4\eta}\frac{\sigma_0}{p\tan\varphi_w}\right) \int_0^{R_0}\int_{\theta_0}^{\frac{\pi}{2}} (-\dot{e}_1)\frac{\zeta^3}{\sqrt{R_0^2 - \zeta^2}}\left[\cos^2\theta - \sin^2\theta\,\tan^2\left(\frac{\pi}{4} + \frac{\varphi}{2}\right)\right] d\zeta\,d\theta \tag{26}$$

where θ_0 is given in eq. (12). The expression in (26) can be integrated analytically to yield

$$\dot{D}_r = \frac{\rho\sigma_0}{3} M\left(1 - \frac{1}{4\eta}\frac{\sigma_0}{p\tan\varphi_w}\right)\dot{e}_1 \tag{27}$$

where M is

$$M = \left(\frac{1}{2} + \frac{\varphi}{\pi} + \frac{1}{\pi}\cos\varphi\right)\tan^2\left(\frac{\pi}{4} + \frac{\varphi}{2}\right) - \frac{1}{2} - \frac{\varphi}{\pi} + \frac{1}{\pi}\cos\varphi \tag{28}$$

If the condition in eq. (8) is satisfied, then pure slip occurs, and the above procedure

leads to an expression for the energy dissipation rate per unit volume independent of the fiber yield stress σ_0

$$\dot{D}_r = \frac{1}{3}\rho\,\eta\,M\,p\tan\varphi_w\,\dot{\varepsilon}_1 \tag{29}$$

Failure Criterion for Fiber-Reinforced Soil

The energy balance equation (4) for isotropic material under plane strain conditions is

$$\dot{\varepsilon}_1\bar{\sigma}_1 + \dot{\varepsilon}_3\bar{\sigma}_3 = \dot{D}_r = \frac{\rho\sigma_0}{3}M\left(1 - \frac{1}{4\eta}\frac{\sigma_0}{p\tan\varphi_w}\right)\dot{\varepsilon}_1 \tag{30}$$

Utilizing (9) one obtains

$$\bar{\sigma}_1 - \tan^2\left(\frac{\pi}{4} + \frac{\varphi}{2}\right)\bar{\sigma}_3 = \frac{\rho\sigma_0}{3}M\left(1 - \frac{1}{4\eta}\frac{\sigma_0}{p\tan\varphi_w}\right) \tag{31}$$

Introducing stress invariant R, convenient for plane-strain conditions (radius of the Mohr circle),

$$R = \sqrt{\frac{(\bar{\sigma}_x - \bar{\sigma}_y)^2}{4} + \bar{\tau}_{xy}^2} \tag{32}$$

and noting that $2p = \bar{\sigma}_1 + \bar{\sigma}_3$, eq. (31) can be transformed to represent the failure criterion of the fiber-reinforced soil in terms of in-plane invariants R and p

$$\frac{R}{\rho\sigma_0} = \frac{p}{\rho\sigma_0}\sin\varphi + \frac{1}{3}N\left(1 - \frac{1}{4\eta\rho}\frac{\cot\varphi_w}{\frac{p}{\rho\sigma_0}}\right) \tag{33}$$

where

$$N = \frac{1}{\pi}\cos\varphi + \left(\frac{1}{2} + \frac{\varphi}{\pi}\right)\sin\varphi \tag{34}$$

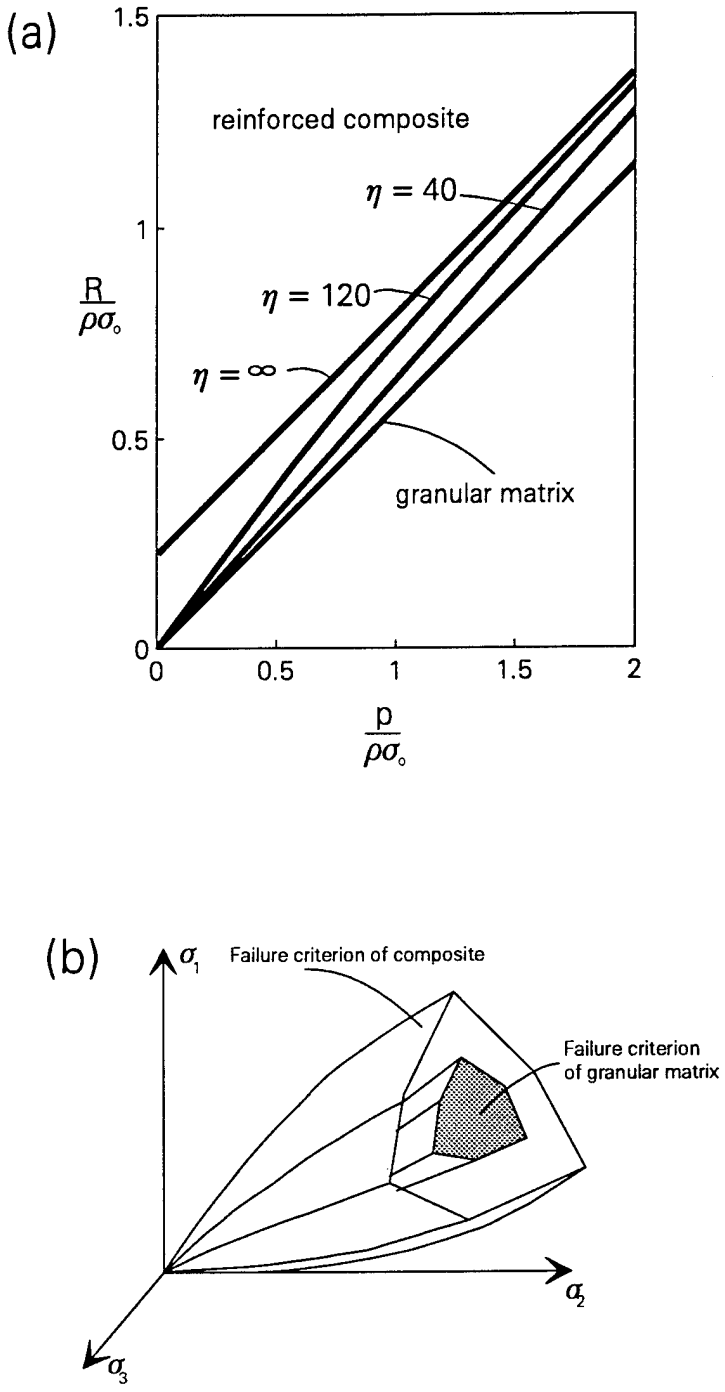

Figure 3. Theoretical failure criterion for isotropic fiber-reinforced granular composite: (a) Failure envelopes as functions of in-plane invariants R and p ($\rho = 0.02$, $\phi = 35^0$, $\phi_w = 20^0$); (b) Failure surface in principal stress space.

When pure slip occurs [eq. (8)] the failure criterion takes the form

$$\frac{R}{\rho\sigma_0} = \frac{p}{\rho\sigma_0}\left(\sin\varphi + \frac{1}{3}N\rho\eta\tan\varphi_w\right) \tag{35}$$

Note that when no fibers are present both (33) and (35) reduce to the standard Mohr-Coulomb failure criterion for granular material

$$R = p\sin\varphi \tag{36}$$

Figure 3(a) presents results from (33) and (35) in the R-p plane. Different curves present failure criteria for fiber-reinforced soil with fibers of various aspect ratios. As indicated in eq. (35), the slip mode is described by a linear function (when the internal friction angle of the soil fill is constant), whereas in the tensile rupture mode the shear strength is not proportional to the mean stress [eq. (33)]. There is no discontinuity in the gradient at the transition point (smooth piece-wise function). Stresses are normalized in Fig. 3(a) by parameter $\rho\sigma_0$ (fiber concentration × fiber yield point). The failure criterion in the principal (macroscopic) stress space is shown in Fig. 3(b).

Failure Criterion for Unidirectionally Reinforced Composite

Homogenization Scheme

The purpose of homogenization is to represent quantities such as stresses and strains or material properties (such as elastic moduli) as average quantities which take into account microstresses in the composite constituents, volumetric proportions of these constituents, their respective properties, and shape of inclusions. Here the objective is to represent the failure criterion of a pressure-dependent (frictional) material reinforced with longitudinal inclusions. Such criterion is to be represented in terms of the macroscopic stress, that is, the stress averaged over the two solid constituents of the composite (matrix and fibers). The term macroscopic here pertains to the average stress, or properties, of the composite, as opposed to the stress or properties in the constituents (microscopic). The terms macro- and microscopic do not relate here to the size of the composite representative element.

The diameter of the inclusions is considered to be at least an order of magnitude larger than the diameter of the grains in the matrix, and the dry friction law is

considered applicable on the soil-fiber interface. The aspect ratio of the inclusions is at least of the order of 10^1 to 10^2, and spacing is of at least one order of magnitude higher than the inclusions' thickness/diameter. Under such circumstances one can expect that, given sufficient confining stresses, a tensile force can be induced in longitudinal reinforcing elements which allows the macroscopic stress in the composite to increase beyond what would be considered a limit stress for the matrix alone.

A kinematics (or energy-based) approach to homogenization will be used in which a plastic velocity field for a representative composite element, such as in Fig. 4, is assumed, and the energy dissipation rate in the constituents of the composite, $\dot{D}(\dot{\varepsilon}_{ij})$, is equated to the work performed by the macroscopic stress $\bar{\sigma}_{ij}$

$$\bar{\sigma}_{ij}\,\bar{\varepsilon}_{ij} = \frac{1}{V}\int_V \dot{D}(\dot{\varepsilon}_{ij})\,dV \tag{37}$$

V is the volume of a representative element of the composite and $\bar{\varepsilon}_{ij}$ is the macroscopic (average) strain rate. This technique is identical to that used earlier (eq. ?), except that now a different kinematics of the composite element will be considered. This homogenization concept was explored earlier in the context of cementitious composites by Hashin (1964), Shu and Rosen (1967), and, for two-dimensional membranes, by McLaughlin and Batterman (1970). Once the energy dissipation rate during the plastic deformation (collapse) of the element is calculated, the macroscopic stress $\bar{\sigma}_{ij}$ can be calculated from eq. (37). This macroscopic stress then can be represented as a point on the failure surface in the macroscopic stress-space.

Of interest are failure criteria associated with plane kinematics where the uniaxial reinforcement is contained in the plane of deformation. In this homogenization scheme we will assume a linear velocity field throughout the representative element in the form

$$v_i = a_{ij}\,x_j \tag{38}$$

where v_i is the velocity vector, x_j is the Cartesian co-ordinate and a_{ij} is a matrix of coefficients subject to constraints imposed by the dilatancy of the base (matrix) material.

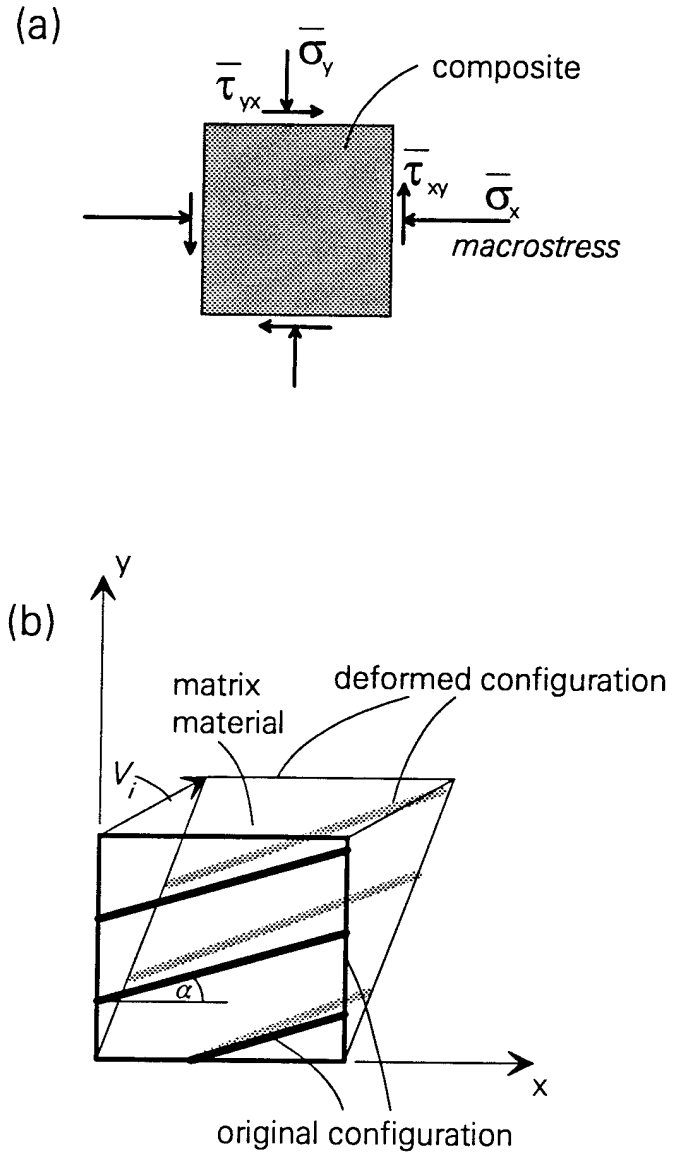

Figure 4. Composite material: (a) Macrostresses; (b) Deformation of a composite element.

Failure Criteria

In order to calculate energy dissipation rate $\dot{D}(\dot{\varepsilon}_{ij})$, the strain rate field, $\dot{\varepsilon}_{ij}$, inside the representative element needs to be known. As the velocity field throughout the representative element is assumed to be linear (eq. (38)), the strain rates are uniform, and the macroscopic strain rate $\bar{\dot{\varepsilon}}_{ij} = \dot{\varepsilon}_{ij}$. While such assumption would not be realistic for elastic deformation or a hardening flow regime, it is a reasonable one when the composite failure is reached (zero hardening modulus).

The matrix of the composite is assumed here to conform to the Mohr-Coulomb failure criterion and the associative flow rule. Consequently, the strain rate field used in the kinematical approach must satisfy the relation (plane strain)

$$\frac{\dot{\varepsilon}_v}{\dot{\varepsilon}_1 - \dot{\varepsilon}_3} = -\sin\varphi \tag{39}$$

where $\dot{\varepsilon}_v = \dot{\varepsilon}_{ii}$ = the volumetric strain rate, $\dot{\varepsilon}_1$ and $\dot{\varepsilon}_3$ are the maximum and minimum principal strain rates, respectively, and φ is the internal friction angle of the matrix, which, for the associative flow rule, also indicates the rate of dilation.

There is some controversy about using the normality rule since the laboratory results for sand indicate less dilation than that predicted by the associative flow law. Here, however, the associative flow rule is used only to select a virtual deformation in the homogenization scheme. It is convenient to use the associative rule, since the energy dissipation rate in the composite matrix becomes, in such case, independent of a particular stress state (zero for a non-cementitious matrix). A discussion of the normality rule versus the non-associative flow law, however, is beyond the scope of this investigation.

The rate of energy dissipation per unit volume of the matrix during plastic deformation under plane strain conditions is

$$\dot{D}^m = \sigma_{ij}^m \dot{\varepsilon}_{ij} = (\dot{\varepsilon}_1 - \dot{\varepsilon}_3)\, c \cos\varphi \tag{40}$$

where σ_{ij}^m satisfies the Mohr-Coulomb failure function (c = cohesion and φ = internal friction angle of the matrix material). The amount of reinforcement inclusions is characterized here by reinforcement concentration (volume density)

$$\rho = \frac{V_r}{V} \tag{41}$$

where V_r is the volume of the inclusions and V is the volume of the entire representative composite element. We are considering composites where the volume of reinforcing inclusions (for instance, fibers) is small compared to the volume of the composite ($\rho << 1$); thus $\dot{D}^m$ in eq. (40) can be interpreted as the dissipation rate in the matrix per unit volume of the composite.

Long Inclusions (Strips/Bars)

First a composite with long reinforcing inclusions is considered, where no slip occurs. Such composite material is representative of "traditional" reinforced soil. The yield point of the reinforcement material is σ_0. Since the deformation of the reinforcing inclusions is assumed to be the same as that for the matrix, the dissipation rate in the inclusions per unit volume of the composite is

$$\dot{D}^f = \rho \sigma^f_{ij} \dot{\varepsilon}_{ij} = \langle \xi \rangle \rho \sigma_0 n_i n_j \dot{\varepsilon}_{ij} \tag{42}$$

where n_i and n_j are the unit vectors in the direction of reinforcement and coefficient $\langle \xi \rangle$ depends on the mobilization of the tensile force in fibers

$$\langle \xi \rangle = \begin{cases} -1 \text{ when } \dot{\varepsilon}_{ij} n_i n_j < 0 \\ 0 \quad \text{otherwise} \end{cases} \tag{43}$$

As most applications of the theory presented here are in soil mechanics, we assume that the tension is negative. Coefficient ξ represents mobilization of the stress in the reinforcement, and, in general, it can vary in the range of $-1 \le \xi \le 0$, but the energy can be dissipated in fibers only when yield point σ_0 is reached ($\xi = \langle \xi \rangle = -1$). Note that, according to eq. (42), the contribution of the longitudinal inclusions (fibers, bars, strips) in the compressive regime to the composite strength is neglected here (due to buckling and kinking).

Eq. (37) can now be written for plane strain conditions as

$$\bar{\sigma}_x \dot{\bar{e}}_x + \bar{\sigma}_y \dot{\bar{e}}_y + 2\bar{\tau}_{xy} \dot{\bar{e}}_{xy} = \dot{D}^m + \dot{D}^f \tag{44}$$

It is convenient to represent the macroscopic failure criterion for plane strain conditions in space p, q, $\bar{\tau}_{xy}$, where $p = (\bar{\sigma}_x + \bar{\sigma}_y)/2$ and $q = (\bar{\sigma}_x - \bar{\sigma}_y)/2$. Introducing angle of inclination of the major principal macrostress to the x-axis ψ

$$\tan 2\psi = \frac{2\bar{\tau}_{xy}}{\bar{\sigma}_x - \bar{\sigma}_y} = \frac{\bar{\tau}_{xy}}{q} \tag{45}$$

eq. (44) takes the form

$$(p+q)\dot{\bar{e}}_x + (p-q)\dot{\bar{e}}_y + 2q \tan 2\psi \dot{\bar{e}}_{xy} = \dot{D}^m + \dot{D}^f \tag{46}$$

It was found to be convenient to calculate points on the failure surface in space p, q, $\bar{\tau}_{xy}$ by calculating in-plane stress invariant R for given values of p and angle ψ

$$R = \frac{1}{2}\sqrt{(\bar{\sigma}_x - \bar{\sigma}_y)^2 + 4\bar{\tau}_{xy}^2} = \sqrt{q^2 + \bar{\tau}_{xy}^2} = |q|\sqrt{1 + \tan^2 2\psi} \tag{47}$$

Using eqs. (40) and (42), solving eq. (46) for q and using the relation in eq. (47), one obtains

$$R(\dot{\bar{e}}_x, \dot{\bar{e}}_y, \dot{\bar{e}}_{xy}) = \left| \frac{c\cos\varphi \sqrt{(\dot{\bar{e}}_x - \dot{\bar{e}}_y)^2 + 4\dot{\bar{e}}_{xy}^2} + \langle\xi\rangle \rho \sigma_0 \dot{\bar{e}}_\alpha - p(\dot{\bar{e}}_x + \dot{\bar{e}}_y)}{\dot{\bar{e}}_x - \dot{\bar{e}}_y + 2\dot{\bar{e}}_{xy}\tan 2\psi} \right| \sqrt{1 + \tan^2 2\psi} \tag{48}$$

where $\dot{\bar{e}}_\alpha$ is the magnitude of the rate of strain in the direction of reinforcing inclusions

$$\dot{\bar{e}}_\alpha = \dot{\bar{e}}_{ij} n_i n_j = \dot{\bar{e}}_x \cos^2\alpha + \dot{\bar{e}}_y \sin^2\alpha + \dot{\bar{e}}_{xy} \sin 2\alpha \tag{49}$$

and α is the angle of inclination of the inclusions to the x-axis. As this approach yields the upper bound to the macroscopic failure criterion, a minimum R was sought from

eq. (48) in an optimization scheme where the strain rates were variable with restriction in eq. (39) and with $\langle\xi\rangle$ determined in eq. (43). Cross-sections of the failure surface calculated (p = const) are shown in Fig. 5. The failure surface in space p, q, $\bar{\tau}_{xy}$ is presented in Fig. 6. It consists of two conical surfaces joined by two plane sectors.

The matrix of the composite was assumed to obey the Mohr-Coulomb yield function and the associative flow rule. The resulting flow rule for the composite also conforms to the normality rule.

The failure criterion of an anisotropic pressure-dependent material under plane-strain conditions can be, in general, written as

$$f(\bar{\sigma}_x, \bar{\sigma}_y, \bar{\tau}_{xy}) = R - F(p,\psi) = 0 \tag{50}$$

where ψ and invariant R are given in (12) and (35), respectively, and p is another in-plane invariant [$p = (\bar{\sigma}_x + \bar{\sigma}_y)/2$]. When function F is independent of ψ, eq. (50) represents an isotropic yield criterion. Representation of failure surface $f(p,q,\bar{\tau}_{xy}) = 0$ can be given as a piece-wise function. Analytical expressions are given below, in which angle α is the angle of inclination of the principal axis of anisotropy to the x-axis (inclination of the direction of reinforcing inclusions). For the part where no influence of fibers is present ($\xi = 0$), *i.e.*, where

$$|2\psi - 2\alpha| \le \frac{\pi}{2} - \varphi \tag{51}$$

the analytic representation of the macroscopic yield function is

$$R = F(p) = p\,\sin\varphi + c\cos\varphi \tag{52}$$

For planar segments in Fig. 6 ($-1 < \xi < 0$), angle 2ψ remains in the range

$$\frac{\pi}{2} - \varphi < |2\psi - 2\alpha| \le \frac{\pi}{2} - \varphi + \tan^{-1}\left(\frac{0.5\rho\sigma_0}{p\tan\varphi + c}\right) \tag{53}$$

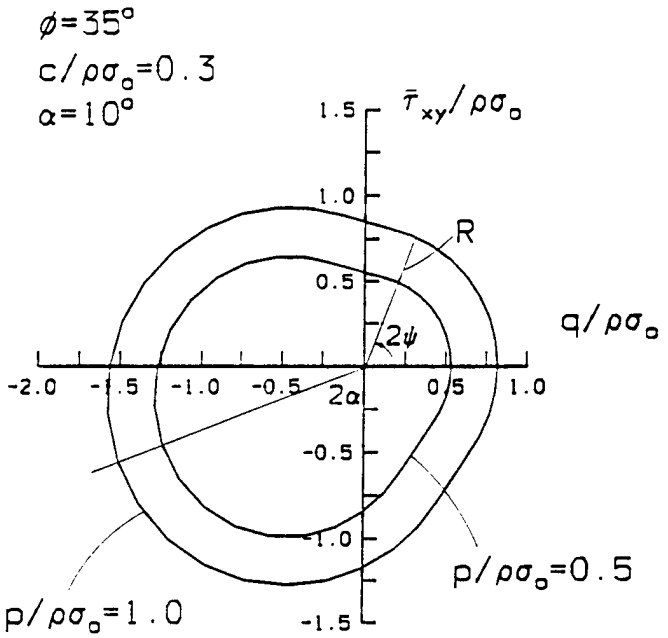

Figure 5. Cross-sections of a failure surface for a unidirectionally reinforced composite with long inclusions (no slip).

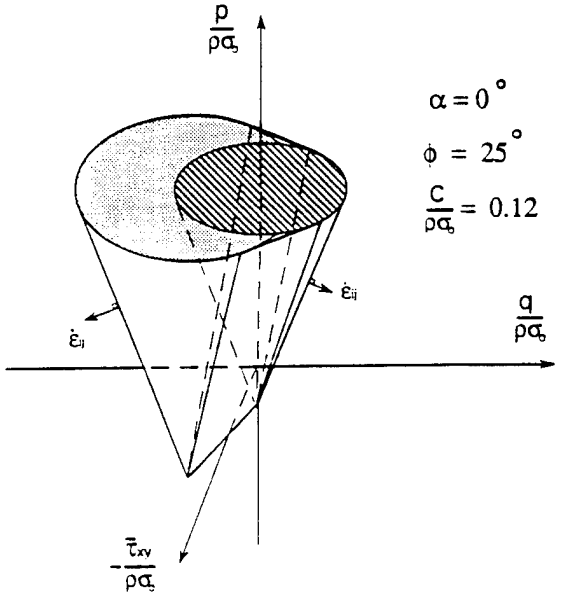

Figure 6. Failure surface for a unidirectionally reinforced composite in space p, q, $\bar{\tau}_{xy}$ (no slip of reinforcing inclusions).

and the failure criterion is

$$R = F(p,\psi) = \frac{p\sin\varphi + c\cos\varphi}{\sin(2\psi - 2\alpha + \varphi)} \tag{54}$$

When the strength in the fibers is fully mobilized ($\xi = -1$), angle 2ψ remains in the range

$$\frac{\pi}{2} - \varphi + \tan^{-1}\left(\frac{0.5\rho\sigma_0}{p\tan\varphi + c}\right) < |2\psi - 2\alpha| \leq \pi \tag{55}$$

and

$$R = F(p,\psi) = -0.5\rho\sigma_0\cos 2(\psi-\alpha) + \sqrt{[(p + 0.5\rho\sigma_0)\sin\varphi + c\cos\varphi]^2 - [0.5\rho\sigma_0\sin 2(\psi-\alpha)]^2} \tag{56}$$

A surface identical to that in Fig. 6 can be obtained through a purely static approach as in the theory of mixtures. This surface is an envelope to the sum of the limit stress in the matrix and stresses at or below failure in reinforcing strips/fibers. Such an approach, however, would be very cumbersome when applied to homogenization of the stress in a composite with short fibers, as presented in the next subsection. The former was considered earlier (de Buhan and Siad, 1989) for the case of a non-cementitious matrix, but the failure surface was presented in a different stress space. A more convenient analytical description for this perfect case was found recently (Michalowski and Zhao, 1995)

No lab test results on composite samples are available to verify the failure criterion derived. Later, in the subsection on implementation, a solution to a boundary value problem (collapse of a vertical slope) is compared to the result from a lab test on a physical model to indicate the rationality of the description proposed.

Short Inclusions (Fibers)

A model of a composite with short inclusions is representative of fiber-reinforced soils. In some applications, such as rolled subgrades of airfields, the preferred orientation of

the fibers is horizontal. If the plane of deformation is any vertical plane, then the failure criterion as presented here can be used to describe the strength of such composite (the effective length of fibers being the average of the fibers' projection on the plane of deformation).

No cohesive bond between the fibers and the matrix is considered, and the load transfer to the fibers has a frictional nature. During plastic deformation of the composite, fibers are expected to slip in the matrix at a low confining pressure, and to fail in tension at large mean stresses. In the latter case the ends of fibers slip to a distance where the yield stress, σ_0, is mobilized in the fibers. Fig. 1(b) presents an expected distribution of shear at the fiber surface and axial stress during deformation of rigid-perfectly plastic fibers in a matrix subjected to the velocity field in eq. (38). Assuming cylindrical fibers with radius r, the length of slip region s (Fig. 1(b)) is

$$s = \frac{r}{2} \frac{\sigma_0}{\sigma_n \tan\varphi_w} \tag{57}$$

where σ_n in the stress normal to the fiber surface and φ_w is the friction angle of the matrix-fiber interface. In order for the tensile collapse of fiber to occur, length s must be smaller than half of the fiber length $l/2$, which occurs when

$$\eta > \frac{1}{2} \frac{\sigma_0}{\sigma_n \tan\varphi_w} \tag{58}$$

where η is the fiber aspect ratio

$$\eta = \frac{l}{2r} \tag{59}$$

We assume here that all fibers have the same aspect ratio η. The energy dissipation rate due to plastic deformation of fibers (yielding) per unit volume of the composite can be calculated now as

$$\dot{D}_1^f = \langle\xi\rangle \rho \sigma_0 \left(1 - \frac{1}{2\eta} \frac{\sigma_0}{\sigma_n \tan\varphi_w}\right) \dot{\varepsilon}_\alpha \tag{60}$$

where $\langle\xi\rangle$ and $\dot{\varepsilon}_\alpha$ are given in eq. (43) and in eq. (49), respectively. The dissipation due

to slip of the fiber ends (per unit volume of the composite) is

$$\dot{D}_2^f = \langle \xi \rangle \rho \sigma_0 \frac{1}{4\eta} \frac{\sigma_0}{\sigma_n \tan\varphi_w} \dot{e}_\alpha \tag{61}$$

Note that no dissipation is accounted for in the compressive regime ($\langle \xi \rangle = 0$). The total energy dissipation rate in fibers per unit volume of the composite now becomes

$$\dot{D}^f = \dot{D}_1^f + \dot{D}_2^f = \langle \xi \rangle \rho \sigma_0 (1 - \frac{1}{4\eta} \frac{\sigma_0}{\sigma_n \tan\varphi_w}) \dot{e}_\alpha \tag{62}$$

When

$$\eta \leq \frac{1}{2} \frac{\sigma_0}{\sigma_n \tan\varphi_w} \tag{63}$$

the fiber energy dissipation occurs in the slip mode only, and it becomes independent of yield point σ_0

$$\dot{D}^f = \dot{D}_2^f = \langle \xi \rangle \rho \eta \sigma_n \tan\varphi_w \dot{e}_\alpha \tag{64}$$

The failure criterion for a frictional matrix reinforced with short fibers can now be obtained following the same procedure as in the preceding section, with the exception that the dissipation rate in the fibers, eq. (42), needs to be replaced with eq. (62) (or eq. (64)). Consequently, the failure condition can be obtained through minimizing function R in eq. (48) where the second term in the numerator is replaced with eq. (62) (or eq. (64)). Notice that when $\eta \to \infty$ eq. (48) is recovered. The influence of the fiber aspect ratio on the macroscopic failure criterion is illustrated in Fig. 7.

While limited laboratory results on random fiber soil reinforcement are available, no experimental data on uni-axially reinforced soils exist that could be presented in terms of a failure surface in the macroscopic stress space. However, in an early work by Yang (1972), one point on the failure surface was obtained for which the major principal stress was perpendicular to the direction of reinforcement. That result was for long reinforcement and it is identical to a particular case of eq. (56) when $2\psi = \pi + 2\alpha$.

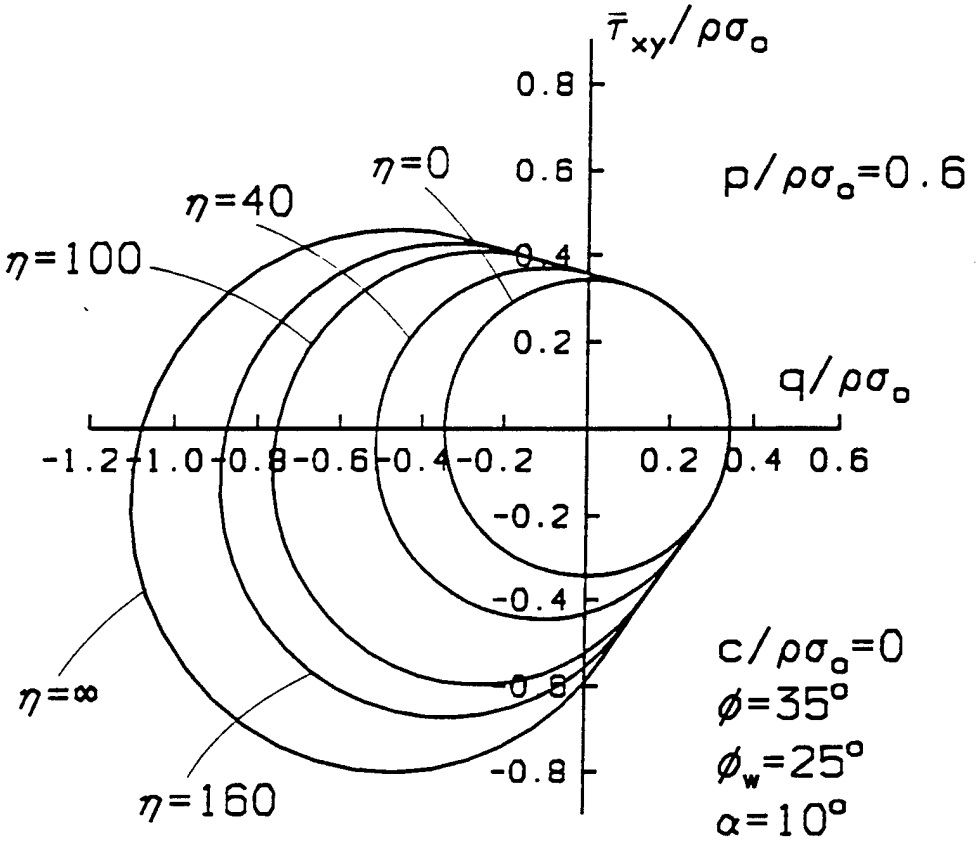

Figure 7. Cross-sections of composite failure surfaces (p = const) for fibers of different aspect ratios.

The length of the fiber slip section (eq. (57)) and the energy dissipation rate due to fibers (eq. (62)) depend on the stress normal to the fiber surface. While the normal stress in the plane of deformation can be represented as a function of the limit macrostress $\bar{\sigma}_{ij}$, distribution of the normal stress along the entire perimeter of the fibers cannot be found, since the resulting failure criterion is independent of the intermediate principal stress. Any attempt at calculation of σ_n then will be approximate. Stress σ_n was taken in calculations here as being equal to the mean of maximum and minimum macrostresses in the plane of deformation (p).

Experimental Tests

An experimental investigation was carried out primarily to determine whether the approach selected for mathematical description of the failure criteria for fiber-reinforced granular materials is reasonable, and, if so, to indicate where the refinement of the suggested failure condition should be pursued.

Material Used

A coarse, poorly-graded sand with d_{50} = 0.89 mm and uniformity coefficient C_u= 1.52 was used in the experiments presented in this section. The specific gravity of the sand was G = 2.65, and minimum and maximum void ratios were 0.56 and 0.89, respectively. Two types of fibers were selected: galvanized or stainless steel (G = 7.85), and polyamide monofilament (G = 1.28). Polyamide is not a material likely to be used as a permanent soil reinforcement (because of its moisture sensitivity and aging/deterioration characteristics), but its availability in a variety of diameters and its mechanical behavior common to other synthetic materials makes it a convenient material to use in tests.

Compaction of the specimens was characterized by the void ratio. In all tests the initial void ratio of prepared specimens was e = 0.66, corresponding to a relative density of I_d = 70% for unreinforced sand. In the definition of the void ratio for reinforced specimens the volume of the fibers is considered part of the skeleton. Relative density is not an appropriate parameter for characterizing fiber-reinforced specimens, since the minimum and maximum void ratios of the composite are very much dependent on the fiber characteristics.

Specimen Preparation

The length of the fibers was approximately 2.5 cm in all tests, and the required aspect ratio was adjusted by selecting an appropriate fiber diameter. Both the height and diameter of the specimens was 9.65 cm. The following procedure of sample preparation was followed in order to achieve uniform distribution of fibers in space and isotropic distribution of fiber orientation in the specimens.

(a) According to the required void ratio (e = 0.66) and fiber concentration by volume (ρ), the corresponding fiber concentration by weight (ρ_w) was calculated as

$$\rho_w = \frac{(1+e)\,G_r\,\rho}{(1+e)(G_r - G_s)\,\rho + G_s} \tag{65}$$

where G_s and G_r are the specific gravity of the sand and fibers, respectively. The weight of the dry sand (W_s) and the fibers (W_r) was then calculated from

$$W_s = \frac{V}{1+e}\,\frac{(1-\rho_w)\,G_s\,G_r}{(1-\rho_w)\,G_r + \rho_w G_s}\,\gamma_w \tag{66}$$

and

$$W_r = \frac{V}{1+e}\,\frac{\rho_w\,G_s\,G_r}{(1-\rho_w)\,G_r + \rho_w G_s}\,\gamma_w \tag{67}$$

where V is the required volume of the mixture (volume of the specimen), and γ_w is the specific weight of water.

(b) The weight of the sand and fibers was divided into five equal portions used later to produce five layers of the specimen.

(c) A 6×6 cm square grid of steel wires (with 3 cm spacing between the wires) was placed at the bottom of the mold.

(d) A small amount of sand was dropped through a funnel into the mold to cover the grid evenly. Each of the five portions (b) was divided into three parts. One-third of the fibers for the first layer was slowly dropped into the mold. Care was taken to produce an even distribution of the fibers on the sand surface. Then, one-third of the sand for that layer was dropped through a funnel with a low mass rate

(fall-height = 40 cm). Following the same procedure, the remaining two parts of the first layer of the specimen were produced.

(e) The grid was slowly pulled (manually) through the first one-fifth portion of the specimen (first layer). The grid was left on the surface of that layer.

(f) The distance from a reference point on the mold to the top of the layer was measured to ensure that the target void ratio was achieved. If the prepared mixture was too loose, the mixture was gently vibrated until the proper density was reached. If the mixture was significantly too loose (or if it was too dense), the entire specimen was recreated.

(g) For the subsequent 4 layers of the specimen, steps (d)-(f) were repeated. The possible influence of vibration on the layers below, when preparing the subsequent layers, was ignored.

The same preparation procedure was followed for unreinforced specimens (except there were no fibers). The grid used in steps (c) and (e) was intended to create an isotropic distribution of fiber orientation. When placing the sand and fiber mixture directly into the mold, the fibers were assuming an anisotropic orientation with the horizontal being the preferred direction. Therefore, the sand and fiber mixture was placed over a grid of wires and the grid was pulled slowly through the mixture, altering the orientation of a portion of fibers. This technique was developed to assure an approximately uniform distribution of fiber orientation (macroscopically isotropic specimens). The distribution of fiber orientation was estimated to be isotropic by visual inspection, and the authors recognize the approximate quality of the conclusion.

Results

Series of triaxial tests were conducted. The fiber concentration, aspect ratio, diameter of fibers and the range of confining pressure for some of the series are given in Table 1. The typical confining pressures for one series were: 50, 100, 200, 300, 400 and 600 kN/m^2. The results of the tests are presented in Figs. 8 through 11. More tests which were performed as part of this research are reported in the Appendix.

The addition of steel fibers to sand led to an increase in the peak shear stress of about 20% (ρ = 1.25%, η = 40) for samples tested under a confining pressure of 100 to 600 kN/m^2 [Fig. 8 (a)]; this relative increase was larger at a very low confining pressure (50 kN/m^2). The samples exhibited a typical compaction effect [Fig. 8(b), ε_v = volumetric strain] at small axial strains ε_1, and dilation at larger strains. The

presence of fibers inhibited the dilation effect to a certain degree. The increase in the content of steel fibers (ρ) leads to a clear increase in the peak shear stress [Fig. 9(a)], and, also, it leads to an increase in the stiffness of the composite prior to reaching failure. An increase in the aspect ratio of the fibers also contributes to a significant increase in the peak shear stress [Fig. 9(b)].

Table 1. Typical series of specimens tested (fiber-reinforced composite with coarse matrix).

Fiber material	Fiber concentration ρ (%)	Aspect ratio η	Fiber diameter $2r$ (mm)	Range of confining pressure σ_3 (kN/m^2)
(1)	(2)	(3)	(4)	(5)
no fibers	0	-	-	50 - 600
steel	0.41	40	0.64	100 - 600
steel	1.25	40	0.64	50 - 600
steel	0.5	85	0.3	50 - 600
polyamide	0.5	85	0.3	50 - 600
polyamide	1.25	85	0.3	400
polyamide	0.5	180	0.14	400

Polyamide fibers produced a significant increase in the peak shear stress [Fig. 10(a)] for large confining pressures, but the effect is associated with a considerable loss of stiffness prior to failure and a substantial increase of strain-to-failure. At a confining pressure of 100 kN/m^2, however, no increase of the peak shear stress (with respect to the granular matrix alone) was recorded.

Addition of the polyamide fibers to the soil inhibits the dilatancy, and the effect is more pronounced for low confining pressures [Fig. 10(b)]. An increase in the fiber content, while the aspect ratio is kept constant, leads to a very significant increase in the peak shear stress, a noticeable decrease in stiffness, and an increase of the strain-to-failure [Fig. 11(a)]. An increase in the aspect ratio of polyamide fibers leads to similar effects [Fig. 11(b)].

An interesting effect is presented in Fig. 12 where the composite (with an amount of fiber reinforcement larger than that in Figs. 8-11) does not fail: the stress-strain curve reaches a point of inflection at rather large strain, and the failure stress increases beyond that point. This occurs because of the structural changes in the specimen due to large

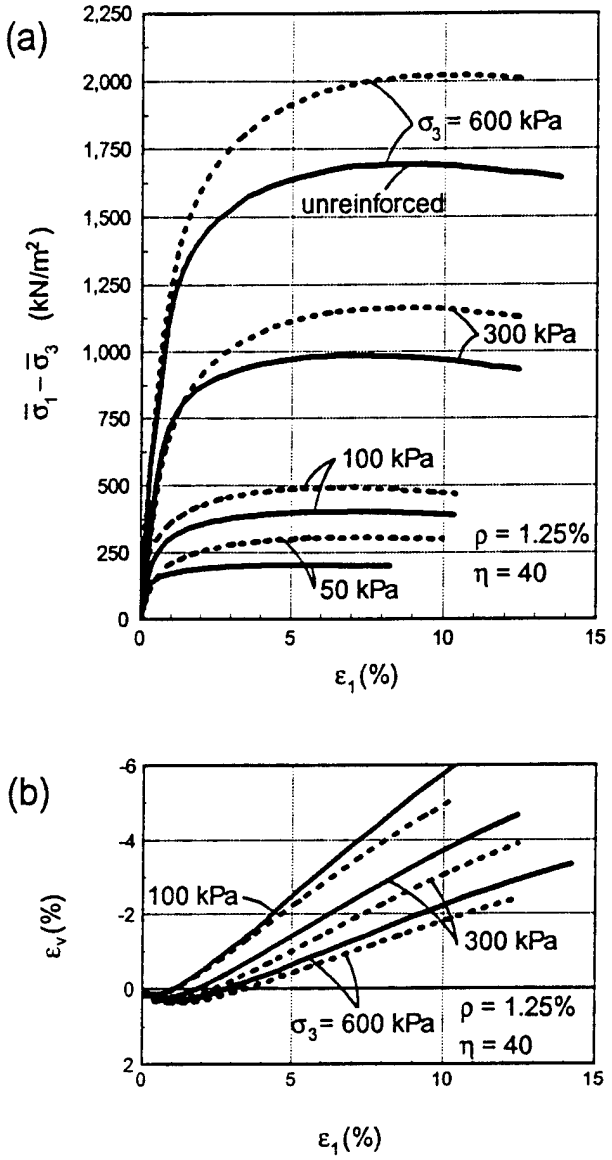

Figure 8. Triaxial compression tests on sand reinforced with steel fibers: (a) Stress-strain relation for different confining pressures; (b) Volumetric strain.

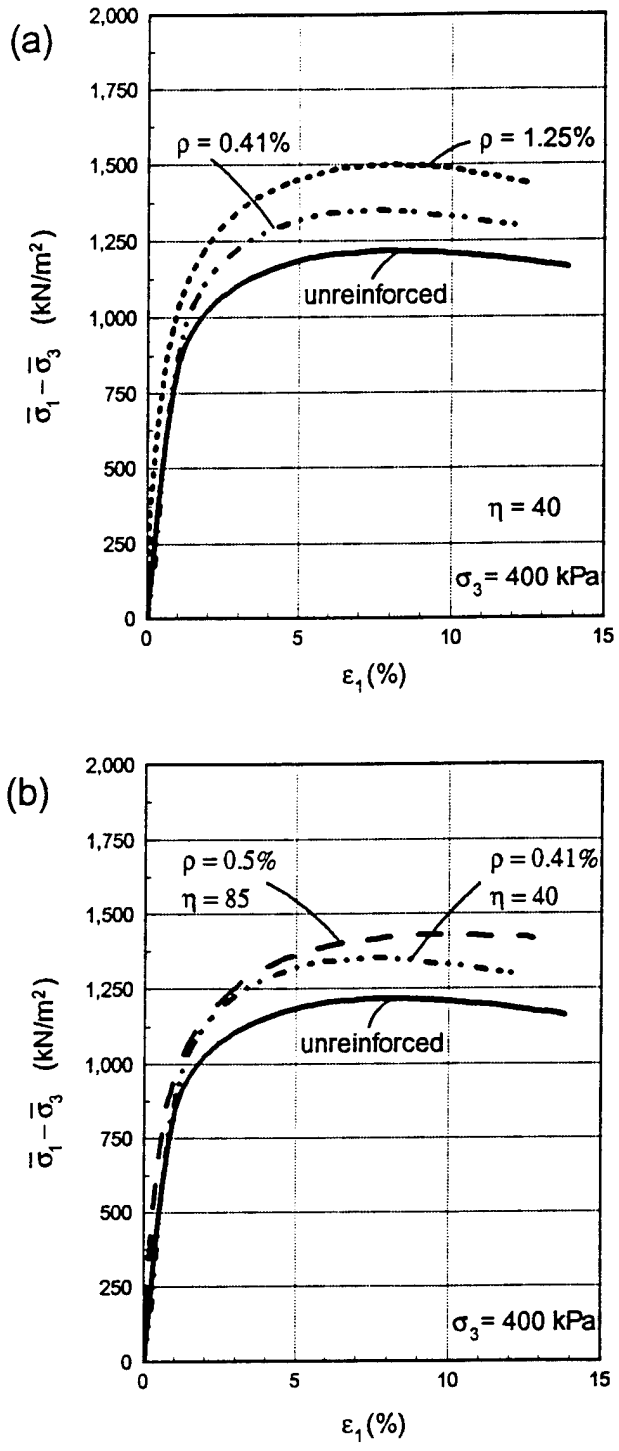

Figure 9. Stress-strain behavior of steel fiber-reinforced sand: (a) Influence of fiber content; (b) Effect of fiber aspect ratio.

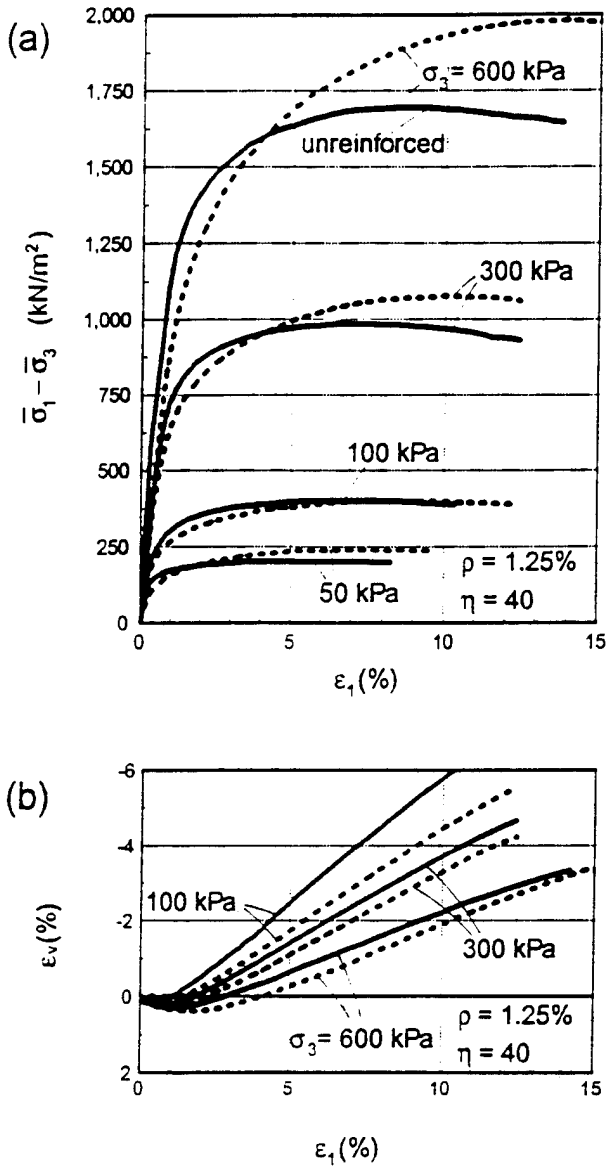

Figure 10. Triaxial compression tests on sand reinforced with polyamide fibers: (a) Stress-strain relation for different confining pressures; (b) Volumetric strain.

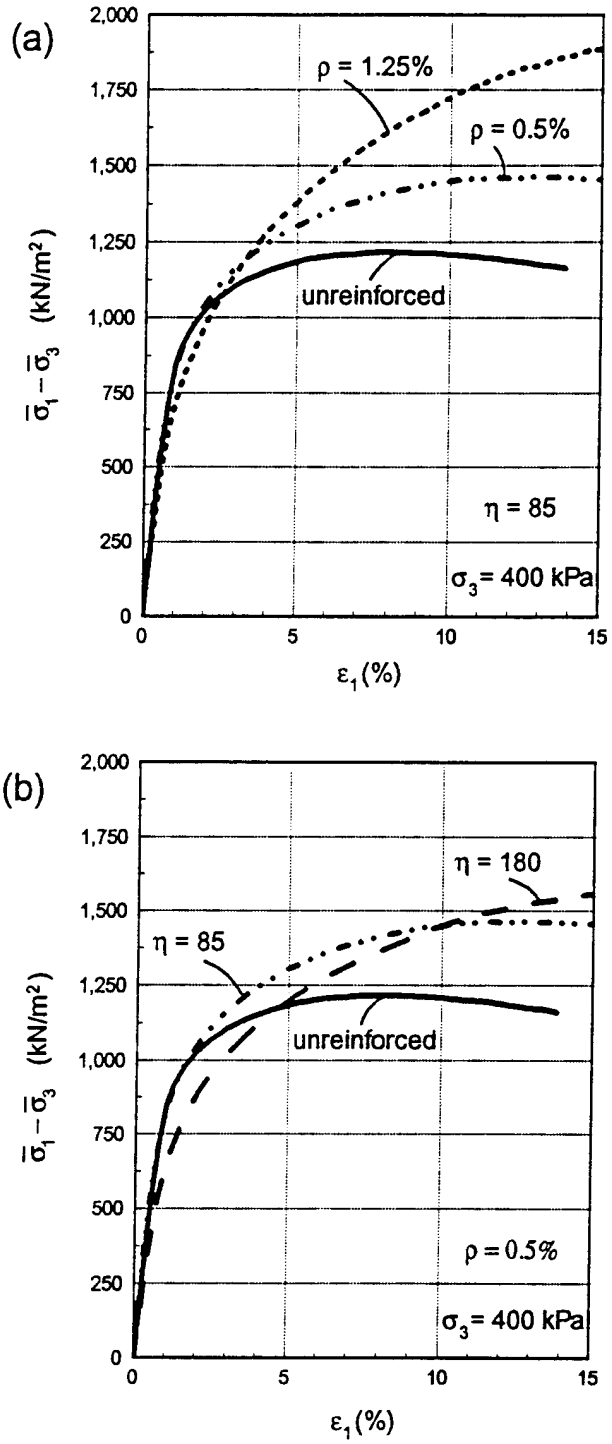

Figure 11. Stress-strain behavior of polyamide fiber-reinforced sand: (a) Influence of fiber content; (b) Effect of fiber aspect ratio.

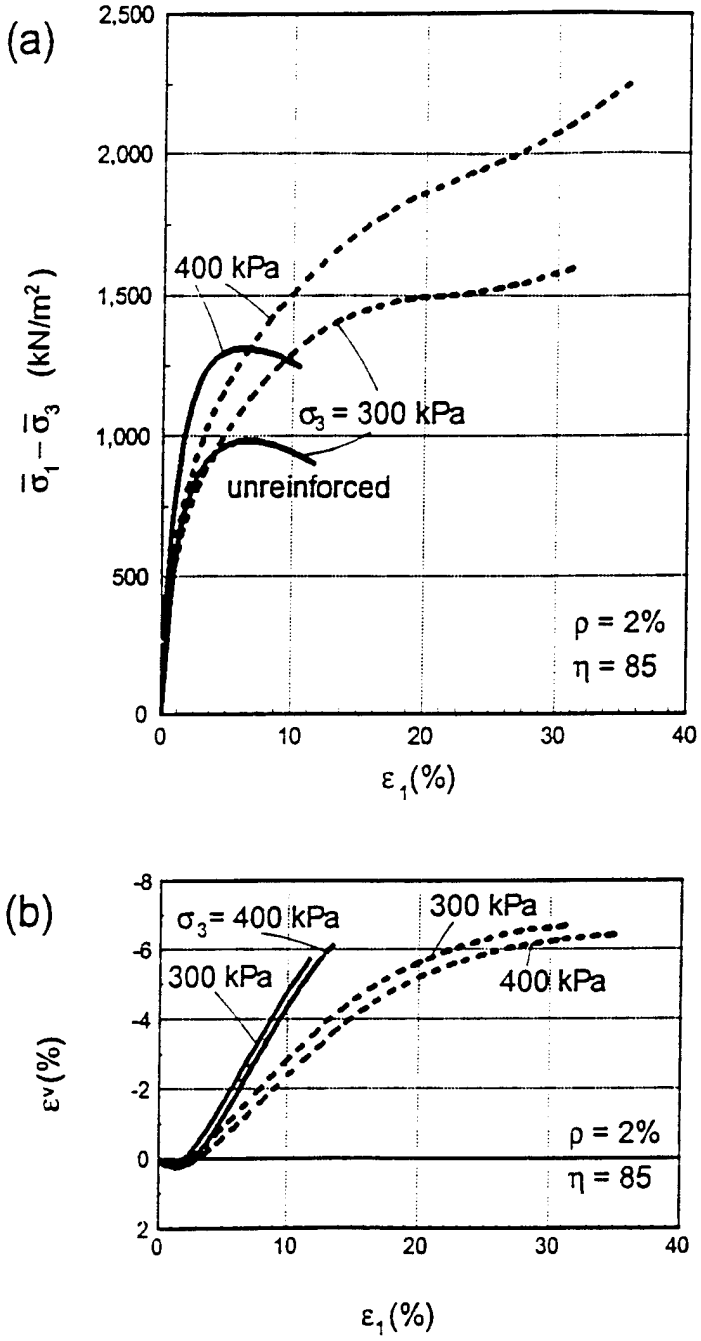

Figure 12. Triaxial compression tests on fine sand reinforced with polyamide fibers: (a) Stress-strain curves with anisotropic hardening effect, and (b) Volumetric strain.

strains. The fibers, originally with random orientation, start to exhibit preferred orientation. The macroscopic properties become therefore anisotropic, causing the kinematic (or anisotropic) hardening effect. A full analysis of this "induced anisotropy" effect and an inclusion of anisotropy in the failure criteria for fiber-reinforced granular composites will be proposed in a request for continuation of this research.

Discussion of the Experiments and Theoretical Predictions

A one-to-one height-to-diameter ratio of the specimens led to failure where no visible localization of strain was present. Also, extra care taken to minimize the effect of friction at the bases of specimens allows one to assert that the macroscopic stress in the composite specimens was close to uniform, and the measured deviatoric stress at failure can be identified with the failure stress of the composite material (macroscopic failure stress state). These stresses, therefore, can be compared directly to those predicted by the suggested theory.

Using different deformation modes in the theoretical derivation (plane strain) and in the experiments (axisymmetrical kinematics) may be disputed. The matrix failure criterion used (Mohr-Coulomb) is independent of the intermediate principle stress, and the theoretical result is not affected by whether the matrix deformation is plain or axisymmetrical. However, the particular deformation mode used in the homogenization process does affect the theoretical result through the fiber component, when only fibers in the tensile regime are considered to contribute to the composite strength. This is because the volumetric strain rate associated with fibers in tension is not invariant, only the total volumetric strain-rate is. As a result of further theoretical considerations, this effect appeared to be small (negligible).

While the influence of the mean principal stress on the granular matrix strength is not contested (see, for instance, Lade 1977), the model presented is a reasonable approximation of the true composite behavior. To reduce the influence of the granular matrix approximation (Mohr-Coulomb criterion) in the theory-experiment comparison, the internal friction angle of the matrix used for theoretical prediction was determined from the axisymmetrical (triaxial compression) tests, and the composite specimens were also tested under axisymmetrical conditions.

No ruptured fibers were found in the specimens upon inspection after the tests. However, for polyamide fibers, some permanent kinking and local damage was noticed.

(a)

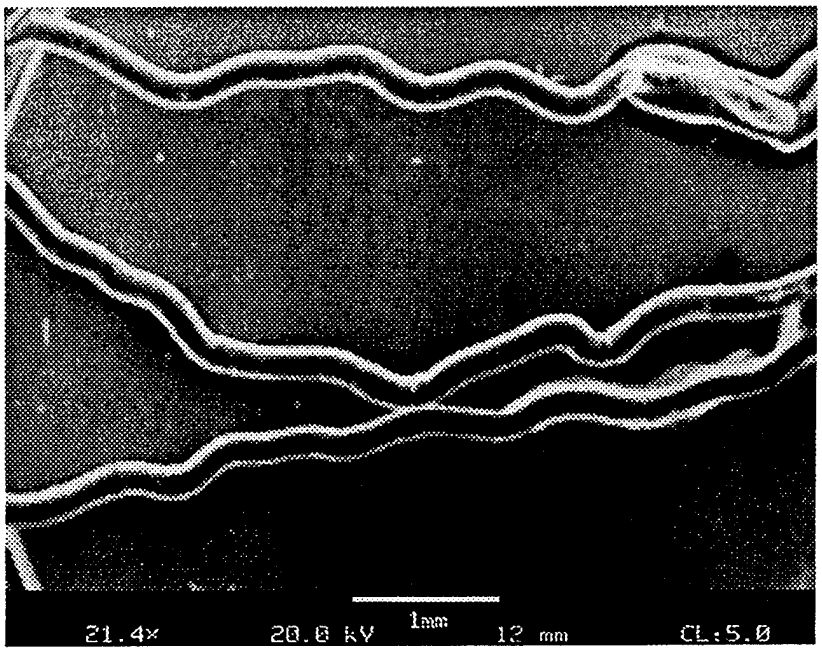

(b)

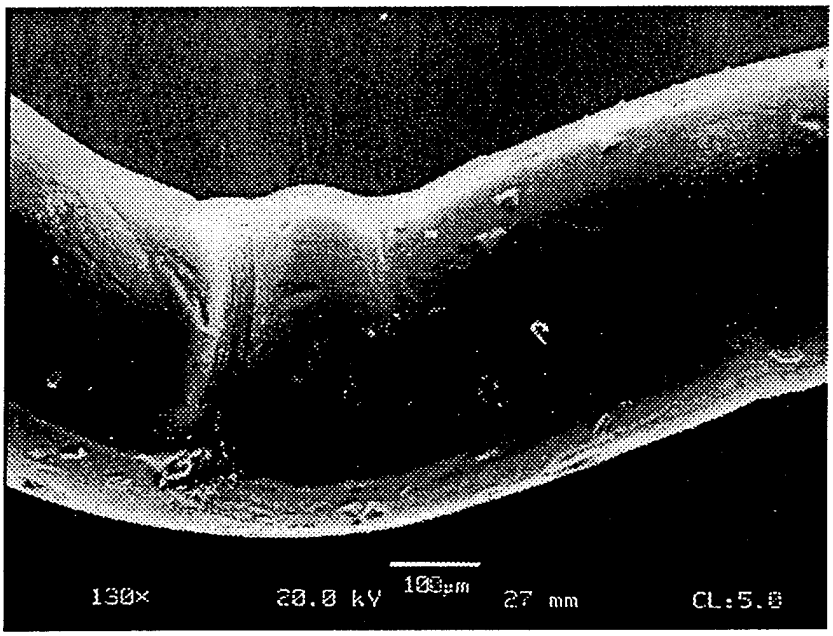

Figure 13. Polyamide fibers after a test; (Scanning Electron Microscope); (a) kinking, (b) irreversible buckling of a single fiber.

(a)

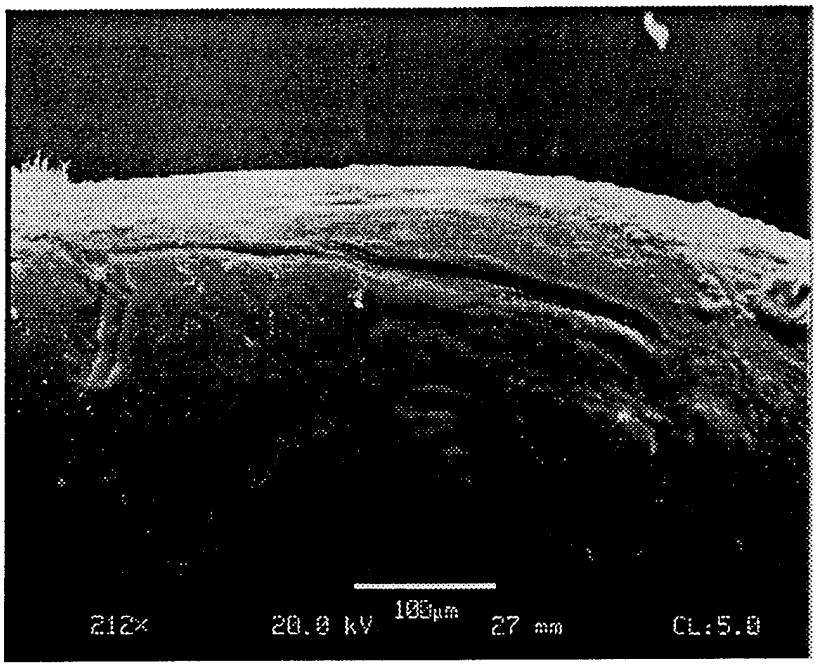

(b)

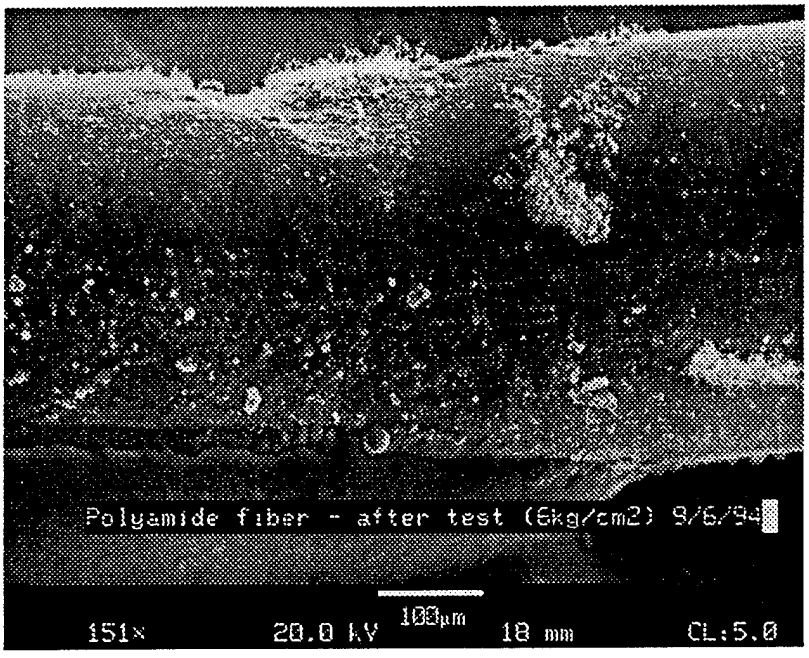

Figure 14. Polyamide fibers after a test, local damage (SEM); (a) ploughing, (b) gouging.

Permanent kinking and plastic buckling of polyamide fibers recovered after a test are shown in Fig. 13. Local damage to fibers is presented in Fig. 14.

The prediction of the composite failure stress for both steel and polyamide fibers is made in Figs. 15-17 using eq. (35). The major principal stress at failure, $\bar{\sigma}_1$, is shown as a function of the confining stress, $\bar{\sigma}_3$ ($\bar{\sigma}_1 = p + R$, $\bar{\sigma}_3 = p - R$). The experimental results came from tests on composite specimens with $\rho = 0.0125$ (1.25%) and $\eta = 40$ (steel fibers), and $\rho = 0.005$ (0.5%) and $\eta = 85$ (polyamide fibers). The internal friction angle for the granular matrix (determined from drained triaxial compression tests) was in the range of 42° to 35.9° for specimens tested under confining pressures from 100 to 600 kN/m^2. This is why the predicted failure criteria in Figs. 15-17 are not straight lines.

The angle of fiber/soil interface friction was determined from pull-out experiments in a modified direct shear apparatus (for steel fibers), and from a direct shear of soil over a polyamide sheet, also in a direct shear device. The friction angle is dependent on the normal pressure at the fiber interface, and was found for steel to be in the range of 24.6° to 19.5°, and for polyamide in the range of 17.9° to 14.7° (normal interface stress changing from approximately 160 to 1600 kN/m^2). In interpretation of the steel fiber pull-out tests the active stress state in the soil was assumed, inhomogeneities in the mobilization of friction along the fiber were ignored, and the peak value of the pull-out force was taken to calculate the interface friction angle (reasonable for short inclusions such as fibers).

The increase in the deviatoric failure stress for fiber-reinforced specimens with respect to the sand tested under identical confining pressure was roughly 20%. This relative increase is smaller when presented in terms of the in-plane invariants R and p since an increase in the deviatoric stress (while confining pressure is constant) also causes an increase in the mean maximum-minimum stress p. While steel fibers with aspect ratio $\eta = 40$ may not seem to be a very effective reinforcement, the theoretical prediction follows the experimental results very closely (Fig. 15). Table 2 presents the data including the internal friction angle for the granular matrix, φ, and the interface friction angle, φ_w. The friction angle (secant) was calculated from sand samples tested under a given (constant) confining pressure (σ_3), and it is related in Table 2 to composite mean stress p for which the confining pressure was the same [*i.e.*, φ in column 2 was not calculated from data in columns (1) and (6)]. The internal friction angle for $p = 203.5$ kN/m^2 was extrapolated. Since tests were performed under a constant confining pressure, mean stress p at failure for reinforced and non-reinforced specimens varied.

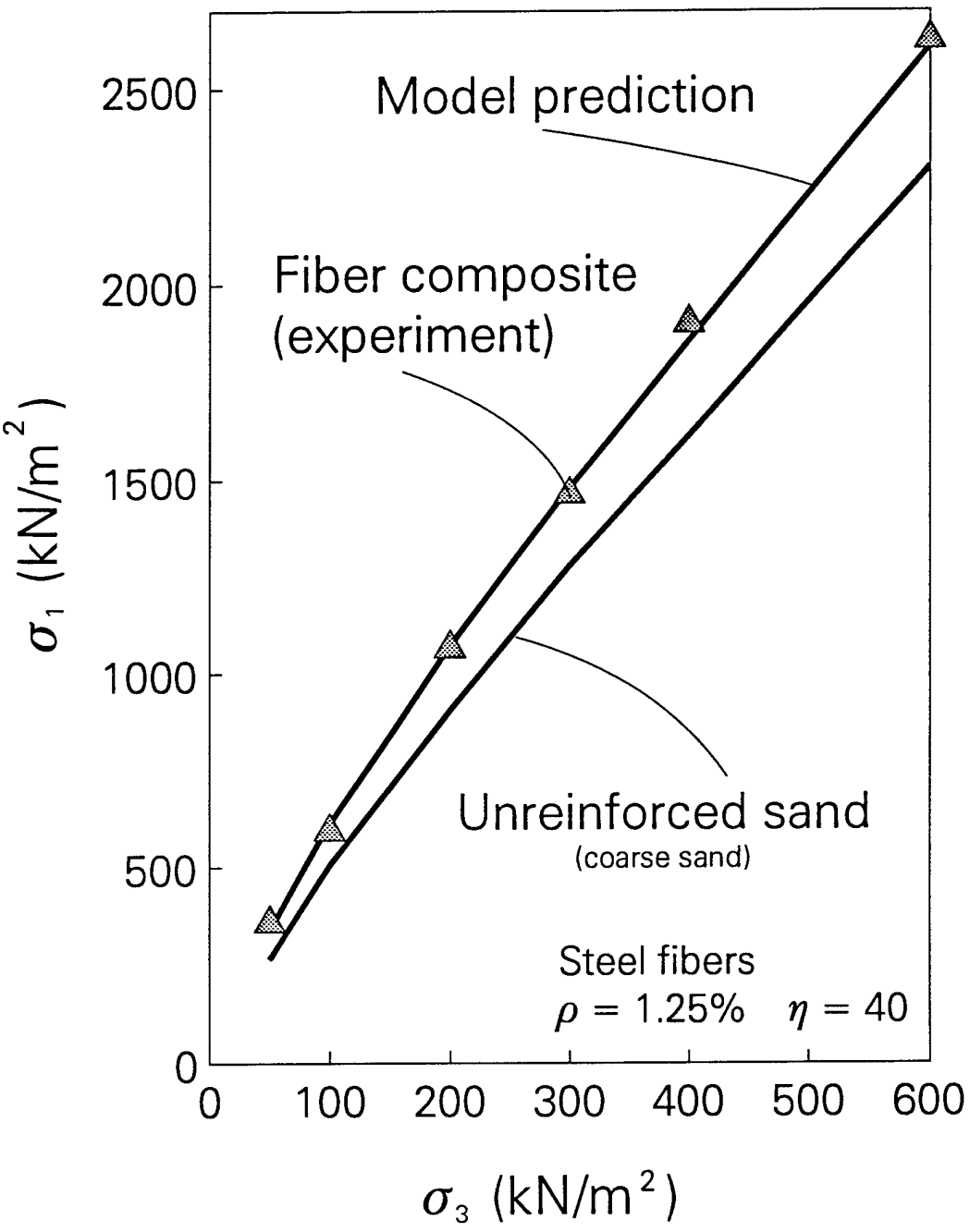

Figure 15. Failure criterion for coarse sand reinforced with steel fibers. Comparison of theoretical prediction to triaxial test results.

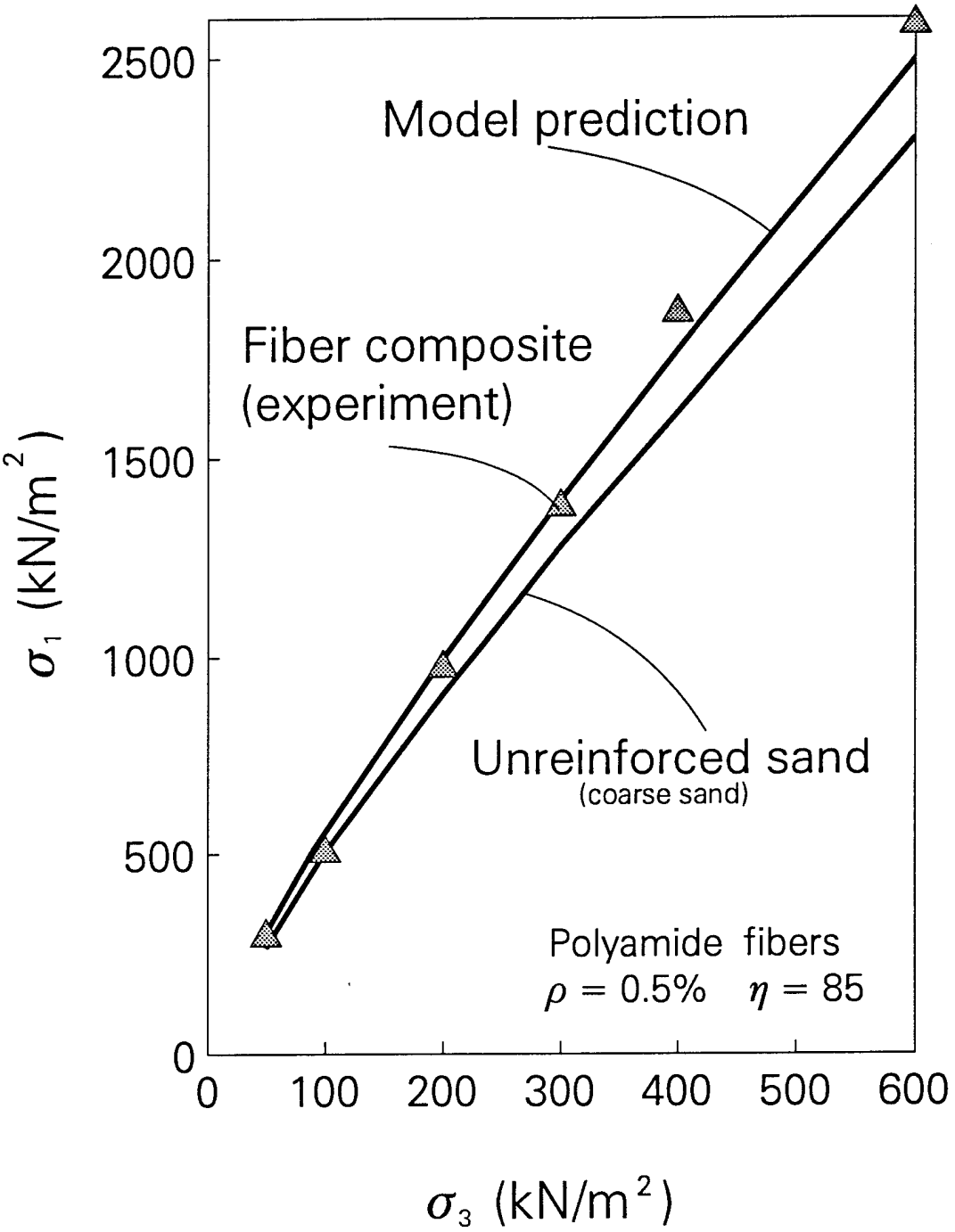

Figure 16. Failure criterion for coarse sand reinforced with polyamide fibers. Comparison of theoretical prediction to triaxial test results.

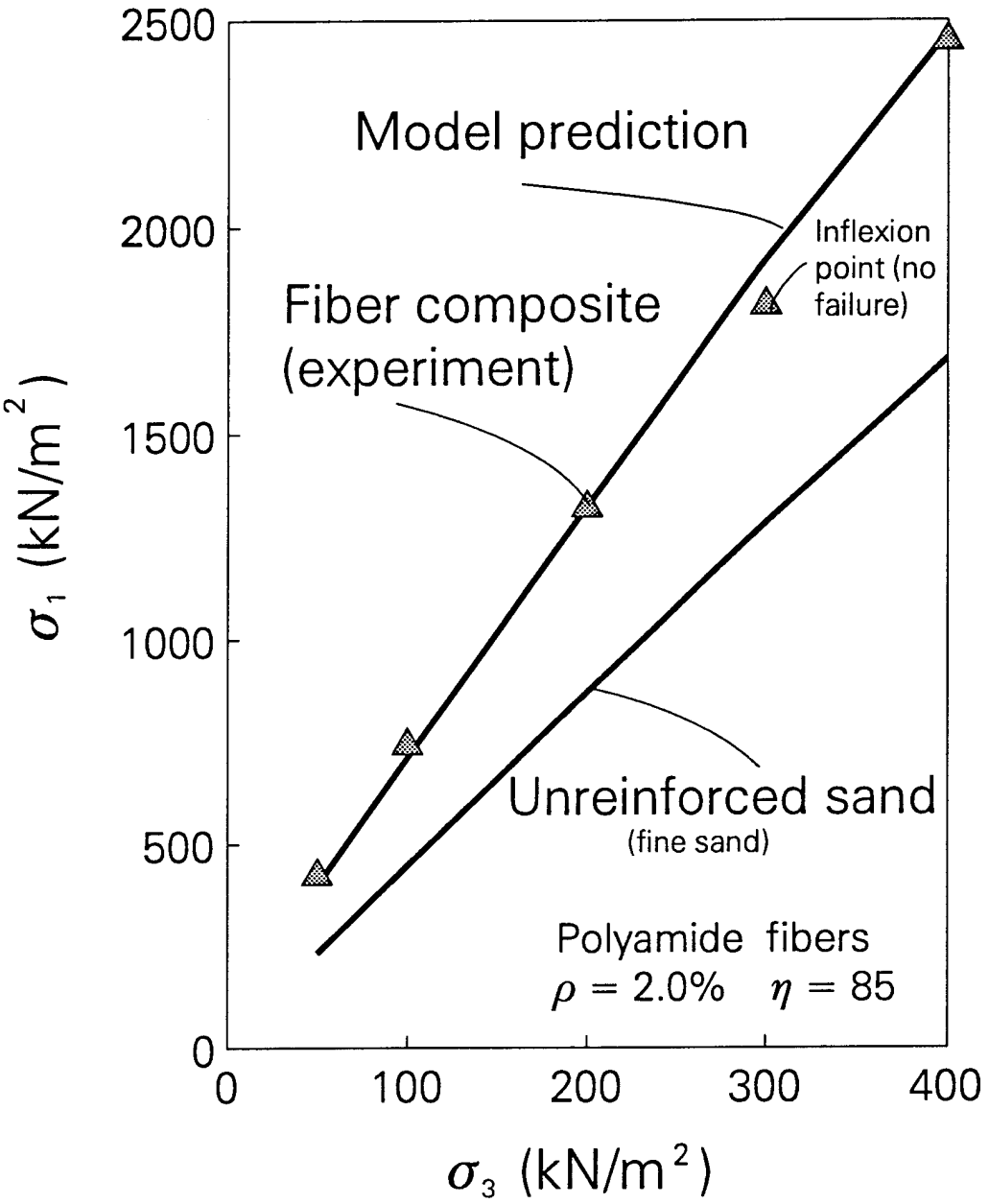

Figure 17. Failure criterion for fine sand reinforced with polyamide fibers. Comparison of theoretical prediction to triaxial test results.

The magnitude of R for the granular matrix alone, column 6 in Table 2, was therefore interpolated to relate to p in column 1.

Table 2. Experimental data and predictions of the failure stress state for a steel fiber-reinforced coarse sand; $\rho = 1.25\%$, $\eta = 40$.

$(\bar{\sigma}_x + \bar{\sigma}_y)/2$ p (kN/m^2) (1)	Int. friction angle φ (2)	Composite (experiment) R (kN/m^2) (3)	Composite (prediction) R (kN/m^2) (4)	Sand R (kN/m^2) (5)
203.6	43°	153.6	147.9	136.3
345.9	42°	245.9	246.7	228.2
633.1	39.7°	433.1	431.5	399.7
881.8	38.3°	581.8	583.5	540.7
1150.8	37.1°	750.8	741.6	686.4
1611.9	35.9°	1011.9	1010.5	936.8

Figure 16 presents predictions for sand reinforced with polyamide fibers. There is a tendency to underestimate the actual influence of fiber reinforcement for large mean stresses. In the theoretical model the fibers were assumed to be straight inclusions, and a possible source of discrepancies may be in ignoring any effects stemming from local damage (gouging, ploughing) and "serpentine" alignment of fibers (which enhances the soil-fiber interaction). These effects are more pronounced for coarse sand and soft fibers, such as polyamide. The prediction is very accurate, however, for polyamide fibers and fine granular matrix (Fig. 17).

It is fair to conclude that the suggested model is consistent with experimental evidence, and the results for applications are promising. A substantial improvement (increase in failure stress) can be expected for inclusions with large aspect ratios and volumetric concentration of 2% (Fig. 17).

Implementation

Eamples of application of the derived failure criterion are presented below. Solutions of boundary value problems were attempted for both random fiber-reinforced soil and unidirectionally reinforced composite (with very long fibers, $\eta \to \infty$, since the closed-form criterion was derived for this case). The influence of the aspect ratio (η) on

the bearing capacity in the first example can be asserted, to a certain extent, from Fig. 7, where the effectiveness of reinforcement as a function of η is illustrated.

A flat smooth punch indentation of a rigid-plastic half-space whose failure criterion is described by the surface in Fig. 6 (see also eqs. (51)-(56)) is considered. The limit load is found using the slip-line method. Eq. (50), along with the set of differential equilibrium equations, leads to a set of two hyperbolic-type partial differential equations which can be solved using the method of characteristics. The equations of characteristics can be expressed as (Booker and Davis, 1972)

$$\begin{aligned} \frac{dy}{dx} &= \tan(\psi - m - \nu), \qquad s_1\text{-characteristic} \\ \frac{dy}{dx} &= \tan(\psi - m + \nu), \qquad s_2\text{-characteristic} \end{aligned} \tag{68}$$

and the stress relations along the characteristics are

$$\begin{aligned} \sin[2(m-\nu)]\frac{\partial p}{\partial s_1} + 2F\frac{\partial \psi}{\partial s_1} + \gamma\cos(2m)\left[\cos(2\nu)\frac{\partial x}{\partial s_1} - \sin(2\nu)\frac{\partial y}{\partial s_1}\right] &= 0, \quad s_1 \\ \sin[2(m+\nu)]\frac{\partial p}{\partial s_2} + 2F\frac{\partial \psi}{\partial s_2} + \gamma\cos(2m)\left[\cos(2\nu)\frac{\partial x}{\partial s_2} + \sin(2\nu)\frac{\partial y}{\partial s_2}\right] &= 0, \quad s_2 \end{aligned} \tag{69}$$

and

$$\tan(2m) = \frac{1}{2F}\frac{\partial F}{\partial \psi}, \qquad \cos(2\nu) = \cos(2m)\frac{\partial F}{\partial p} \tag{70}$$

where γ is the unit weight of the soil. The gravity acceleration is assumed here to be directed opposite to co-ordinate y.

Solutions to two boundary value problems are given below. The application in Fig. 18 is similar to the smooth punch-indentation problem considered by Hill (1950), with the exception that the half-space is now pressure-dependent and anisotropic. The failure criterion is represented by equations (51)-(56). Such a composite is representative

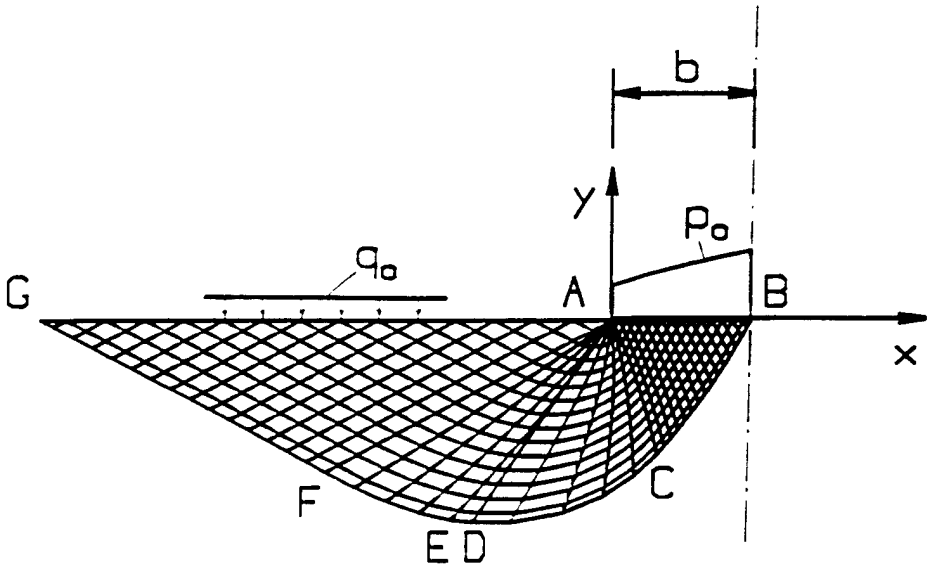

Figure 18. Stress characteristics field for a smooth punch indentation into an anisotropic half-space (simulating soil reinforced in horizontal direction).

of a soil subgrade reinforced with horizontal reinforcement strips or blankets of geosynthetic material. The matrix (fill) material is cohesionless with internal friction angle $\varphi = 35°$. The geometry of the punch and the amount of reinforcement is characterized by coefficient $\gamma b/\rho\sigma_o = 0.4$ (γ = specific weight, b = punch half-width). The stress boundary condition is given along AG (Fig. 18) as a vertical pressure, $q_o/\gamma b = 0.25$, and the direction of the limit pressure along AB is vertical (smooth punch).

Along AG we have $\psi = 0$, and the force in the reinforcement is not mobilized in the entire triangle AFG. The failure criterion is described here by the classical Mohr-Coulomb failure function, eq. (52), and the Cauchy boundary value problem in AFG reduces to the isotropic case as in Sokolovskii (1965). Fan of characteristics AFC represents the slip-line solution for a boundary value problem with a singular point at A. The case where no force is mobilized in the reinforcement extends from characteristic AF to AE. At point A of characteristic AE angle $2\psi = \pi/2 - \varphi$. Beyond characteristic AE a tensile force is mobilized in the reinforcement, but the reinforcement stress does not reach yield point σ_0 (see eqs. (53) and (54)).

Using eqs. (70) and (54), expressions for $2m$ and 2ν are found, and, after substituting these into eq. (68), the equations of characteristics become

$$\frac{dy}{dx} = \tan\alpha, \qquad s_1 - \text{characteristic}$$

$$\frac{dy}{dx} = \tan\left(\frac{\pi}{2} - \varphi + \alpha\right), \qquad s_2 - \text{characteristic} \tag{71}$$

where α is the angle of inclination of the reinforcing inclusions to the x-axis (inclination angle of the axis of anisotropy). This comes as a surprise, since the inclination of the characteristic lines is now independent of the principal stress directions. Further increase in angle ψ at singular point A does not generate more characteristics in fan AFC until angle ψ reaches the range expressed in eq. (55). The latter is indicative of the reinforcement reaching yield point σ_0, which occurs in the region to the right of line AE; line AE is a stress discontinuity. This is quite different from slip-line fields for isotropic materials where a stress characteristic cannot become a stress discontinuity. This peculiar type of discontinuity was first reported by Rice (1973) for a pressure-independent (non-frictional) material. Such discontinuities are always associated with plane segments of failure criterion in the space presented in Fig. 6.

The stress state in the plastic region to the right of stress discontinuity AE satisfies eq. (56) (yield point reached in the reinforcement). The average limit pressure along boundary AB is $\bar{p}_o/\gamma b$ = 39.93, a 2.03 times increase above the limit pressure over an unreinforced half-space.

The second example of application is shown in Fig. 19. This is a simulation of a collapse of a 3-meter-tall vertical slope built of cohesive soil reinforced with 12 horizontal reinforcing layers. A physical model of the wall was laboratory tested, and the details can be found in Wu (1992). The material parameters (based on data reported in Wu, 1992) are: cohesion c = 82.7 kN/m^2, internal friction angle φ = 12.6°, and unit weight γ = 18.9 kN/m^3. The reinforced soil mass is homogenized here, and its failure condition is described by equations (51)-(56). There were 12 layers of geosynthetic reinforcement used with strength estimated from tests as 6 kN/m which, for a wall height of 3m, yields a macroscopic strength of $\rho\sigma_o$ = 24 kN/m^2. The wall was loaded using air bags, and a pressure of 227 kN/m^2 was regarded as the failure load since it was associated with a disproportionately large increment of displacement.

The stress state at failure and the limit load is calculated here using the method of characteristics. The slip-line network is shown in Fig. 19. Zero traction is given at boundary AD, and the collapse load along AB is vertical. The tensile stress in the reinforcing inclusions is now mobilized everywhere in the composite mass, and the failure criterion is expressed by eq. (56). The average collapse load at AB was calculated to be $\bar{p}_0$ = 216 kN/m^2, while the model of the slope collapsed at $\bar{p}_0$ = 227 kN/m^2. While such coincidence of results cannot be regarded as verification of the failure criterion derived, it indicates that the stability analyses based on such criterion are reasonable. In an associated velocity field discontinuities could occur along slip-lines. Shear bands examined at the side wall of the test tank, however, do not coincide with characteristics from the theoretical solution. This is probably caused by the small depth-to-height ratio of the wall backfill in the experiment, which did not allow for a full development of the field similar to that in Fig. 19.

It needs to be mentioned that the model wall was loaded with air bags, and the structure used to brace the air bags probably restricted the freedom of horizontal displacement of the top boundary. A concentrated load cannot be included in the slip line solution, but this support condition could be simulated approximately with a distributed horizontal component of the load on boundary AB. The limit load calculated then would have increased. In such a case, point A would become a singular point in

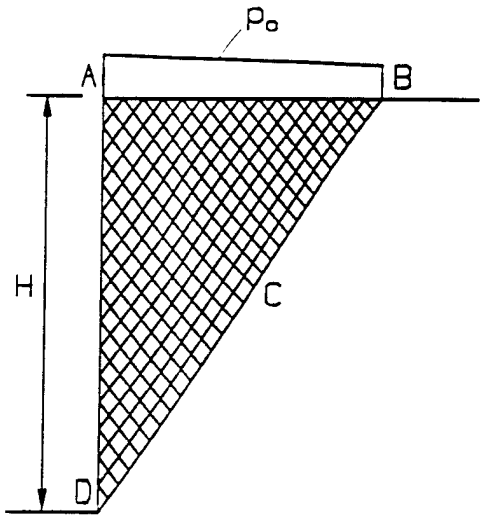

Figure 19. Stress characteristics field for an anisotropic vertical slope (simulation of a reinforced soil slope).

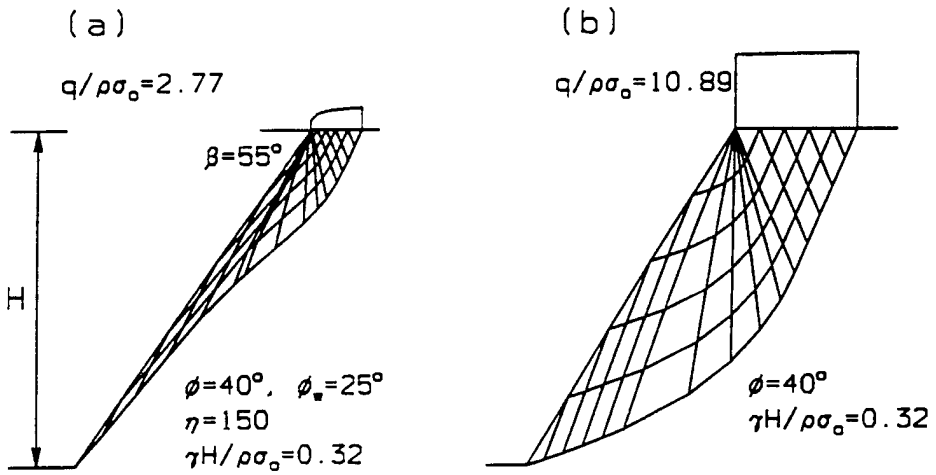

Figure 20. Slip-line fields for slope limit load calculations: (a) fiber reinforcement; (b) unidirectional (horizontal) reinforcement.

the stress field, giving rise to a fan of slip lines between the Cauchy stress region in triangle ADC and the mixed stress boundary value problem in ABC.

The quantity of the horizontal force at the support was not measured in the experiment. Without an accurate measurement of the horizontal load and without including it in the boundary condition, one cannot make an assessment as to whether the vertical component of the failure load calculated would become even closer to the actual collapse load or would overestimate it.

Another example of implementation, a slope stability problem, is shown in Fig. 20. The slip-line fields for a slope of inclination angle of 55° and soil randomly reinforced with fibers (isotropic composite), with internal friction angle of 40° is shown in Fig. 20(a). The slip-line field for a unidirectionally reinforced soil (anisotropic composite) is presented in Fig. 20(b). The aspect ratio of the fibers is 150, interfacial friction angle $\varphi_w = 25°$, and the slope is characterized by dimensionless parameter $\gamma H/\rho\sigma_o = 0.32$ (γ = unit weight of soil, H = slope height). The average limit load was calculated, and it is given in dimensionless fashion: for a fiber-reinforced slope $\bar{q}/\rho\sigma_o = 2.77$, and for horizontal reinforcement $\bar{q}/\rho\sigma_o = 10.89$.

FINAL REMARKS

This research focused on the limit behavior of granular composites reinforced with fibers. In particular, failure criteria for such composites for both a macroscopically isotropic case (random fiber reinforcement) and a composite with a preferred direction of fibers have been derived. An experimental program was also carried out to validate the findings of the theoretical considerations.

An energy-based homogenization technique was found to be a viable method for describing the macroscopic (average) stress at failure for fiber-reinforced granular composites. Two composites were considered: one was uniform with respect to both the spatial distribution of fibers and the distribution of fiber orientation, and the second one had a uniform distribution of fibers in space, but a preferred direction of orientation. Consequently, an isotropic yield condition was obtained for the former, and an anisotropic one for the latter. In both cases piece-wise and closed-form failure criteria were obtained in terms of the macroscopic (average) stress-state. Since the granular matrix was described by the Mohr-Coulomb failure function, the limit condition for the

composite is independent of the mean principal stress.

The failure criterion for the randomly fiber-reinforced soil (isotropic case) consists of two segments: the first one describes failure of the composite due to fiber slip, and the second one is associated with the tensile rupture (or plastic flow) of fibers. However, the transition from one mode to another is continuous and smooth (continuous derivative).

The failure criterion for the composite reinforced in one preferred direction consists of four segments: one which includes the strength of the matrix only (with all reinforcement under compression) and is represented in the macroscopic stress space as a segment of a cone, a segment of a larger cone which includes the strength of the granular matrix and the fibers under tension, and two plane segments, tangent to the two cones, which are associated with the transition of the stress in the reinforcement from compression to maximum (limit) tension.

The following parameters are needed to predict theoretically the failure stress using the proposed criteria: volumetric fiber concentration ρ, fiber aspect ratio η, fiber yield point σ_0, soil/fiber interface friction angle φ_w, the internal friction angle of the granular matrix, φ, and, for the unidirectionally reinforced composite, the angle of inclination of the reinforcement. For a pure fiber slip failure mode, the failure criterion is independent of the fiber yield stress (although σ_0 was used to present the results in a dimensionless fashion in Figs. 3 and 6).

For the derived failure criteria to be applicable, the fiber concentration needs to be low enough so that the interaction between fibers can be neglected. This is a common limitation of self-consistent schemes of homogenization. The diameter of the inclusions (fibers) is considered to be at least an order of magnitude larger than the diameter of the grains in the matrix, and the dry friction law is considered applicable on the soil-fiber interface. The aspect ratio of the inclusions is at least of the order of 10^1 to 10^2, and spacing (for the unidirectionally reinforced composite) is of at least one order of magnitude higher than the inclusions' thickness/diameter. Under such circumstances one can expect that, given sufficient confining stresses, a tensile force can be induced in longitudinal reinforcing elements which allows the macroscopic stress in the composite to increase beyond what would be considered a limit stress for the matrix alone.

The derived failure criterion for the randomly fiber-reinforced soil predicts the

strength of such composite well, particularly for cases where fibers retain their straight shape when placed in soil and loaded (such as steel fibers in a coarse matrix). The predictions are also very sound for fine-grain composites with flexible fibers. This criterion yields reasonable results for flexible fibers in a coarse matrix, although the prediction could possibly be improved by including the effect of a "serpentine" alignment of fibers when mixed with a coarse granular soil.

The failure criteria derived are directly applicable in numerical methods for solving boundary value problems. Immediate applications of the failure model derived are foreseen in design of airfields, aircraft parking facilities, and roads. Future research needs to include a refinement of the fiber/matrix interaction, and it needs to include the anisotropy patterns due to more realistic distribution of fiber orientation. A description of the entire stress-strain behavior also needs to be attempted, which is likely to reveal the possibility of such phenomena as snap-back of individual fibers.

Future research will concentrate on making the description of the mechanical behavior of fibrous granular composites more comprehensive (the entire stress-strain behavior). The fundamental question that was partly answered in this research was: under what circumstances can the process of deformation of a fiber composite become unstable? Issues of fundamental and practical importance that will be addressed in future research are in the questions: Can the deformation process of the composite be controlled by stiffness or length (aspect ratio) of fibers? What is the capability of the granular/particulate matrix based composite to dissipate energy? Does a residual interfacial stress remain upon removing the loads, and can shakedown occur in a cyclic process?

REFERENCES AND BIBLIOGRAPHY

Aboudi, J. (1987). Closed form constitutive equations for metal matrix composites. *Int. J. Eng. Sci.*, 25, 1229-1242.

Aboudi, J. (1991). *Mechanics of Composite Materials. A Unified Micromechanical Approach.* Elsevier, Amsterdam.

Abramento, M. and Whittle, A.J. (1995). Analysis of pullout tests for planar reinforcements in soil. *J. Geot. Eng.*, 121, 176-485.

Adams, D.F. (1970). Inelastic analysis of a unidirectional composite subjected to transverse normal loading. *J. Composite Mat.*, 4, 310-328.

Andersland, O.B. and Khattak, A.S. (1979). Shear strength of kaolinite/fiber soil mixtures. *Int. Conf. Soil Reinforcement*, I, Paris, 11-16.

Arenicz, R.M. and Chowdhury, R.N. (1988). Laboratory investigation of earth walls simultaneously reinforced by strips and random reinforcement. *Geot. Test. J.*, 11, 241-247.

Bentur, A. and Mindess, S. (1990). *Fiber Reinforced Cementitious Composites.* Elsevier, London.

Bažant, Z.P. and Desmorat, R. (1994). Size effect in fiber or bar pullout with interface softening slip. *J. Eng. Mech.*, 120, 1945-1962.

Bažant, Z.P. and Cedolin, L. (1991). *Stability of Structures.* Oxford University Press, New York.

Booker, J.R. and Davis, E.H. (1972). *A general treatment of plastic anisotropy under conditions of plane strain*, J. Mech. Phys. Solids, 20, 239-250.

Bowling, J. and Groves, G.W. (1979). The debonding and pull-out of ductile wires from a brittle matrix. *J. Mat. Sci.*, 14, 431-442.

Budiansky, B. (1965). On the elastic moduli of some heterogeneous materials. *J. Mech. Phys. Solids*, vol. 13, 223-227.

Budiansky, B. (1983). Micromechanics. Computers and Structures, 16, 3-12.

de Buhan, P. and Siad, L. (1989). Influence of a soil-strip interface failure condition on the yield-strength of reinforced earth, *Computers and Geotechnics*, 7, 3-18.

de Buhan, P., Mangiavacchi, R., Nova, R., Pellegrini, G. and Salençon, J. (1989). Yield design of reinforced earth walls by homogenization method, *Géotechnique*, 39, 189-201.

de Buhan, P. and Taliercio, A. (1991). A homogenization approach to the yield strength of composite materials. *Eur. J. Mech., Ser. A/Solids*, 10(2), 129-154.

Cox, H.L. (1952). The elasticity and strength of paper and other fibrous materials, *Brit. J. Appl. Phys.*, 3, 72-79.

Dieterich, J.H. (1972). Time-dependent friction in rocks. *J. Geophys. Res.*, 77, 3690-3697.

Dieterich, J.H. (1979). Modeling of rock friction. 1. Experimental results and constitutive equations. *J. Geophys. Res.*, 84, 2161-2168.

Dieterich, J.H. (1979). Modeling of rock friction. 2. Simulation of preseismic slip. *J. Geophys. Res.*, 84, 2169-2175.

Drescher, A. and de Josselin de Jong (1972). Photoelastic verification of a mechanical model for the flow of granular material, *J. Mech. Phys. Solids*, 20, 337-351.

Drescher, A. Vardoulakis, I. and Han, C. (1990). A biaxial apparatus for testing soils. *Geotech. Testing Journal*, 13, 226-234.

Drucker, D.C, Greenberg, H.J and Prager, W. (1952). Extended limit design theorems for continuous media, *Q. Appl. Math.*, 9, 381-389.

Dvorak, G.J., Rao, M.S.M. and Tarn, J.Q. (1974). Generalized initial yield surfaces for unidirectional composites. *J. Appl. Mech.*, 41, 249-253.

Dvorak, G.J., Rao, M.S.M. and Tarn, J.Q. (1973). Yielding in unidirectional composites under external loads and temperature changes. *J. Composite Mat.*, 7, 194-216.

Dvorak, G.J. and Bahei-El-Din, A.Y. (1982). Plasticity analysis of fibrous composites. *J. Appl. Mech.*, 49, 327-332.

Gopalaratnam, V.S. and Shah, S.P. (1987). Tensile failure of steel fiber-reinforced mortar. *J. Eng. Mechanics*, 113, 635-652.

Gray, D.H. and Al-Refeai, T. (1986). Behavior of fabric versus fiber-reinforced sand. *ASCE J. Geot. Eng.*, 112, 804-820.

Gray, D.H. and Ohashi, H. (1983). Mechanics of fiber reinforcement in sand. *ASCE J. Geot. Eng.*, 109, 335-353.

Gray, R.J. (1984). Analysis of the effect of embedded fibre length on fibre debonding and pull-out from an elastic matrix. *J. Mat. Sci.*, 19, 861-870.

Greszczuk, L.B. (1969). Theoretical studies of the mechanics of the fibre-matrix interface in composites. *Interface and Composites.* ASTM STP 452, Philadelphia, 42-58.

Hashin, Z. (1964). Transverse strength. in *Evaluation of Filament Reinforced Composites for Aerospace Structural Applications*, Dow. N.F and Rosen, B.W., eds., NASA CR-207, 36-43.

Hashin, Z. (1983). Analysis of composite materials - A survey. *J. Appl. Mech., Trans ASME*, vol.50, 481-505.

Hermann, L.R. and Al-Yassin, Z. (1978). Numerical analysis of reinforced soil systems, Proceedings of the Symposium on Earth Reinforcement, Pittsburgh, 1978, 428-457.

Hill, R. (1950). *Mathematical Theory of Plasticity.* Academic Press, Oxford.

Hill, R. (1963). Elastic properties of reinforced solids: some theoretical principles. *J. Mech. Phys. Solids*, 11, 357-372.

Hill, R. (1964a). Theory of mechanical properties of fiber-strengthened materials. 1. Elastic behaviour. *J. Mech. Phys. Solids*, 12, 199-212.

Hill, R. (1964b). Theory of mechanical properties of fiber-strengthened materials. 1. Inelastic behaviour. *J. Mech. Phys. Solids*, 12, 213-218.

Hill, R. (1965). A self-consistent mechanics of composite materials. *J. Mech. Phys. Solids*, 13, 213-222.

Hoare, D.J. (1979). Laboratory study of granular soils reinforced with randomly oriented discrete fibers. Int. Conf. on Soil Reinforcement: Reinforced soil and other techniques. Paris, Vol. 1, 47-52.

Huang, W. (1973). Elastoplastic transverse properties of a unidirectional fibre reinforced composite. *J. Composite Mat.*, 7, 482-498.

Jewell, R.A. and Wroth, C.P. (1987). Direct shear test on reinforced sand, *Géotechnique*, 37, 53-68.

Jommi, C., Nova, R. and Gomis, F. (1995). Numerical analysis of reinforced earth walls via a homogenization method. in *5th Int. Symp. on Numerical Models in Geomechanics (NUMOG V)*, G.N. Pande and S. Pietruszczak, eds. Balkema, 231-236.

Juran, I. and Schlosser, F. (1978). Theoretical analysis of failure in reinforced earth structures, Proceedings of the Symposium on Earth Reinforcement, Pittsburgh, 1978, 528-555.

Lade, P.V. (1977). Elasto-plastic stress-strain theory for cohesionless soil with curved yield surfaces. *Int. J. Solids Structures*, vol. 13, 1019-1035.

Leflaive, E. (1985). Soil reinforced with continuous yarns: The Texsol. *XIth Int. Conf. Soil Mech. Found. Eng.*, III, San Francisco, 1787-1790.

Leflaive, E. and Liausu, Ph. (1986). The reinforcement of soils by continuous threads. Proc. 3rd Int. Conf. on Geotextiles, Vienna, Vol. 4, 1159-1162.

Liausu, Ph. and Juran, I. (1995). Texsol: material properties and engineering performance. *Transp. Research Record*, No. 1474, 3-12.

Lin, T.H., Salinas, D. and Ito, Y.M. (1972). Initial yield surface of a unidirectional reinforced composite. *J. Appl. Mech.*, 39, 321-326.

Maher, M.H. and Gray, D.H. (1990). Static response of sands reinforced with randomly distributed fibers, *ASCE J. Geot. Eng.*, 116, 1661-1677.

Maher, M.H. and Woods, R.D. (1990). Dynamic response of sand reinforced with randomly distributed fibers, *ASCE J. Geot. Eng.*, 116, 1116-1131.

Mallick, P.K. (1988). *Fiber-Reinforced Composites*. Marcel Dekker, New York.

Maugin, G.A. (1992). *The Thermomechanics of Plasticity and Fracture*. Cambridge University Press.

McGown, A., Andrawes, K.Z. and Mercer, F.B. (1985). Soil strengthening using randomly distributed mesh elements. *XIth Int. Conf. Soil Mech. Found. Eng.*, III, San Francisco, 1735-1738.

McLaughlin, P.V. (1972). Plastic limit behavior and failure of filament reinforced materials, *Int. J. Solids Struct.*, 8, 1299-1318.

McLaughlin, P.V. and Batterman, S.C. (1970). Limit behavior of fibrous materials, *Int. J. Solids Struct.*, 6, 1357-1377.

Michalowski, R.L. and Mróz, Z. (1978). Associated and non-associated sliding rules in contact friction problems, *Arch. Mech. Stos.*, 30, 259-276.

Michalowski, R.L. and Zhao, A. (1994). *Failure criteria for fibrous granular composites*, in Proceedings, 8th. Int. Conf. International Association for Computer Methods and Advances in Geomechanics, Morgantown WV, vol. 2, 1385-1390.

Michalowski, R.L. (1995). *Failure criterion for a fiber-reinforced granular composite*, Proc. ASCE X Engineering Mechanics Conference, ed. S. Sture, Boulder, CO, Vol. 2, 1143-1146.

Michalowski, R.L. and Zhao, A. (1995). Continuum versus structural approach to stability of reinforced soil. *J. Geotech. Eng.*, 121, 152-161.

Michalowski, R.L. and Zhao, A. (1995b). *Limit condition for fiber-reinforced granular soil*, Transportation Research Record, No. 1474, 102-107.

Michalowski, R.L. and Zhao, A. (1996). Failure of fiber-reinforced granular soils. *J. Geot. Eng.*, 122, 226-234. See also: Failure of granular composites with fiber

reinforcement, Particulate Mechnics Contractor/Grantee Meeting, Tyndall AFB, Panama City, September 1995 (AFOSR Report).

Mindess, S. (1983). The fracture of fiber reinforced and polymer impregnated concretes. A review. *Fracture Mechanics of Concrete,* ed. F.H. Whittmann, Elsevier,, Amsterdam, 481-501.

Mori, T. and Tanaka, K. (1973). Average stress in matrix and average elastic energy of materials with misfitting inclusions. *Acta Metallurgica,* vol.21, 571-574.

Naanan, A.E. and Shah, S.P. (1976). Pull-out mechanism in steel fiber reinforced concrete. *ASCE J. Struct. Div.,* 112, 1537-1548.

Naylor, D.J. and Richards, H. (1978). Slipping strip analysis of reinforced earth, Int. J. Num. Analyt. Meth. Geomech., 2, 343-366.

Piggott, M.R. (1980). *Load Bearing Fibre Composites,* Pergamon Press, Oxford.

Pinchin, D.J. and Tabor, D. (1978). Inelastic behavior in steel wire pull-out from Portland cement mortar. *J. Mat. Sci.,* 13, 1261-1266.

Pindera, M.J. and Aboudi, J. (1988). Micromechanical analysis of yielding of metal matrix composites. *Int. J. Plasticity,* 4, 195-214.

Pindera, M.J., Aboudi, J. and Brayshaw, J.B. (1991). Micromechanical investigation of the convexity of yield surfaces of metal matrix composites. *Int. J. Plasticity,* 7, 549-566.

Plesha, M.E. (1987). Constitutive models for rock discontinuities with dilatancy and surface degradation. *Int. J. Num. Analyt. Meth. Geomech.,* 11, 345-362.

di Prisco, C. and Nova, R. (1993). A constitutive model for soil reinforced by continuous threads. *Geotextiles and Geomembranes,* 12, 161-178.

Rice, J. (1973). "Plane strain slip line theory for anisotropic rigid/plastic materials." *J. Mech. Phys. Solids,* vol. 21, No. 1, 63-74.

Rice, J. and Ruina, A.L. (1983). Stability of steady frictional slippng. *J. Appl. Mech.,* ASME, 50, 343-349.

Romstad, K.M., Hermann, L.R. and Shen, C.K. (1976). Integrated study of reinforced earth - I: Theoreticam formulation, *ASCE J. Geot. Eng. Div.,* 102, 457-471.

Romstad, K.M., Al-Yassin, Z, Hermann, L.R. and Shen, C.K. (1978). Stability analysis of reinforced earth retaining structures, Proceedings of the Symposium on Earth Reinforcement, Pittsburgh, 1978, 685-713.

Ruina, A. (1983). Slip instability and state variable friction laws. *J. Geophys. Res.,* 88, 10,359-10,370.

Sawczuk, A. and Boehler, J.-P. (1972). Plastic anisotropy of soils, Proceedings of the workshop on Theoretical and Experimental Problems of Limit Analysis of Granular Materials, Jablonna 1971.

Sawicki, A. (1983). Plastic limit behavior of reinforced earth. *ASCE J. Geot. Eng.,* 109(7), 1000-1005.

Sawicki, A. and Lesniewska, D. (1989). Limit analysis of cohesive slopes reinforced with geotextiles, *Computers and Geotechnics,* 7, 53-66.

Shu, L.S. and Rosen, B.W. (1967). Strength of fiber-reinforced composites by limit analysis methods. *J. Composite Materials,* vol.1, 366-381.

Sokolovskii, V.V. (1965). *Statics of Granular Media.* Pergamon Press, New York.

Spencer, A.J.M. (1972). *Deformations of Fibre-reinforced Materials.* Clarendon Press, Oxford.

Stang, H. and Shah, S.P. (1986). Failure of fiber reinforced composites by pullout fracture. *J. Mat. Sci.*, 21, 953-957.

Stauffer, S.D. and Holtz, R.D. (1995). Stress-strain and strength behavior of staple fiber and continuous filament-reinforced sand. *Transp. Research Record*, No. 1474, 82-97.

Steif, P.S. (1990). A model for kinking in fiber composites - I. Fiber breakage via micro-buckling. *Int. J. Solids Struct.*, 26, 549-561.

Steif, P.S. (1990). A model for kinking in fiber composites - I. Kink band formation. *Int. J. Solids Struct.*, 26, 563-569.

Tanaka, K., Wakashima, K. and Mori, T. (1973). Plastic deformation anisotropy and work-hardening of composite materials. *J. Appl. Mech.*, 21, 207-214.

Villard, P. and Jouve, P. (1989). Behaviour of granular materials reinforced by continuous threads, *Computers and Geotechnics*, 7, 83-98.

Wakashima, K., Suzuki, Y. and Umekawa, S. (1979). A micromechanical prediction of initial yield surfaces of unidirectional composites. *J. Composite Mat.*, 288-302.

Waldron, L.J. (1977). The shear resistance of root-permeated homogeneous and stratified soil. Soil Sci. Soc. Am., vol. 41, 843-849.

Wu, T.H., McKinnell III, W.P. and Swanston, D.N. (1979). Strength of tree roots and landslides on Prince of Wales Island, Alaska. Can. Geot. J., Vol. 16, No. 1, 19-33.

Wu, J.U.H. (1992). "Predicting performance of the Denver Walls: General Report." Proc. Int'l. Symp. on Geosynthetic-Reinforced Soil Retaining Walls. Balkema, Rotterdam, 3-20.

APPENDIX

An extensive experimental program was carried out in addition to theoretical considerations. Experimental results were used in this report to verify the assumptions of the failure model presented, and to validate the model-based predictions.

Specimens of fiber-reinforced fine and coarse sand were tested. Specimens were subjected to an axisymmetrical stress state ($\sigma_1 > \sigma_2 = \sigma_3$) in a triaxial apparatus (kinematically controlled), and drained tests were carried out. The specimens had a one-to-one height-to-diameter ratio (*diam.* = 9.65 cm). Over 80 specimens were tested.

The procedure of specimen preparation is described on pages 35-36. Fine and course quartz sand and three types of fibers were used (steel, polyamide and polypropylene). Description of the specific confining stress, fiber content and fiber aspect ratio is given in the figures and in the figure captions. All fibers were approximately 2.54 cm long (1"), except where the influence of the length was tested (and this is noted in the captions). The aspect ratio is not given for the polypropylene fibers, as they were groups (strands) of thin monofilament fibers with no unique diameter.

The majority of the specimens were macroscopically isotropic (with a uniform distribution of fiber orientation in all directions). Eight specimens (Figs. A10, A16, A24, and A32) had fibers placed in a preferred direction (vertical or radial).

The following 32 pages present the stress-strain behavior for all specimens: (a) deviatoric stress vs. axial strain, and (b) volumetric strain vs. axial strain.

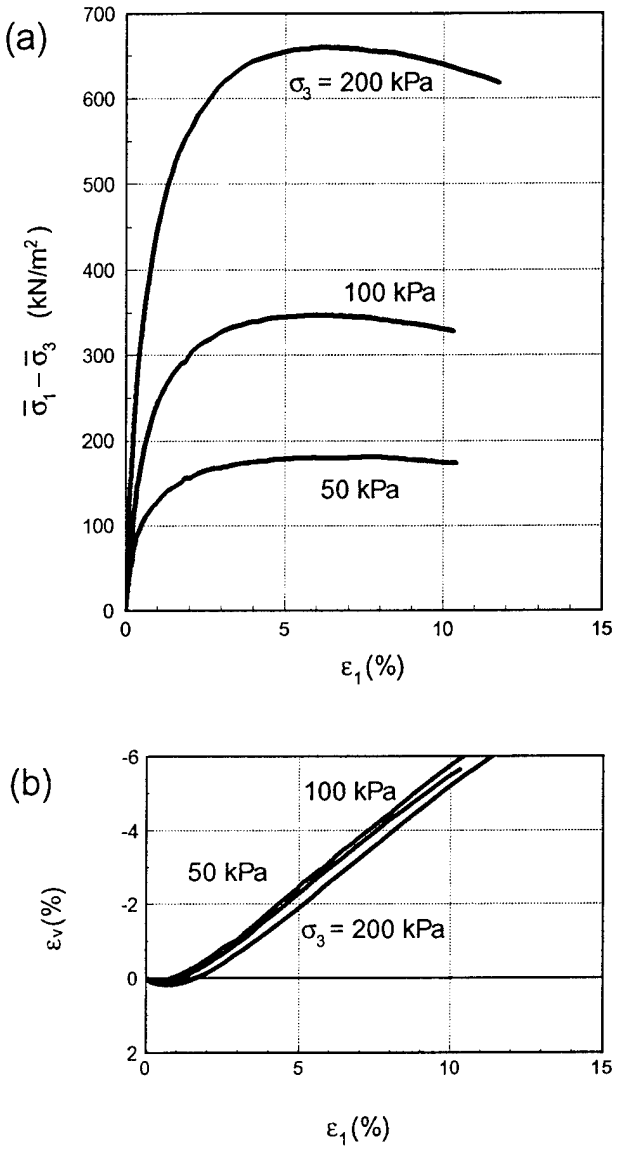

Figure A1. Triaxial test results: (a) deviator stress vs. strain, (b) volumetric strain.
Fine sand, unreinforced.

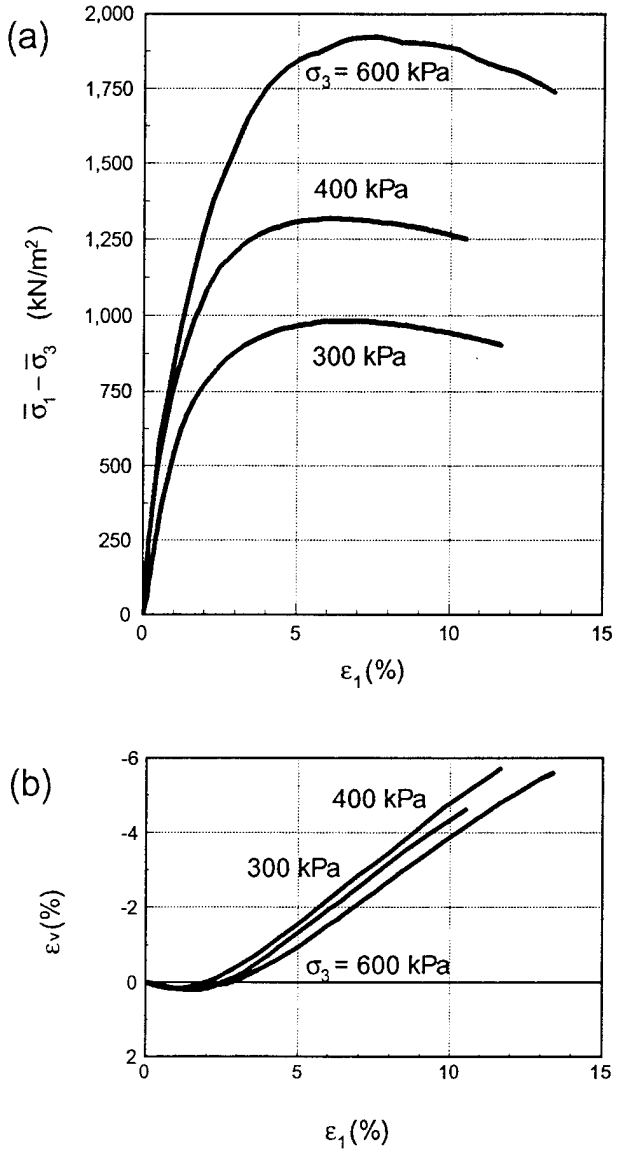

Figure A2. Triaxial test results: (a) deviator stress vs. strain, (b) volumetric strain.
Fine sand, unreinforced.

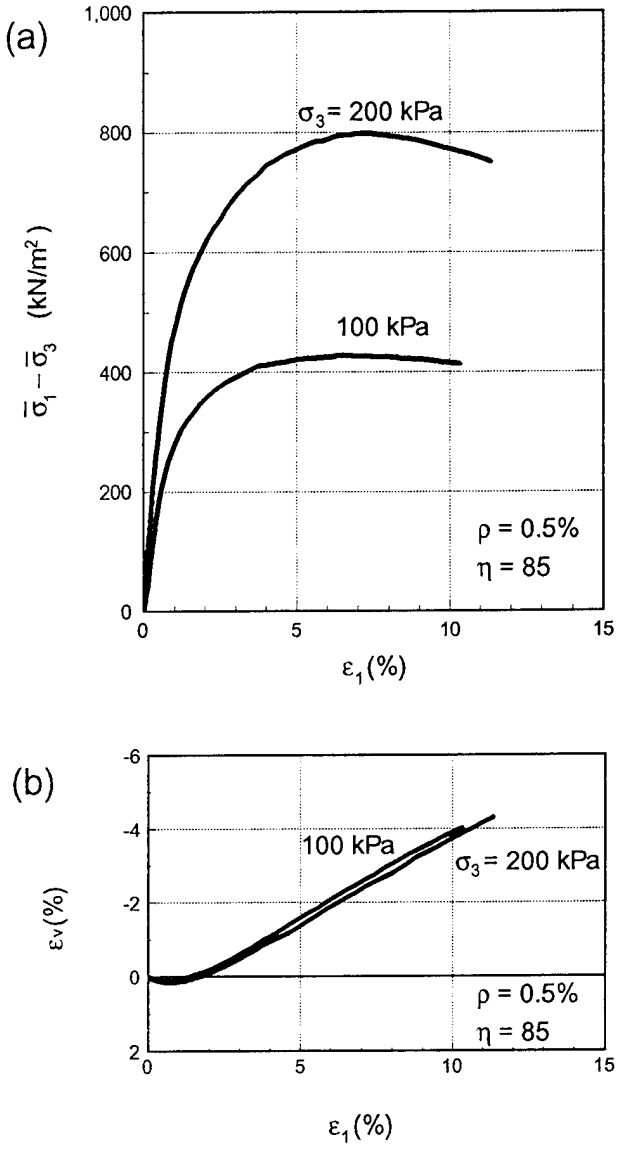

Figure A3. Triaxial test results: (a) deviator stress vs. strain, (b) volumetric strain.
Fine sand, polyamide fibers.

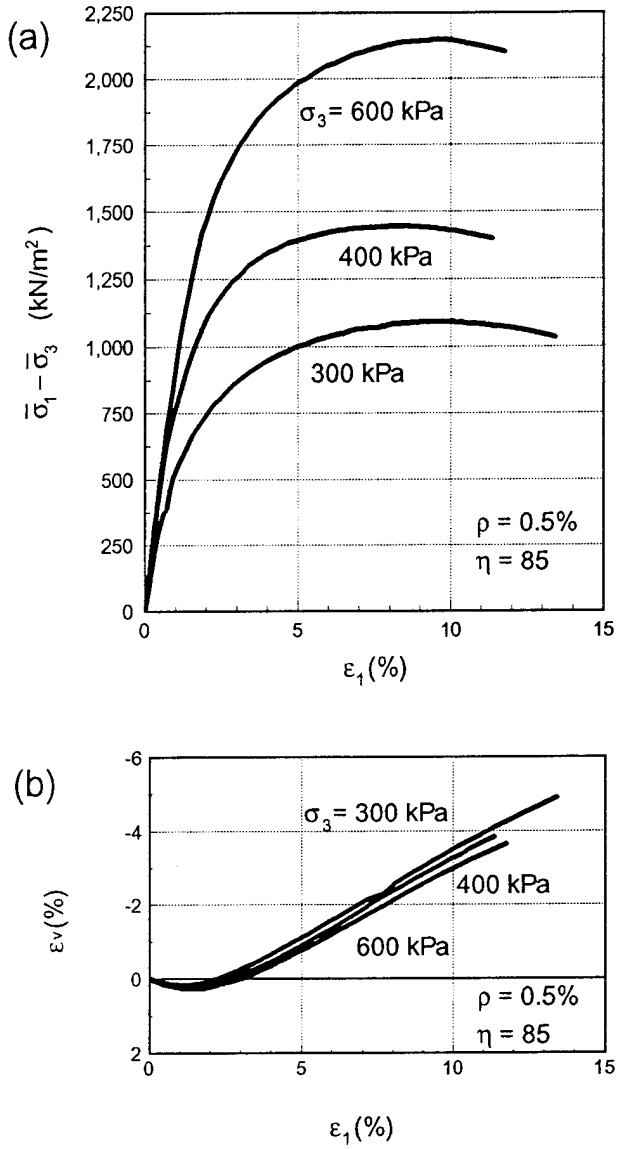

Figure A4. Triaxial test results: (a) deviator stress vs. strain, (b) volumetric strain.
Fine sand, polyamide fibers.

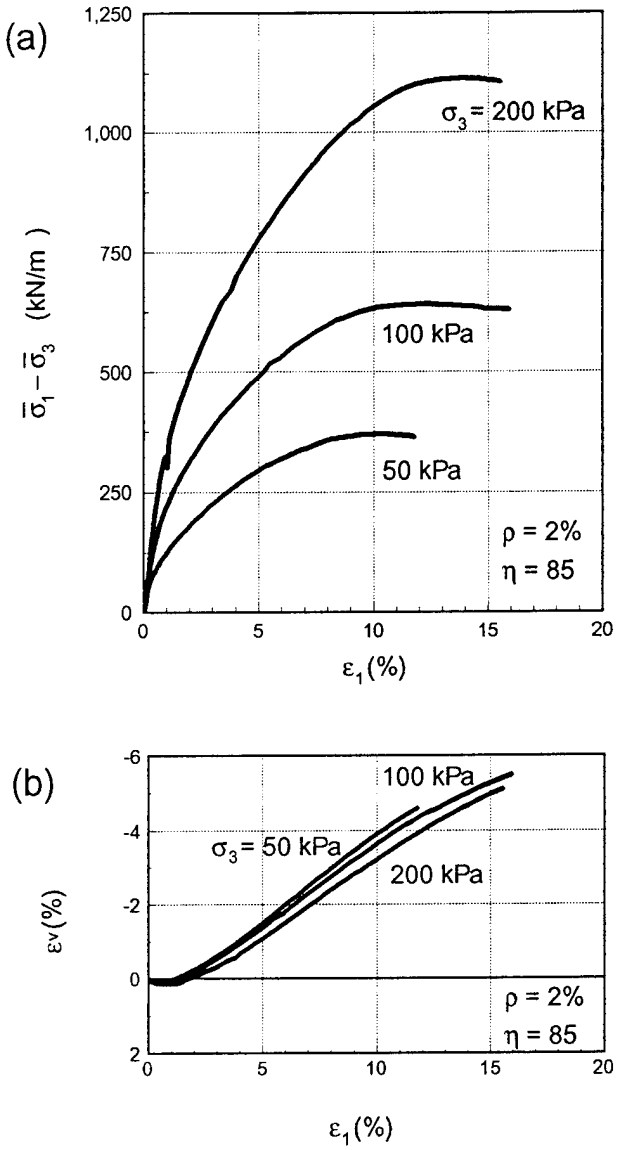

Figure A5. Triaxial test results: (a) deviator stress vs. strain, (b) volumetric strain.
Fine sand, polyamide fibers.

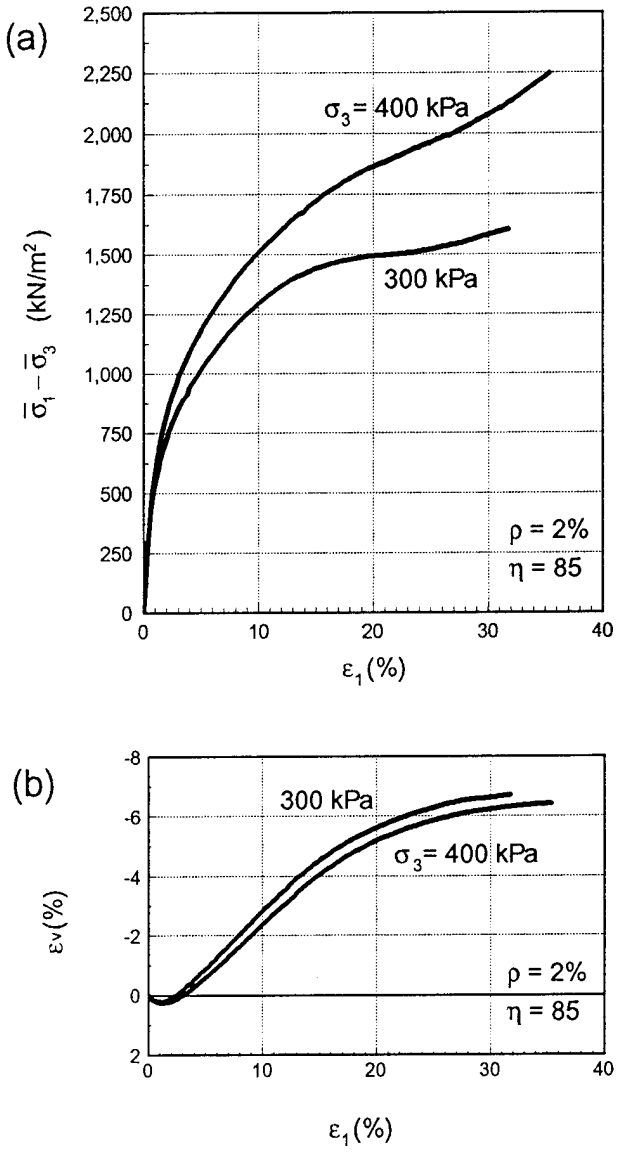

Figure A6. Triaxial test results: (a) deviator stress vs. strain, (b) volumetric strain.
Fine sand, polyamide fibers.

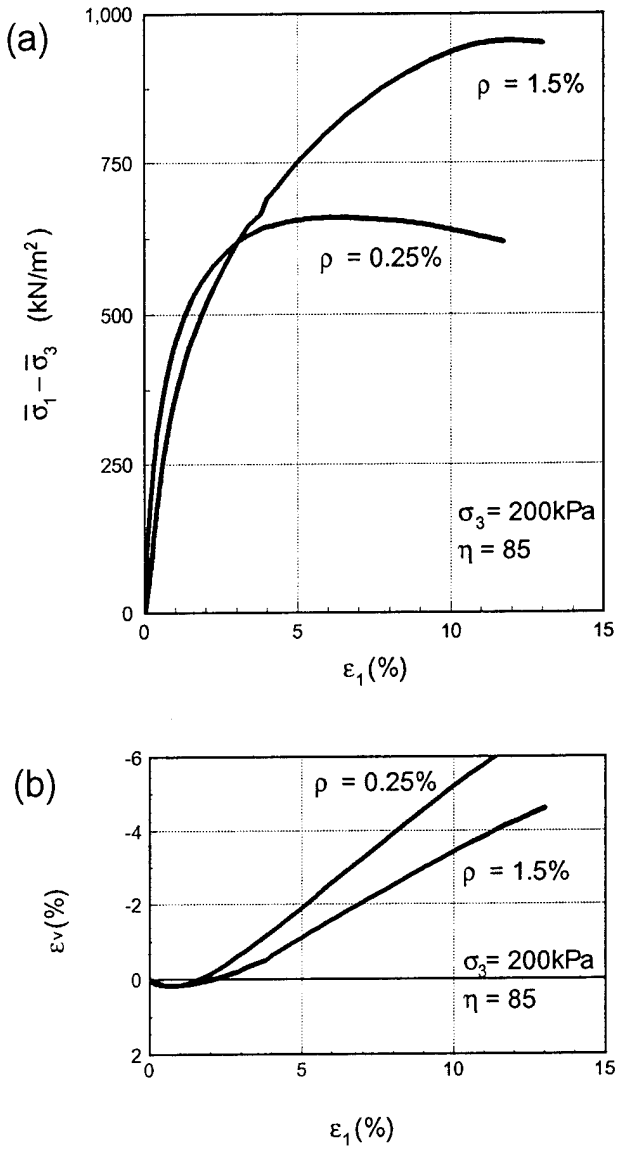

Figure A7. Triaxial test results: (a) deviator stress vs. strain, (b) volumetric strain.
Fine sand, polyamide fibers.

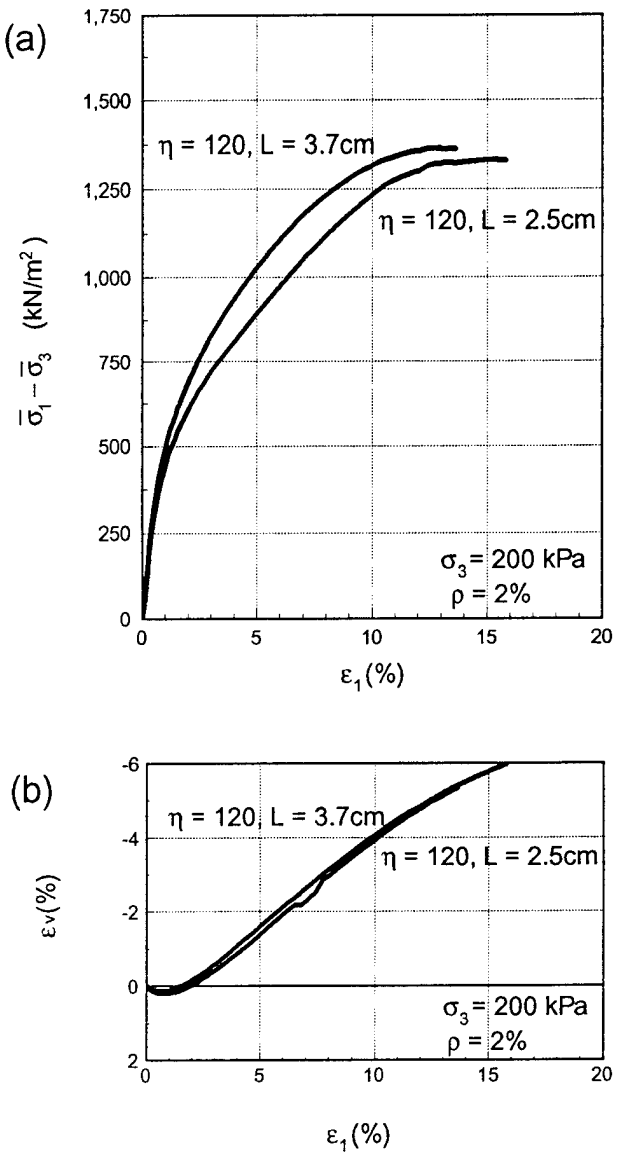

Figure A8. Triaxial test results: (a) deviator stress vs. strain, (b) volumetric strain.
Fine sand, polyamide fibers.

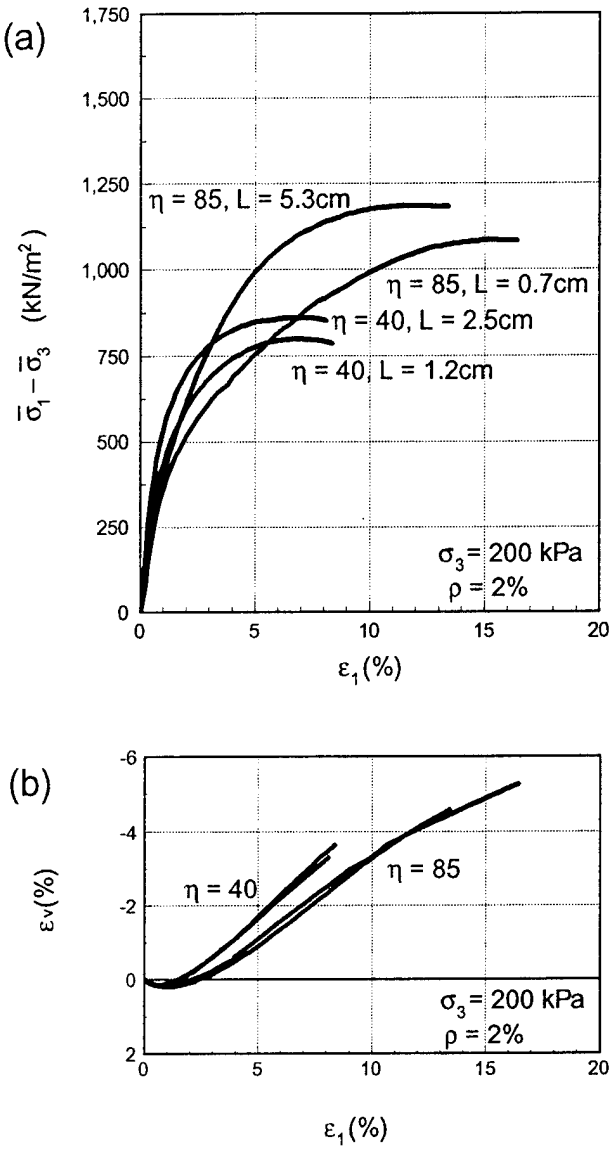

Figure A9. Triaxial test results: (a) deviator stress vs. strain, (b) volumetric strain.
Fine sand, polyamide fibers.

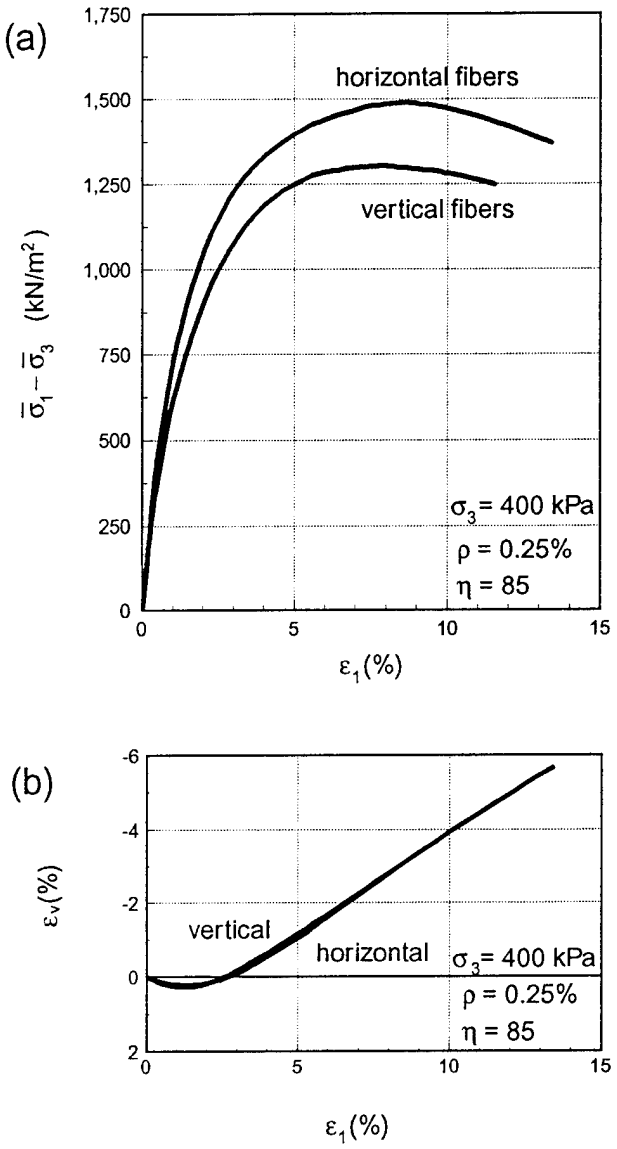

Figure A10. Triaxial tests on macroscopically anisotropic specimens with all fibers in the horizontal (radial) direction, or all fibers in the vertical direction; (a) deviator stress vs. strain, (b) volumetric strain. Fine sand, polyamide fibers.

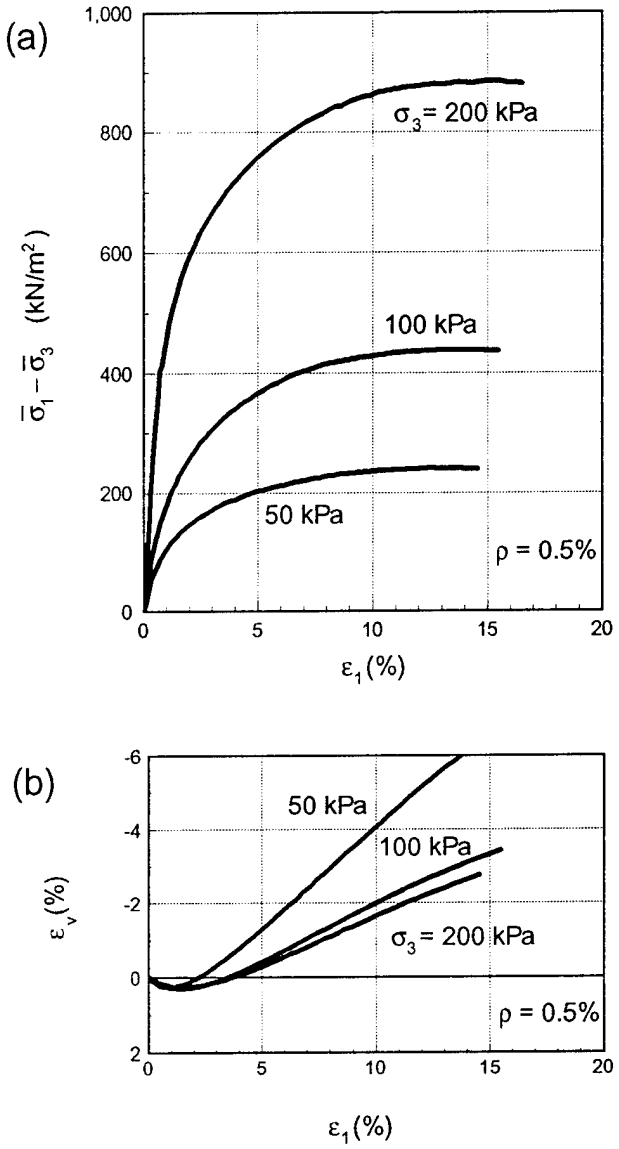

Figure A11. Triaxial test results: (a) deviator stress vs. strain, (b) volumetric strain.
Fine sand, polypropylene fibers.

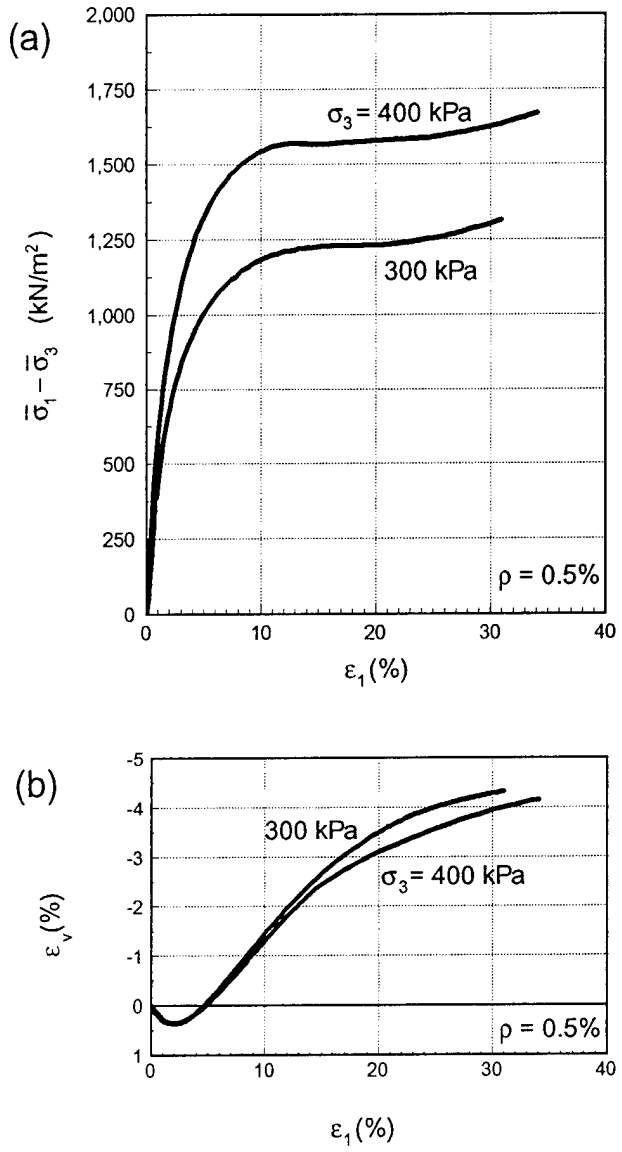

Figure A12. Triaxial test results: (a) deviator stress vs. strain, (b) volumetric strain.
Fine sand, polypropylene fibers.

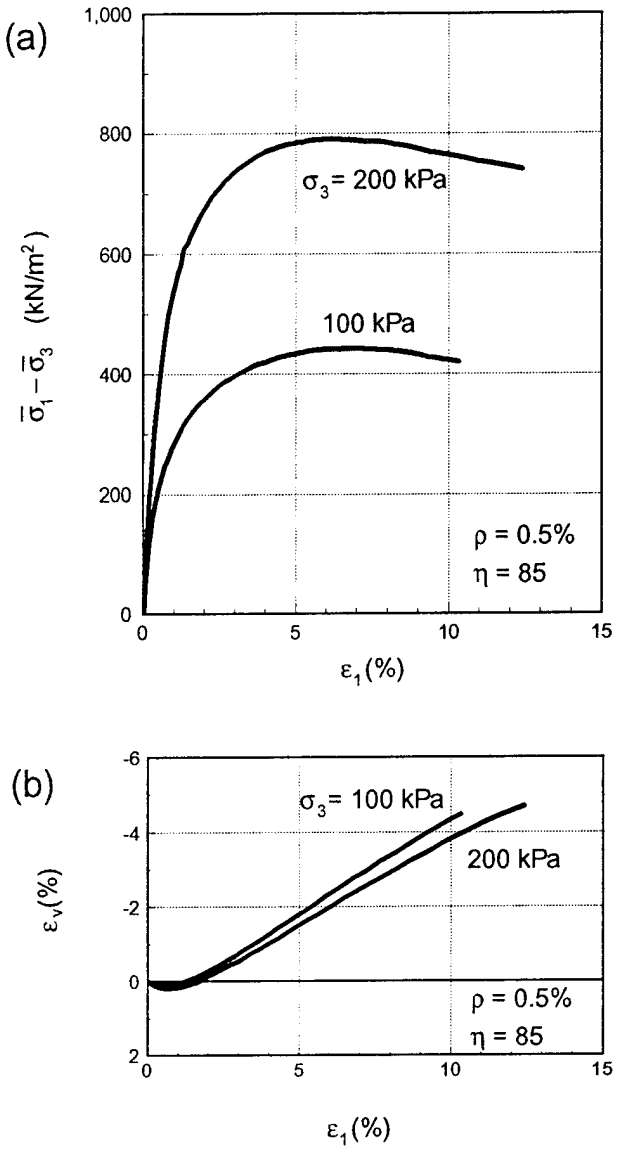

Figure A13. Triaxial test results: (a) deviator stress vs. strain, (b) volumetric strain.
Fine sand, steel fibers.

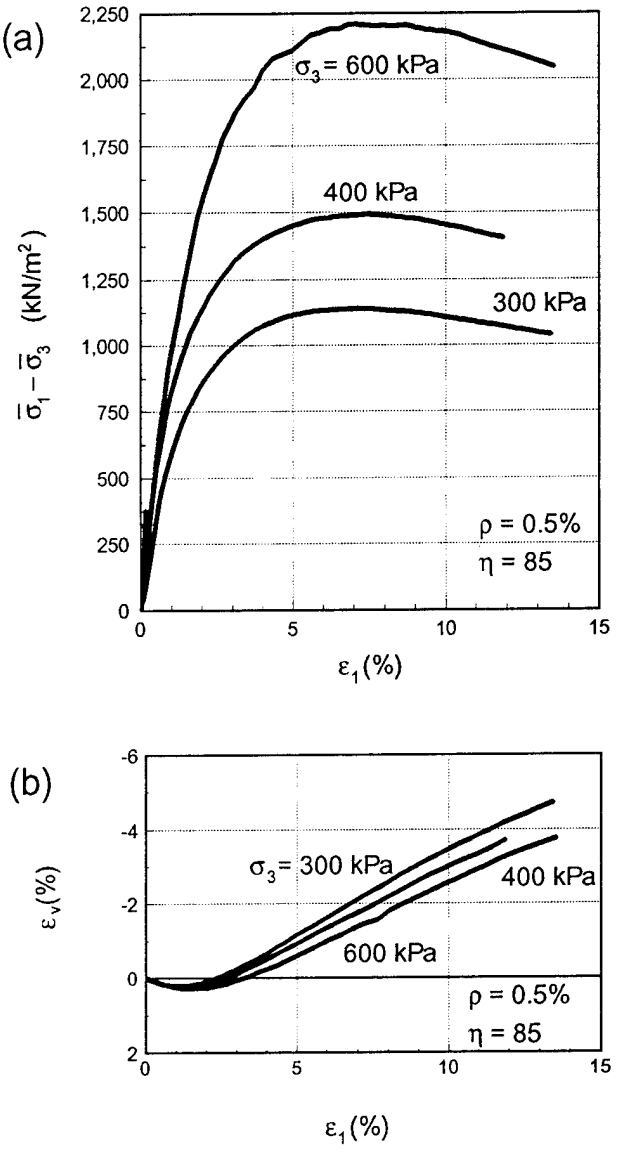

Figure A14. Triaxial test results: (a) deviator stress vs. strain, (b) volumetric strain.
Fine sand, steel fibers.

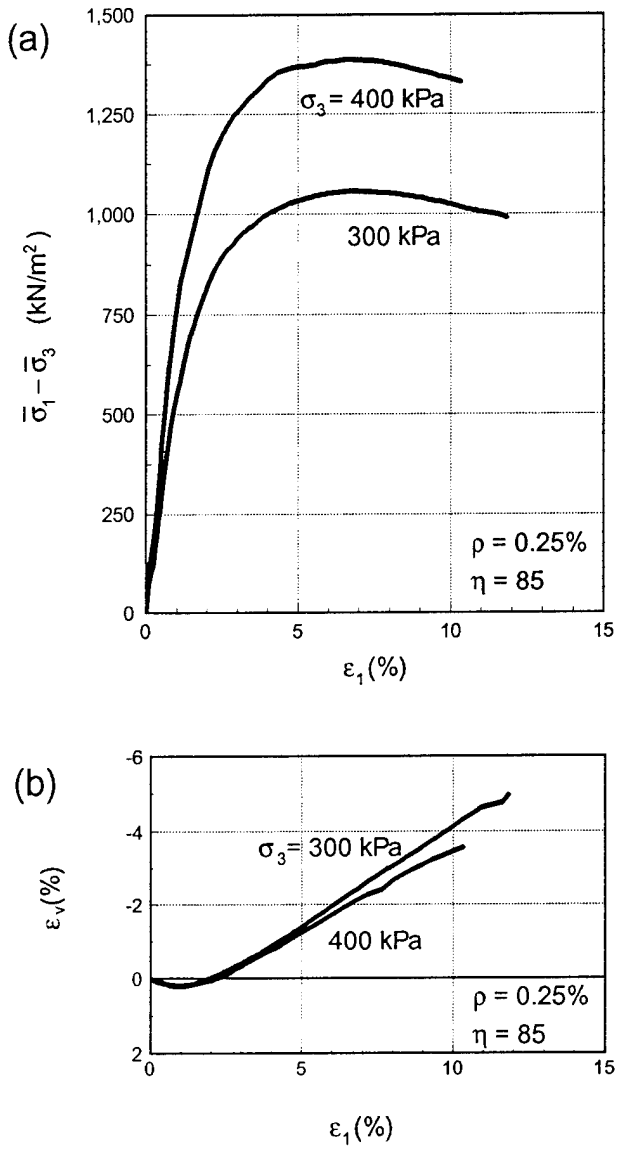

Figure A15. Triaxial test results: (a) deviator stress vs. strain, (b) volumetric strain.
Fine sand, steel fibers.

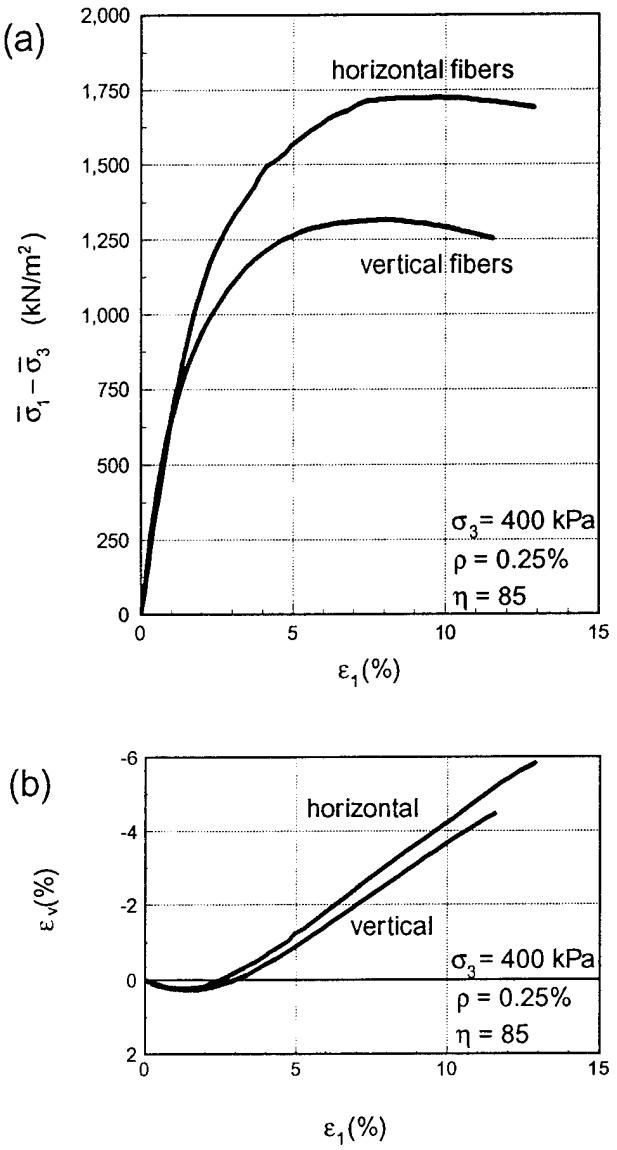

Figure A16. Triaxial tests on macroscopically anisotropic specimens with all fibers in the horizontal (radial) direction, or all fibers in the vertical direction; (a) deviator stress vs. strain, (b) volumetric strain. Fine sand, steel fibers.

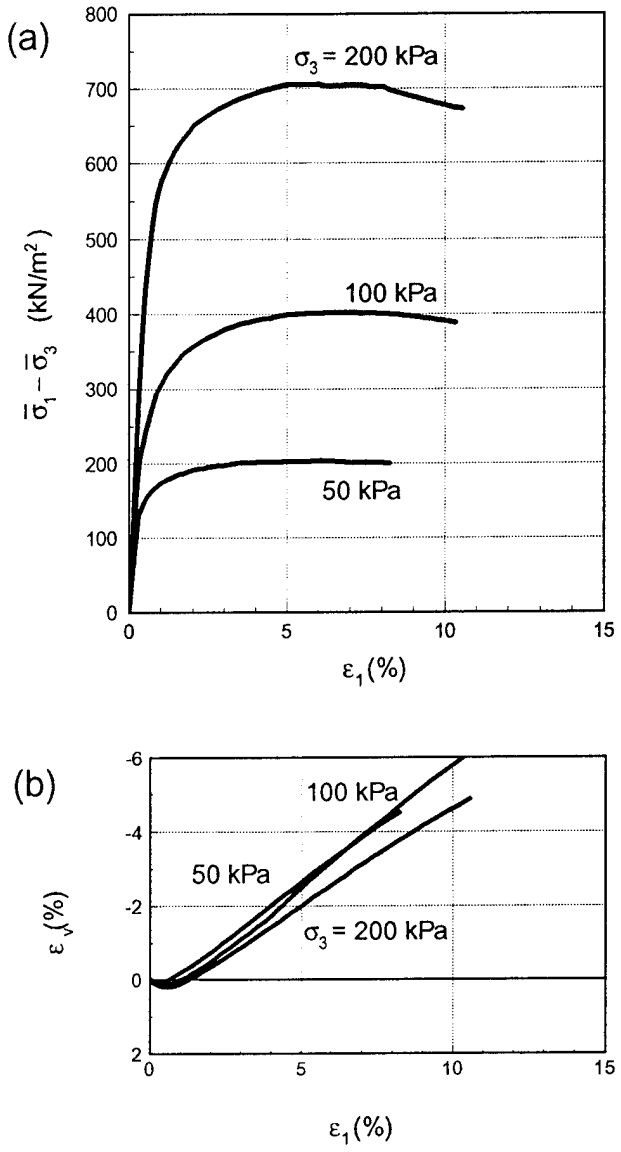

Figure A17. Triaxial test results: (a) deviator stress vs. strain, (b) volumetric strain. Coarse sand, unreinforced.

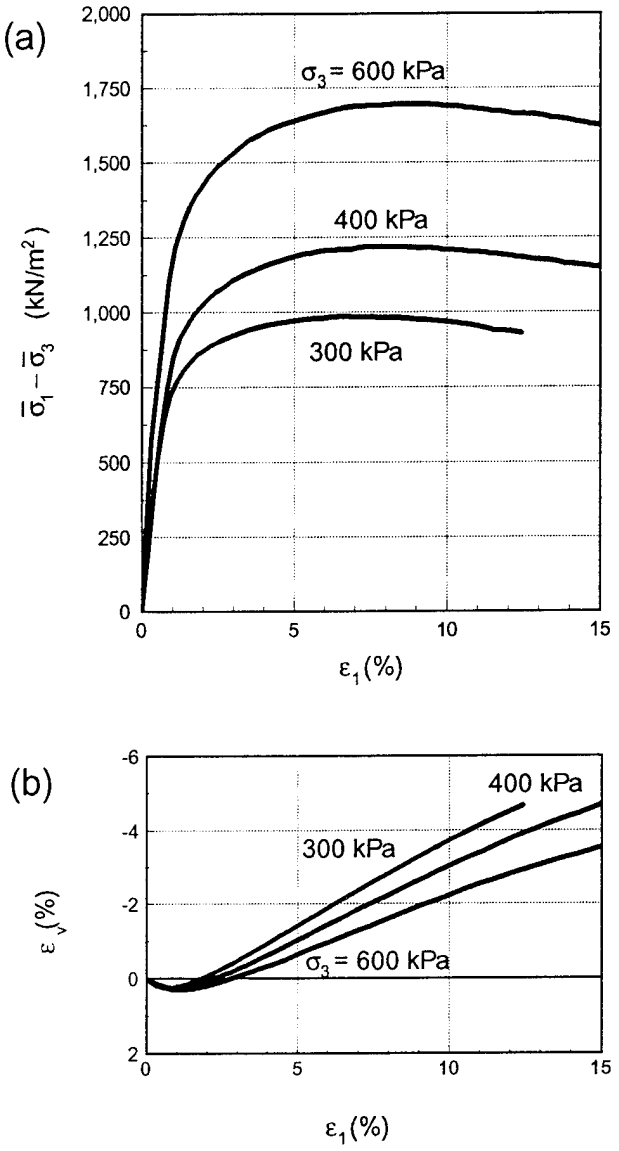

Figure A18. Triaxial test results: (a) deviator stress vs. strain, (b) volumetric strain. Coarse sand, unreinforced.

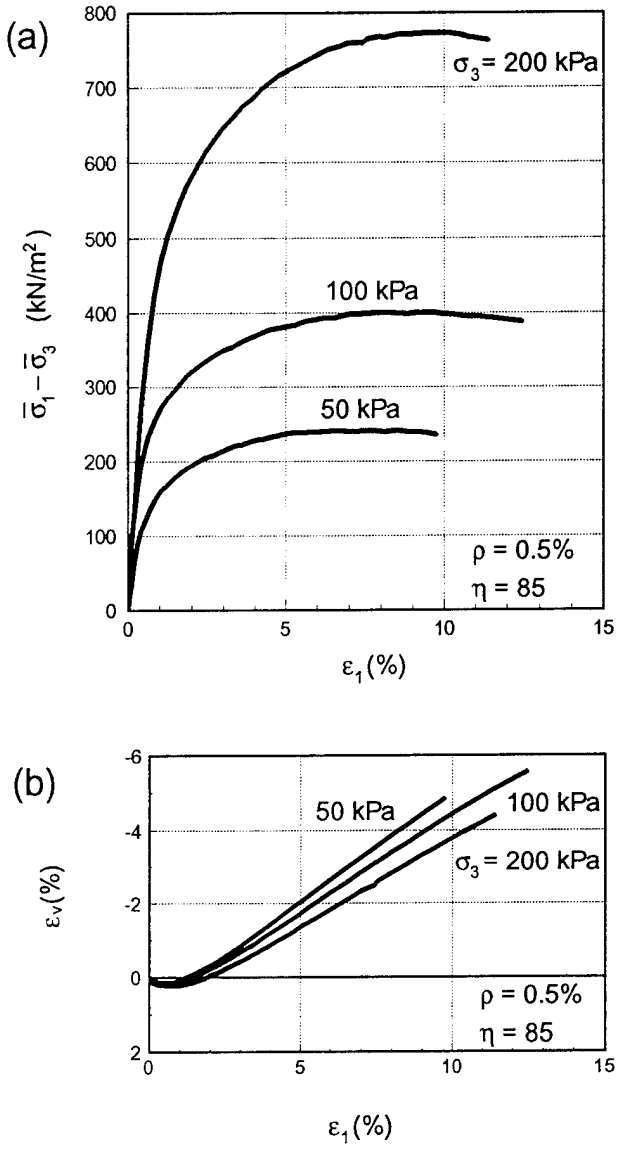

Figure A19. Triaxial test results: (a) deviator stress vs. strain, (b) volumetric strain.
Coarse sand, polyamide fibers.

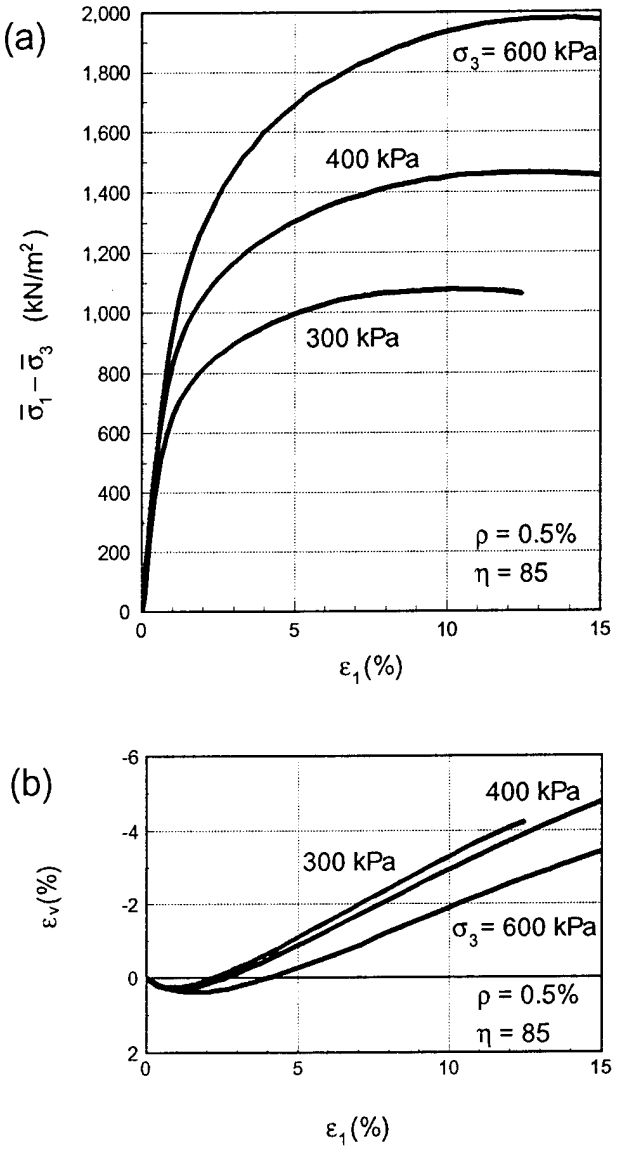

Figure A20. Triaxial test results: (a) deviator stress vs. strain, (b) volumetric strain. Coarse sand, polyamide fibers.

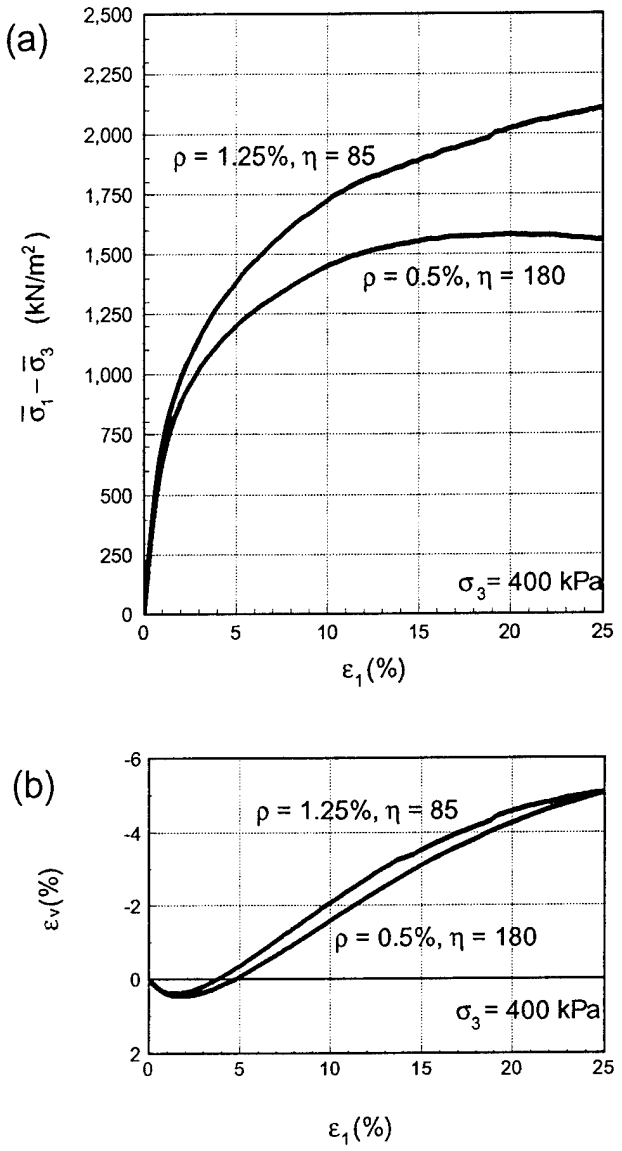

Figure A21. Triaxial test results: (a) deviator stress vs. strain, (b) volumetric strain.
Coarse sand, polyamide fibers.

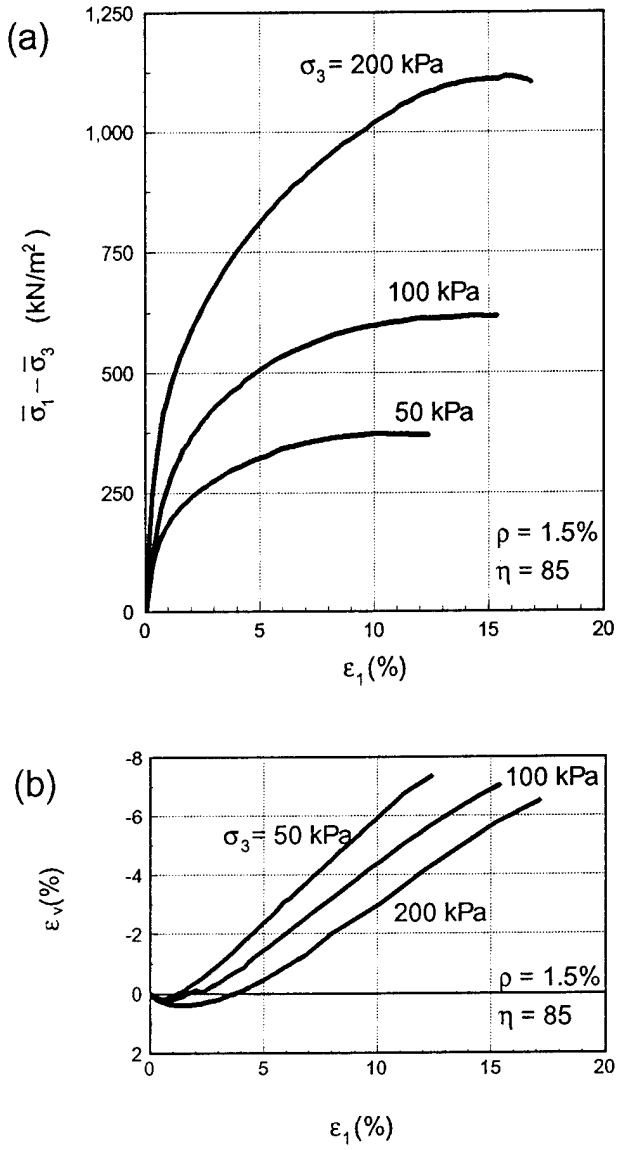

Figure A22. Triaxial test results: (a) deviator stress vs. strain, (b) volumetric strain.
Coarse sand, polyamide fibers.

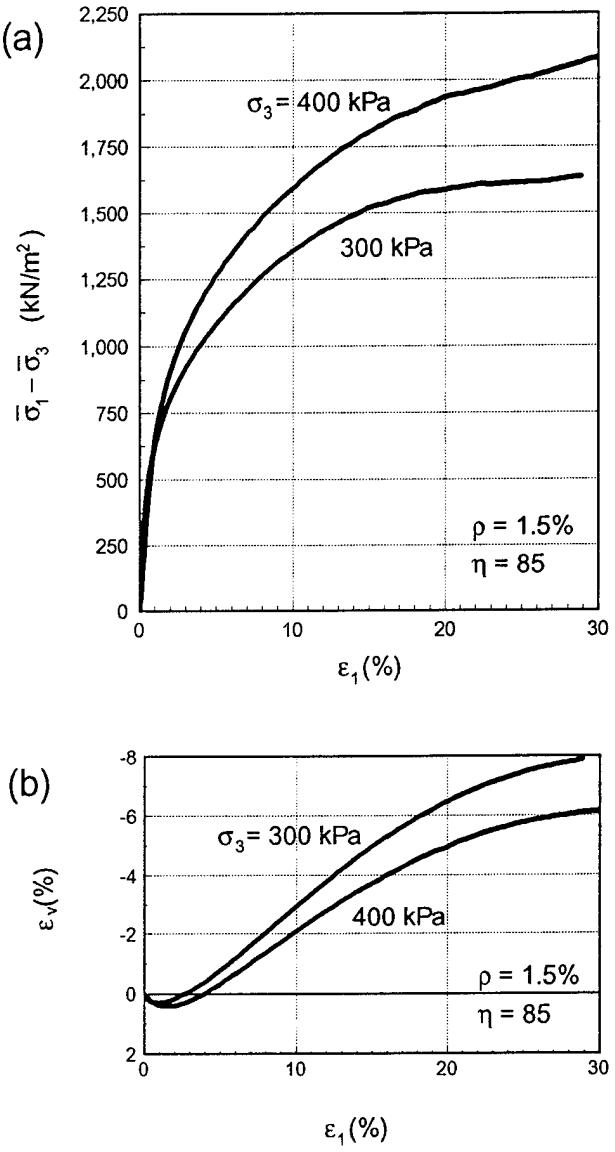

Figure A23. Triaxial test results: (a) deviator stress vs. strain, (b) volumetric strain.
Coarse sand, polyamide fibers.

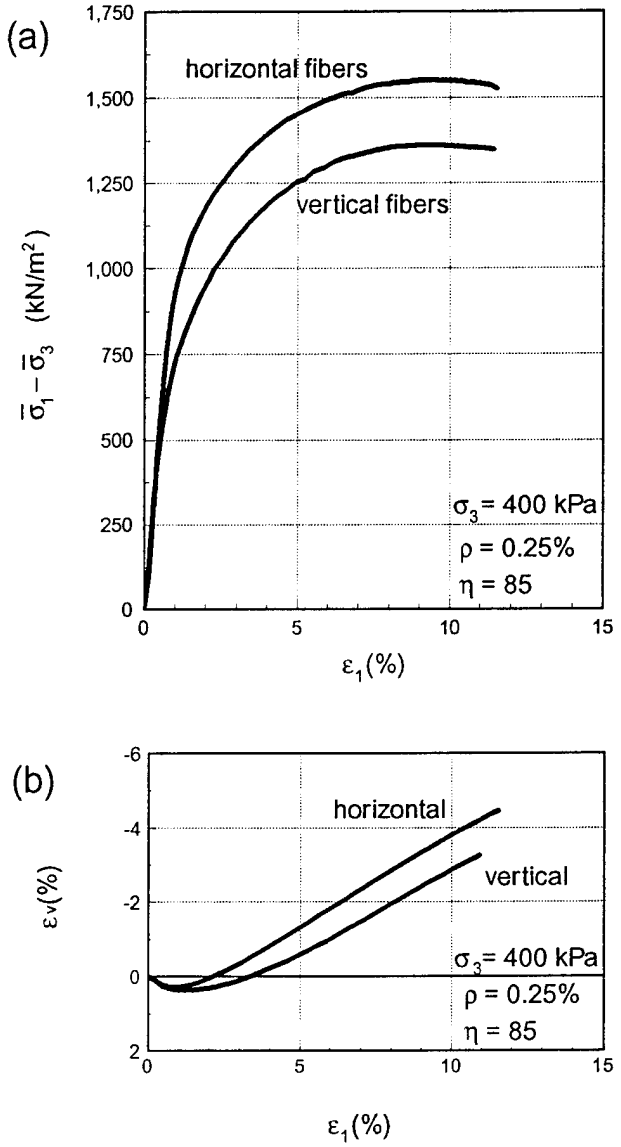

Figure A24. Triaxial tests on macroscopically anisotropic specimens with all fibers in the horizontal (radial) direction, or all fibers in the vertical direction; (a) deviator stress vs. strain, (b) volumetric strain. Coarse sand, polyamide fibers.

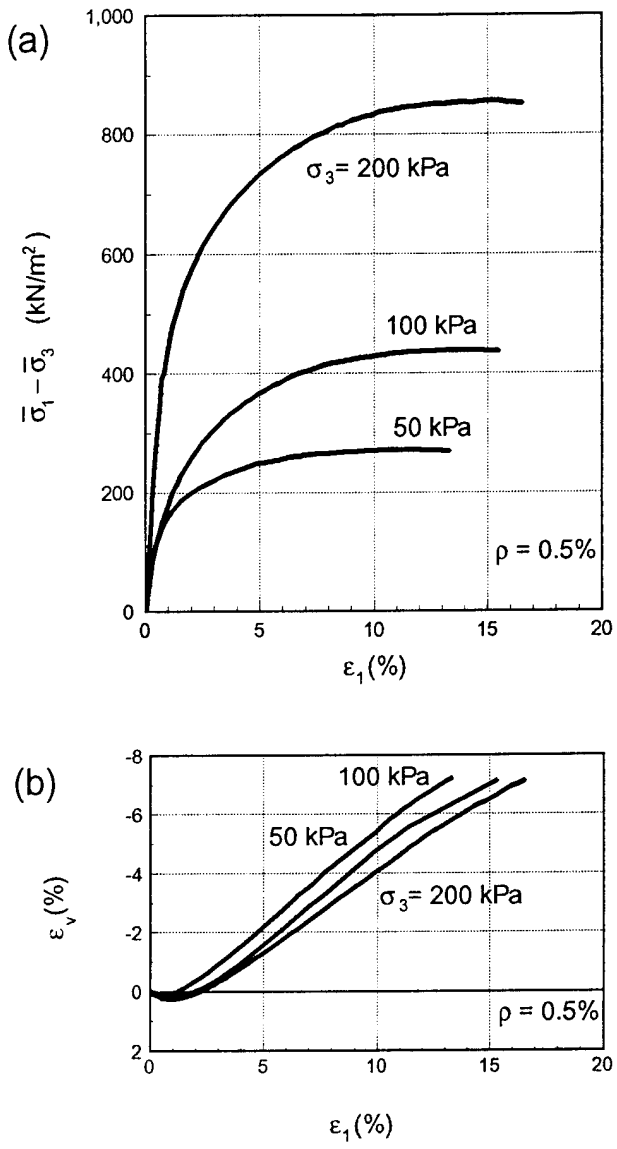

Figure A25. Triaxial test results: (a) deviator stress vs. strain, (b) volumetric strain.
Coarse sand, polypropylene fibers.

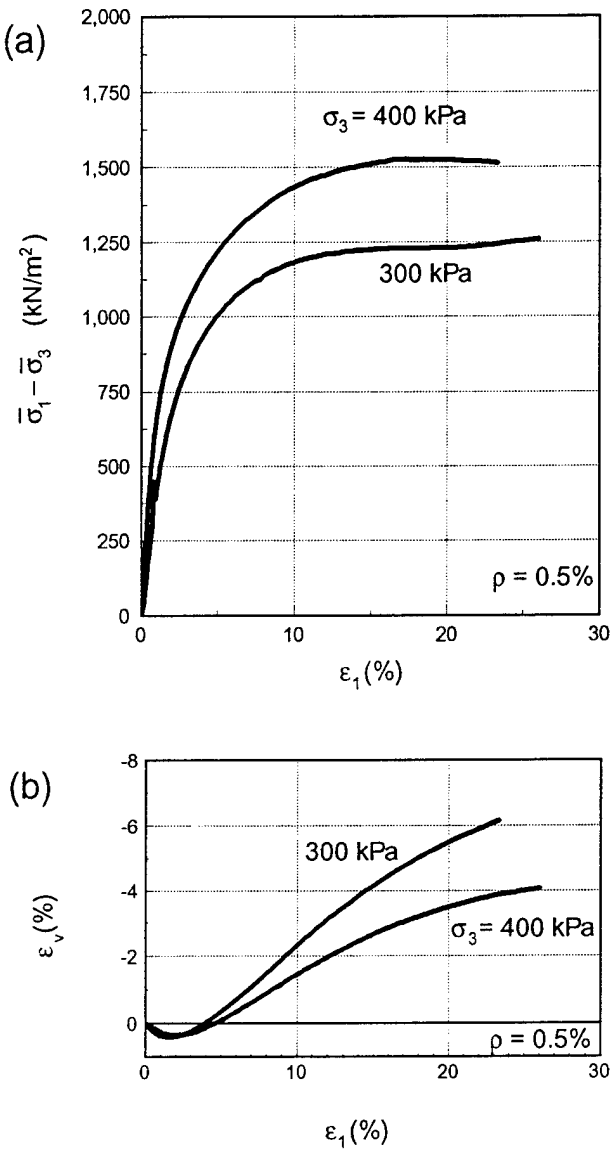

Figure A26. Triaxial test results: (a) deviator stress vs. strain, (b) volumetric strain.
Coarse sand, polypropylene fibers.

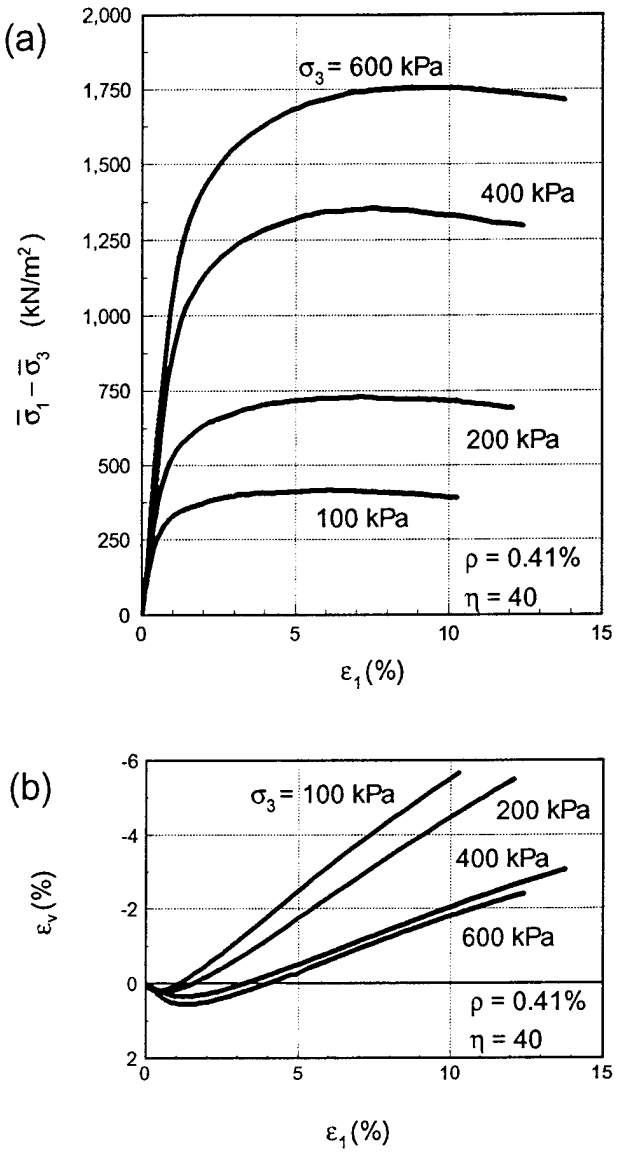

Figure A27. Triaxial test results: (a) deviator stress vs. strain, (b) volumetric strain.
Coarse sand, steel fibers.

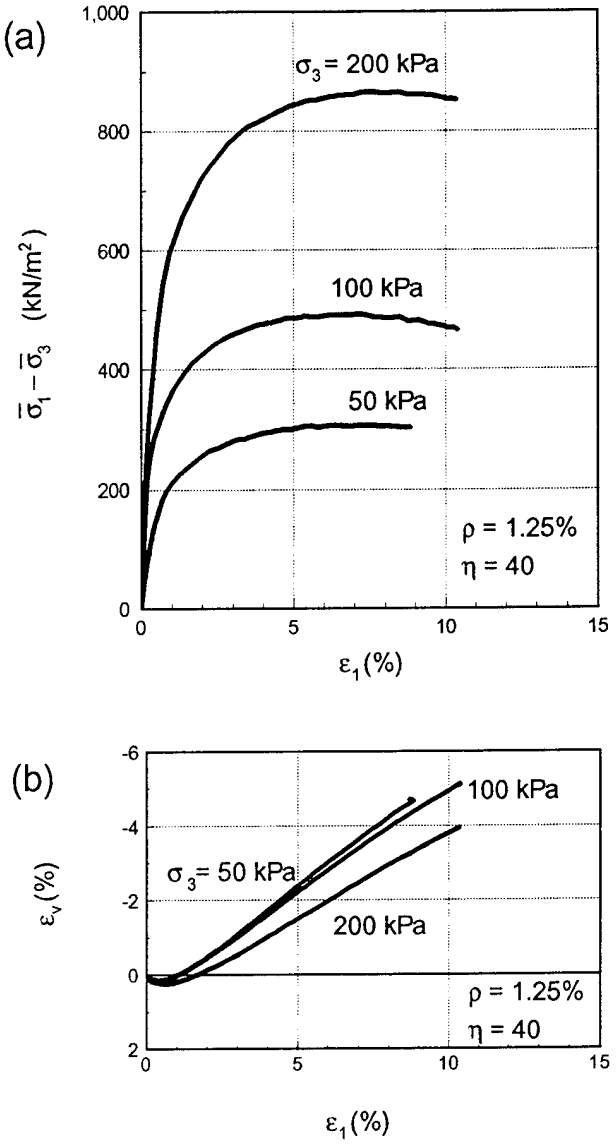

Figure A28. Triaxial test results: (a) deviator stress vs. strain, (b) volumetric strain.
Coarse sand, steel fibers.

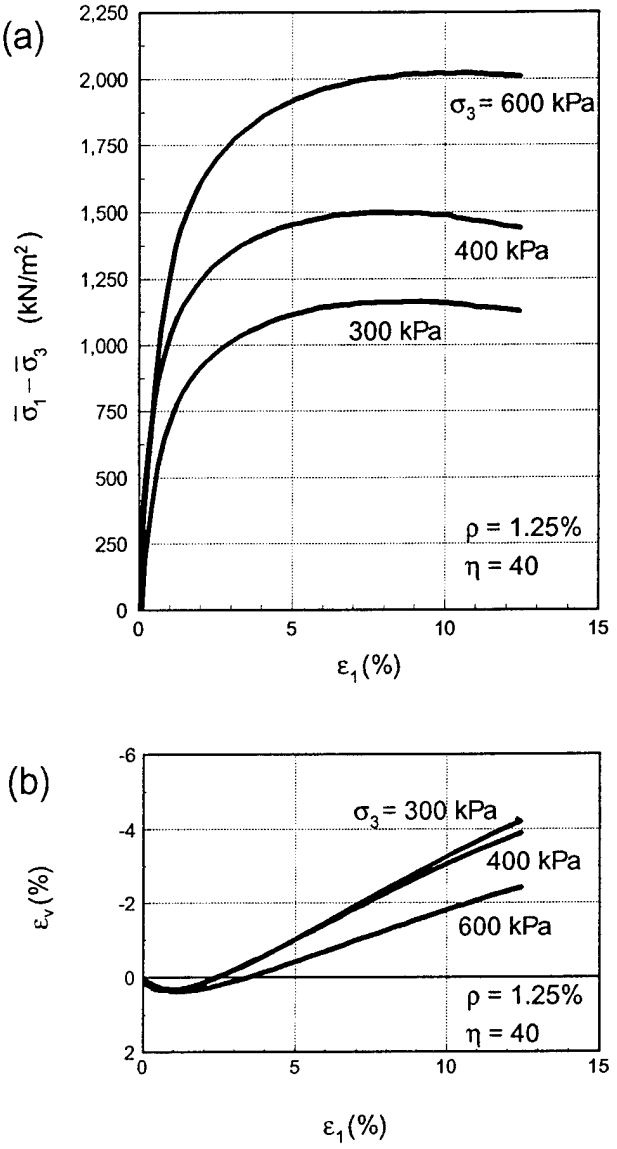

Figure A29. Triaxial test results: (a) deviator stress vs. strain, (b) volumetric strain.
Coarse sand, steel fibers.

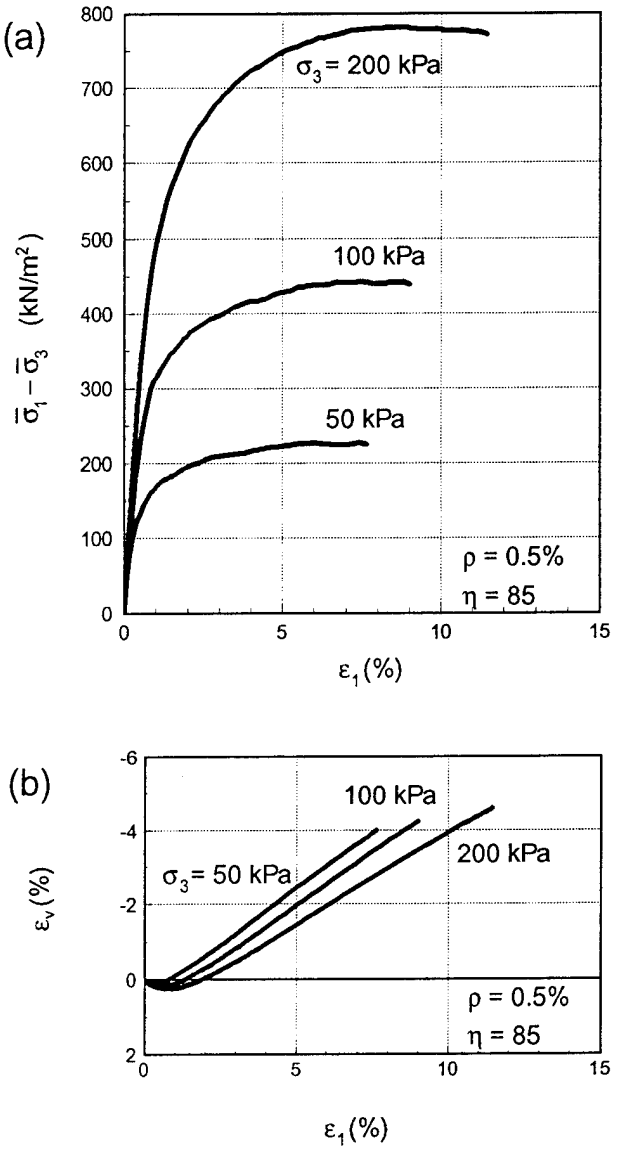

Figure A30. Triaxial test results: (a) deviator stress vs. strain, (b) volumetric strain.
Coarse sand, steel fibers.

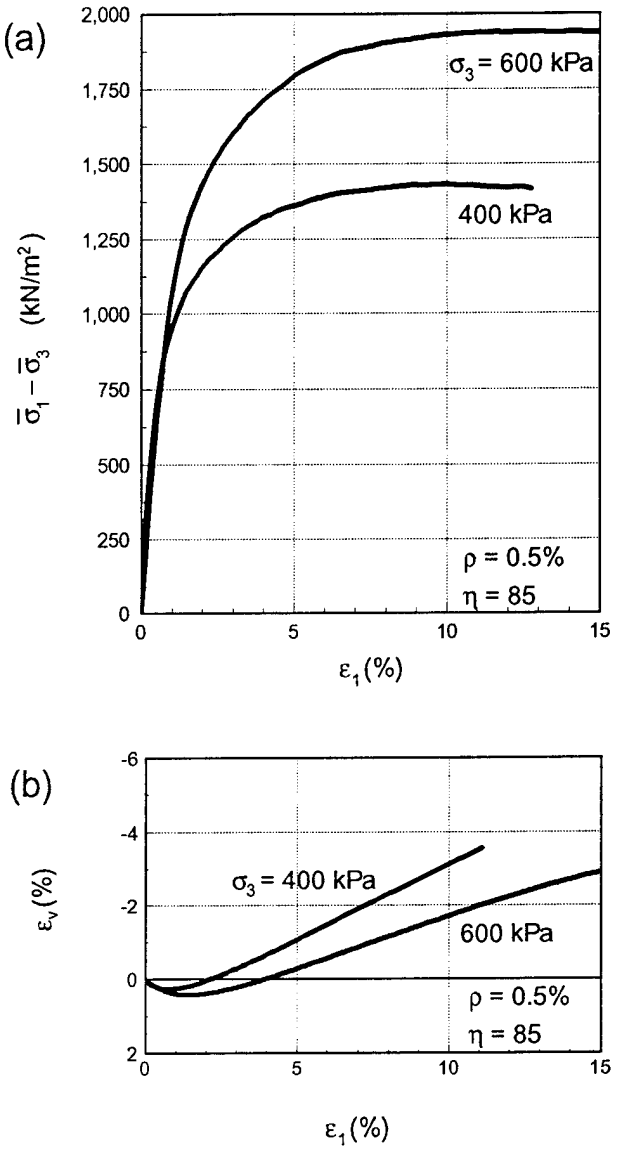

Figure A31. Triaxial test results: (a) deviator stress vs. strain, (b) volumetric strain.
Coarse sand, steel fibers.

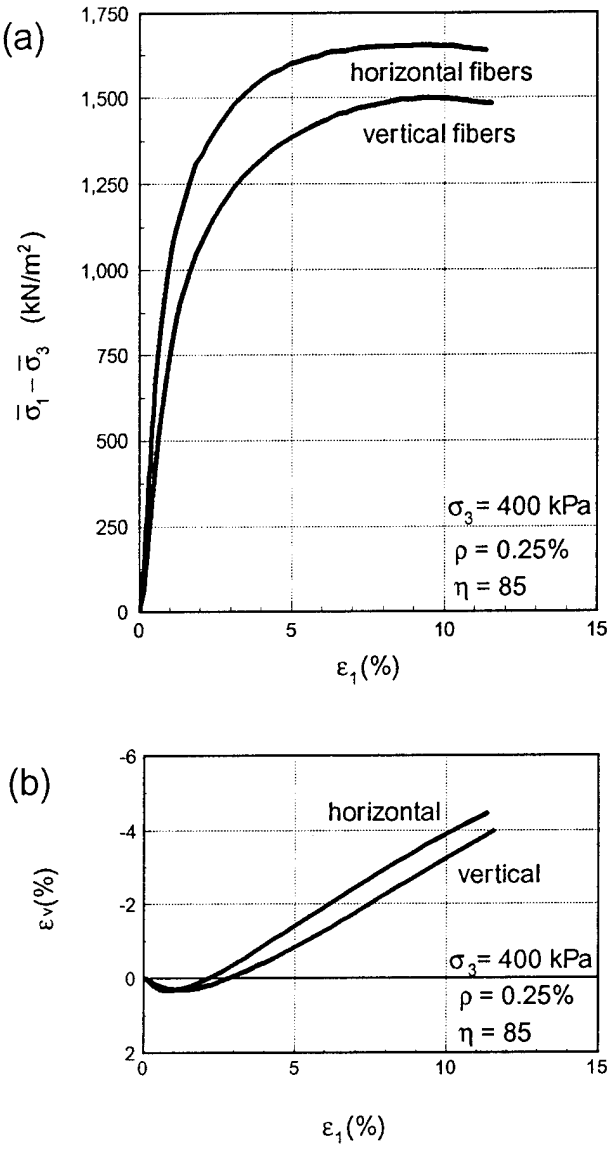

Figure A32. Triaxial tests on macroscopically anisotropic specimens with all fibers in the horizontal (radial) direction, or all fibers in the vertical direction; (a) deviator stress vs. strain, (b) volumetric strain. Coarse sand, steel fibers.